Impact of per-cycle changes in spatial and temporal pattern of dose and biokinetics in neuroblastoma patients receiving 177Lu-DOTATATE

Javian Malcolm

A thesis presented for the degree of

Doctor of Philosophy

Department of Oncology

Oxford University

Date: 01 16 20

Abstract

A thesis submitted to the University of Oxford

for the degree of Doctor of Philosophy

Green Templeton College, Michaelmas Term 2019

Recently, there has been a growth in using post-treatment dosimetry after the first treatment cycle to plan the prescription for subsequent administrations to achieve an acceptable safe dose to kidneys and therapeutic dose to tumour. This level of personalisation recognises inter-patient variability in the uptake and clearance of 177Lu-DOTATATE by the kidneys and tumours. Increasingly, studies are showing additional variation in pharmacokinetics between cycles in an individual patient which may be particularly relevant in NETs cases in paediatric cases like NBL. The central goals for this work were to characterise variability in the spatial and temporal patterns of renal and tumour biokinetics and dose during a four cycle course of 177Lu-DOTATATE and investigate relationships between these variabilities and patient response.

To accomplish this, an open-source software platform was written to facilitate calculation of per cycle pharmacokinetics of organs at risk and lesions using published clinical protocols. Subsequently, we applied these protocols on a single pre-therapy Ga68-DOTATATE PET/CT and intra-therapy longitudinal SPECT/CT image sets acquired in six children with NBL after each cycle to understand the temporal change in physical dose and effective half life over a course of treatment in two anatomical and one functional region. The kinetics of radiobiological dose in the tumour was explored using parameters derived from in-vitro experiments.

The effective half life of 177Lu-DOTATATE in the tumour showed the greatest variation between cycles. Overall, the temporal and spatial variability in renal and tumour pharmacokinetics and dose showed no clear relationship with response in this small cohort. This thesis is a significant step towards further understanding intra-cycle variability during a course of treatment which may impact dosimetry-based treatment planning aimed at delivering a set dose per cycle.

Declarations

I confirm that this thesis I am submitting is wholly my own work except where otherwise indicate. No portion of this work has been presented previously for another qualification at this or any other university. Part of this thesis was published in peer review journals[1, 2, 3].

Word Count

The word count exclusive of figures is 27,672.

Acknowledgements

First I would like to thank Cancer Research UK and University of Oxford Clarendon Fund for providing a fantastic framework and generous funding for my training and research. Further, I would like to recognise my supervisors Katherine Vallis and Nadia Falzone for their guidance, support and discussions.

Importantly, I would like to acknowledge Matthew Aldridge and Mark Gaze who contributed the clinical data and discussions for the project completing. I would also like to acknowledge Boon Quan Lee for his help on the technical and coding elements of the project.

Importantly, I would like to show appreciation for the time of Katherine Vallis for proofreading my thesis.

For day to day support in the lab, I have been fortunate to work in a fantastic team of friend and colleagues in the lab over the past three years. I would like to thank especially Bas B, Edyta A, Elliot A, Irini SK, Martin G and Sarah A for being the first persons I met in Oxford and making it a wonderful experience. Of course, I am grateful to many incredible people at Green Templeton College and beyond who made my time in Oxford unforgettable like Ben D, Timo R, Moritz R, .. and many more.

Finally, my deepest appreciation goes to Mira, my family and friends, without whose continuous support this work would not be possible.

"A chapter a day"

Contents

List of Figures

List of Tables

Abbreviations

131I-mIBG Iodine-131 meta-iodobenzylguanidine. 6, 18, 53

177Lu Lutetium-177. 34, 35, 38, 46, 48

177Lu-DOTATATE Lutetium-177 (177Lu)-DOTA-TATE. 1, 5, 6, 9–11, 16–20, 22–26, 28, 29, 31–38, 40–42, 51, 56, 58–60, 62, 65, 71–73, 75–77, 81, 82, 84, 85, 87, 88, 94, 95

2D 2-dimensions. 34, 36

3D 3-dimensions. 34, 36, 78

AD absorbed dose. 51

AUC area under the curve. 41–43, 45

BED Biological Effective Dose. 20, 29, 30, 39, 40, 48, 58, 62, 75, 77, 78, 85

CCC Concordance Correlation Coefficient. 80, 83, 84, 92

CT Computed Tomography. 35, 36, 45, 51

DICE Sorenson-Dice coefficient. 48

DICOM Digital Imaging and Communications in Medicine. 61

EANM European Association of Nuclear Medicine. 42

EBRT External Beam Radiation Therapy. 53

EUBED Equivalent Uniform Biological Effective Dose. 20, 40, 76, 78, 83, 95

68Ga-DOTATATE PET/CT 68Ga-DOTATATE Positron Emission Computed Tomography/Computer Tomography. 10, 19, 58, 59, 80, 81, 85, 95

IA Injected Activity. 29, 30

LED Local Energy Deposition. 38, 39

LOA Limits of Agreement. 9, 51, 54

LQ Linear-Quadratic. 39, 40, 48, 82

MC Monte Carlo. 38

MIRD Medical Internal Radiation Dosimetry Committee. 35, 36, 38, 48

MTA Maximum Tolerable Activity. 29

MTAD Maximum Tolerable Absorbed Dose. 29

NBL Neuroblastoma. 1, 6, 16, 18–20, 26, 28, 32, 39, 51, 53, 59, 71, 73, 77, 85, 87, 94, 95

NETs Neuroendocrine Tumours. 1, 22–26, 30–32, 40, 46, 58, 71, 72, 75–77, 86, 95

OS Overall Survival. 76

OS Overall Survival. 30

OSEM Ordered Subsets Expectation Maximization. 60

PBPK physiologically based pharmacokinetic. 41

PET Positron Emission Computed Tomography. 20, 21, 83–87

PET/CT Positron Emission Computed Tomography/Computer Tomography. 76, 78, 81

PFS Progression Free Survival. 76

PRRT Peptide Receptor Radionuclide Therapy. 29

PVE Partial Volume Effect. 86

PVE Partial Volume Effects. 35

RECIST Response Evaluation Criteria in Solid Tumors. 61, 80, 81, 84

RT-STRUCT RT-Structure Set. 48, 61

SPECT Single Photon Emission Computed Tomography. 9, 10, 19, 20, 35, 36, 38–40, 45, 47, 48, 51, 60, 62, 73, 76, 78, 81, 83–87

SPECT/CT Single Photon Emission Computed Tomography/Computed Tomography. 1, 9, 11, 18, 21, 34, 36, 37, 42, 43, 47, 48, 50, 51, 58, 60, 62, 73, 76, 80, 81, 86, 95

SSTR somatostatin receptor. 23, 77, 85, 86

TRT Targeted radionuclide therapy. 17, 22, 26, 28, 32, 39

UCLH University College London Hospital. 51, 59, 87

VDK Voxel Dose Kernels. 38, 39, 48

VOI Volume of Interest. 45, 48, 51, 55, 61, 78

Chapter 1

Introduction

1.1 Establishing a context

The European directive 2013/59/Euratom is concerned with basic safety standards in European nuclear medicine centers for protection against the dangers arising from exposure to ionising radiation[4]. For Neuroblastoma (NBL) patients treated with 177Lu-DOTATATE this means individually planning patient prescriptions to reduce inter-patient variability in renal and tumour uptake, retention and clearance, and subsequent radiation dose.

While inter-patient variability in pharmacokinetics is widely accepted for 177Lu-DOTATATE, the best strategy to individualise prescription to reduce the variability and subsequent unexpected results in patient response remains controversial [5]

Fixed dosages or dosages adapted to clinical parameters may result in lack of tumour control through low dose to the tumour and is not in line with the EURATOM Directive. Dosimetric estimates of the absorbed tumour and normal organ dose allow optimisation among patients by delivering a set dose.The rationale for absorbed dose planning is the treatment outcome (for any given patient) depends on how much radiation is delivered to which tissue and less dependent on how much drug is administered. This effort enables each patient to receive the maximum cumulative activity based on the individual rates of their tumour and normal organs. There is an opportunity in the field to enable a more even distribution of radiation dose

throughout the course of treatment. The advantages of dosimetry-based approach are the optimisation of radionuclide therapy, the estimation of the cost-benefit ratio of treatment in single patients, minimisation of risks of toxicity and individualisation according to clinical needs.

The first stage of personalisation was to no longer assume invariable or similar biokinetics among a cohort of patients. Instead, for the most part, investigators have assumed minimal variability in renal and lesion biokinetics, as measured by serial SPECT/CT, across cycles within the same patient. This assumption has lead to clinically feasible protocols and simplified methods to reduce sampling points and make planning multi-cycle 177Lu-DOTATATE treatment simpler and cost-effective [6, 7, 8].

However, it ignores the possibility of tumour responses at earlier points in the therapy leading to clinically relevant changes in the patient biokinetics, in terms of effective half lives, at later cycles of the treatment.

For some time, changes to the intra-cycle pharmacokinetics were inconclusive with authors reporting significant changes for Lu177-based therapies in kidneys and no significant change with caveats. The recent increase in post-therapy dosimetry studies due to feasible protocols have shown a reduction in the radiation dose to the tumour per injected activity as the number of treatments increase [9, 10, 11]. These reports have been confirmed by studies claiming a change in the pharmacokinetics of the patient as a function of tumour load [12, 13, 14, 15, 16, 17, 18]. There has been increasing evidence indicating the temporal change in pharmacokinetics should be considered. Especially in TRT, where the organ doses may change dramatically because of altered organ function, tumor burden and altered hormone release from the tumor, individualized patient dosimetry is indispensable. These findings indicate that patients with cardio-vascular risk factors, borderline kidney dysfunction, and those with dramatic decrease of tumor burden may warrant more caution

The interpretation of these results is hampered by the lack of standardized dosimetry protocols across clinical centers with differences in the major steps in-

cluding the pharmacokinetic modeling (to obtain total number of disintegrations - the cumulated activity - within a given region of interest) precludes a direct comparison of results and strategies among centers.

While inter-subject(cycle) variation makes a strong argument for the application of dose individualisation, the potential for dose individualization is undermined when there is a large degree of intra-patient variation in pharmacokinetics and a lack of studies on the per-cycle changes in tumour and renal effective half life and dose. Changes in the spatial and temporal pattern of uptake and biological clearance of the radiopharmaceutical between earlier and later cycles kinetics may also lead to underdosing at later cycles within a patient for a constant per cycle activity.

1.2 Aim and Scope of the study

In this study we hypothesized that variables capable of reflecting various longitudinal changes in quantitative image features extracted from serial imaging over the course of treatment would be capable of superior prognosis prediction in NBL patients receiving 177Lu-DOTATATE.

1.2.1 Specific Aim 1

Design and build a freely available, cross-platform tool to perform multiple various published pharmacokinetic and radiobiological calculations at the voxel level

Working Hypothesis 1

It is possible to contribute to comparisons of clinical results generated with varied nuclear medicine dosimetry protocols by providing a freely available tool for pharmacokinetic and radiobiological modelling.

- Study 1.1 Demonstrate use case of XINDA using longitudinal 177Lu-DOTATATE SPECT/CT in NBL patients to compare multiple fitting methods

- Study 1.2 Demonstrate use case of XINDA using longitudinal 131I-mIBG gamma counter measurements to model pharmacokinetics in NBL mouse models.

1.2.2 Specific Aim 2

Determine the relationship between treatment response and changes in the temporal pattern of renal and tumour biokinetics and radiation dose during a four-cycle course of 177Lu-DOTATATE.

Working Hypothesis 2

Changes in the biokinetics and absorbed dose so called delta parameters of the tumour and kidneys during treatment can be detected and may have predictive value

- Study 2.1: Characterisation of changes in kidney and tumour biokinetics and radiation dose during treatment using the mean effective half life and absorbed dose metrics derived from per-cycle longitudinal SPECT
- Study 2.2: Investigation of the relationship between delta parameters on tumour response and optimal number of treatment administrations and cycles

1.2.3 Specific Aim 3

Determine the relationship between 177Lu-DOTATATE therapy response and changes in the spatial distribution of pre-treatment 68Ga-DOTATATE PET/CT and intra-treatment 177Lu-DOTATATE SPECT

Working Hypothesis 3

Investigation of the change in the pattern of the dose and effective halflife before and during four cycles of 177Lu-DOTATATE can be used to understand NBL patients that are more likely to respond

- Study 3.1: Provide the first demonstration of quantifying temporal change in spatial distribution of the absorbed dose and effective half life before and during treatment in functionally defined subvolume of the tumour
- Study 3.2: Investigation of the relationship between pre-treatment PET and SPECT based per-cycle physical dose and effective halflife images heterogeneity and tumour response

1.2.4 Specific Aim 4

To explore delta radiobiology parameters in predicting patient response.

Working Hypothesis 4

Changes in radiobiological dose to the tumour may correlate with response.

- Study 4.1 Determine radiobiological parameters experimentally to apply to clinical calculations
- Study 4.2: Investigation of the relationship between delta EUBED for tumour and delta BED for kidneys over a course of treatment.

1.3 Significance

One intended outcome of this study, on a theoretical level, is to extend what is known about the variability and predictive value of intra-patient variability in normal organ at risk and tumour kinetics and dose in 177Lu-DOTATATE therapy in NBL patients. On a practical level, a second intended outcome is to provide a freely available platform for applying the various clinical protocols in a step to justify the effort of dosimetry and towards harmonisation of dosimetry and intercomparison of clinical trials from different centers.

1.4 Overview of the study

The thesis consists of three main parts within five further chapters.

In PART I (Chap. 2 & 3) the current study is situated in related literature and established research methodology. In Chap 2. I provide a critical review of the historical context, current practice and the place of dose optimisation in clinical practice of peptide radionuclide therapy. Chap 2 argues for the need to investigate longitudinal kinetics in a course of repeated Lu177-based treatments. Based on that, the most pressing gaps in the literature are identified and research questions are posed accordingly. Given the detailed method development, Chap 3 deals with the methodological issues and research design providing a theoretical and procedural description as well as a critical examination of the issues of the dosimetry and radiobiology methodology used in this study to collect, present and analyse data.

In PART II (Chap. 4,5 & 6), I present the features of the protocol-agnostic open source platform to implement different pharmacokinetic models using protocols published from multiple centers within Europe. This platform forms the basis for results of data analysis of the potential per-cycle variation of absorbed dose and effective half life in the organs and kidneys. I also present an investigation of a phenomena where there is an identifiable measurable change in the temporal variation of the tumour radiobiological dose and the spatial variation of the dose in the tumour in both the SPECT/CT and PET of a phenomena where there is an identifiable measurable change in the organ and tumour biokinetics over treatment. The analysis of a radiobiological cell survival culture for the generation of alpha beta values was also done. Each chapter ends with a discussion of the key findings expanded to appropriate concepts within the field.

Part III (Chap. 7) contains the discussion, recommendations, and conclusions of the thesis. In Chap 7, the findings of the individual chapters are summarised and fit into the overall theme of the thesis with a reflective evaluation of the study and suggestions for further research agendas.

Chapter 2

Background

2.1 Targeted Radionuclide Therapy: 177Lu-DOTATATE

Targeted radionuclide therapy (TRT) involves the use of a radio-labelled biologic or other vehicle to target and deliver a cytotoxic amount of radiation to inoperable or disseminated disease by emitting Auger, β- or α-particles. In the past five years, three radiopharmaceuticals have been approved by the FDA for clinical use of TRT: Radium-223-based Xofigo for the treatment of metastatic castration-resistant prostate cancer (mCRPC patients) with symptomatic bone metastases without visceral metastases, Iodine-131-based Azedra for the treatment of patients with metastatic pheochromocytoma or paraganglioma and Lutetium-177 (177Lu)-DOTATATE (Lutathera) for the treatment of somatostatin receptor-positive (SSTR) gastroenteropancreatic neuroendocrine tumours (NETs).

Management of NETs has proved problematic since the disease is often diagnosed when metastatic and therapeutic options are limited. A recent phase III, randomized, controlled trial of midgut NETs, progressive on standard-dose octreotide (NETTER-1), demonstrated Lutetium-177 (177Lu)-DOTA-TATE (177Lu-DOTATATE) to be more effective than high-dose octreotide for progression free survival (PFS) with improvement in quality of life and symptom control [19].The NETTER trial showed efficacy when using a basic prescription based on 4 repeat administrations or cycles of 7.4 GBq with no consideration for BSA and Dosimetry

Table 2.1: Historical fixed dose strategies in nuclear medicine

Radiophaceutical	Tumour Type	Prescribed Activity x No of cycles	Ref
90Y-SIR-Spheres	Liver Metastases	3 GBq x 1-10	[20]
131I-mIBG	Paediatric Neuroendocrine	444 MBq/kg x 2	[21]
90Y-DOTATATE	Adult Neuroendocrine	3.7 GBq/m^2 x variable	[22]
177Lu-DOTATATE	Adult Neuroendocrine	7.4 GBq x 4	[19]
177Lu-PSMA	Metastatic castration-resistant prostate cancer	4-9 GBq x 1-5	[23, 24]
223Ra-dichloride	Bone Metastases	55 kBq/kg x6	[25]

and as such the historical standard prescription of 177Lu-DOTATATE for NETs is based on fixed-level empirical dosing consisting of up to four cycles with a time interval between 6 - 10 weeks. These simplified fixed dosing regimens are commonplace in nuclear medicine treatment as shown in Table 2.1 and although beneficial for ease of use may be flawed.

2.2 Variability in Pharmacokinetics of Patients

2.2.1 Inter-Patient variability

The pattern of accumulation and excretion of 177Lu-DOTATATE is governed by the same principles as most anti-cancer drugs. Briefly, after intravenous administration, 177Lu-DOTATATE circulates in the bloodstream and enters the capillaries where it is extravasated into the interstitium mainly driven by convection and diffusion. There it attaches to cells via the SSTR antigens Figure 2.1 By that, it accumulates in sites of NETs cells. Upon radioactive decay, the $\beta-$ particles released by the unstable Lu177 nuclei deposits its kinetic energy within the range of millimeters of tumour tissue to damage and ultimately kill the cancer cells. The main routes of excretion are through the kidneys making the kidneys the major normal organ at risk. Quantification of the accumulation, clearance and radioactive decay process is termed Internal Dosimetry.

The amount and rates of 177Lu-DOTATATE uptake and excretion in the tumour

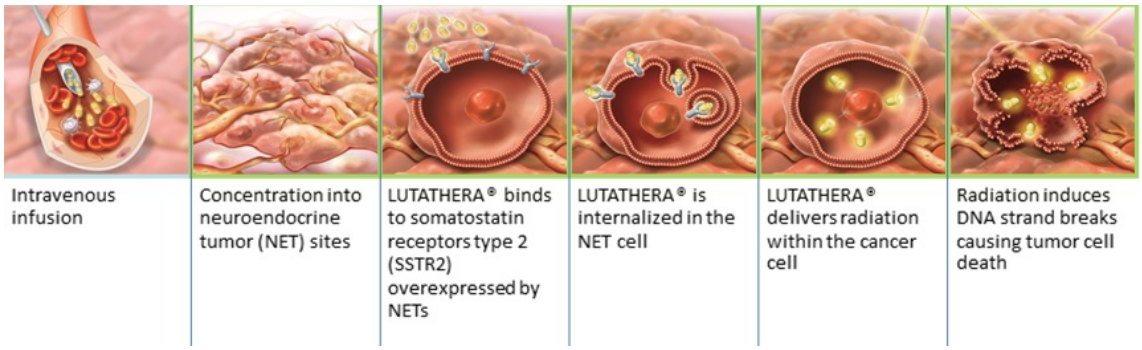

Figure 2.1: Steps in pharmacokinetic process from administration to metabolism for 177Lu-DOTATATE in NETs cells. reprinted from © 2015 Advanced Accelerator Applications and used under a Creative Commons Attribution-Noncommercial license: http://creativecommons.org/licenses/by-nc/3.0/."

and normal organs at risk like the kidneys are governed by passive physiological mechanisms, as well as active mechanisms, such as receptors and happens at differing rates amongst individuals. It should be noted that in addition to receptors, P-glycoprotein (P-gp) is another active mechanism and a key player in the multidrug-resistant phenotype in cancer. P-gp is a drug efflux plasma membrane protein which acts as a localised drug transport mechanism, actively exporting drugs from the cell membrane and cytoplasm and reducing sensitivity to anticancer drugs. As a consequence, the pharmacokinetic parameters of (exposure, i.e., area under the dose-time curve [AUC], and rate of clearance, i.e., dose divided by exposure) may vary substantially among NETs patients for a set radioactivity 177Lu-DOTATATE activity of 7.4 GBq, which is expressed by the term interindividual variation.

This phenomena has been observed in clinical studies. Ilan and colleagues showed in 24 patients receiving a radioactivity dose of 7.4 GBq, that the most frequent radiation dose to tumour was approximately 20 ± 10 Gy during the first therapy cycle, with a median of approximately 50 Gy (range, 10–170 Gy) [10]. In a bigger study, Larsson et al [26] showed a large individual variation, with absorbed dose per unit administered activity of 0.33 to 2.4 Gy/GBq per treatment cycle for kidneys (mean value 0.80 Gy/GBq; SEM= 0.02, SD= 0.30).

This interindividual variation leads to an unpredictable variety in clinical response and adverse effects. It is therefore acknowledged that rational prescribing

of 177Lu-DOTATATE requires not only an understanding of how much drug is administered, but also careful consideration of the factors known to affect how much radiation is delivered and retained in a particular NETs patient. This individualisation can be done on empirical adaptation of the level of activity administered or the number of administrations to patient specific clinical and laboratory parameters like tumour burden, patient weight and renal function, radiosensitivities or patient pharmacokinetics.

2.2.2 Intra-Patient variability

The recent increase in the use of image-based intra-cycle dosimetry to verify radiation exposure of the normal organs and NETs post repeated cycles of 177Lu-DOTATATE has highlighted variability in pharmacokinetics between cycles in the same patient. A summary of these clinical studies and findings on per-cycle changes in the kidneys and tumour can be found in Table 2.2.

For the normal organs, Sandstrom and colleagues [27] noticed 177Lu-DOTATATE changed the organ and tumor uptake as well as the elimination of the administered activity in consecutive cycles, for some patients in a dramatic way. The ratio between the absorbed doses to the bone marrow at later therapy cycles divided by that of the first cycle had a median ratio was 0.82 (interquartile range, 0.64–0.98), and the reduction in absorbed dose was significant for the bone marrow and kidneys ($P < 0.001$). For the tumour, [9] showed the contribution to the accumulative absorbed dose to the tumor after each therapy cycle was gradually reduced. [12] In individual patients, significant changes in activity elimination during therapy indicating a tendency towards increased activity elimination during therapy were found for all organs, often when a large tumor burden reduction occurred during treatment. Del Prete was the first author to personalise every cycle of a 177Lu-DOTATATE treatment by assuming unchanged pharmacokinetics from the previous cycle. It was noted that the renal absorbed dose per IA received at a given cycle was predicted by that received at the previous cycle with an accuracy of $4.9 \pm 26.7\%$ (range, -48.8

– +89.1%; n = 83) [28]

Per-cycle variability in the pattern of γ-H2AX kinetics [29] and progressive reduction of uptake in tumours at interim 177Lu-DOTATATE scans or 68Ga-DOTATATE performed after the first 177Lu-DOTATATE cycle have been found to correlate with predicted time to progression and correlated with an improvement in clinical symptoms response in NETs patients [30, 31].

In much the same way, the variability in dose between patients was an indication for personalisation, it stands that the variability between cycles may be a case for further personalisation.

2.3 Neuroblastoma - The Paediatric Neuroendocrine Tumour

The patient groups that are particularly vulnerable to intra-cycle pharmacokinetic variability are paediatric cases with growing organs, where age-related changes in body composition and tissue boundaries affecting drug distribution and effects on radionuclide drug clearance are not well documented. Further, the "elimination" organs, for example, kidneys, are growing and developing at different rates.

Neuroblastoma (NBL) is a neuroendocrine cancer predominantly in infants and young children and arises in the developing sympathetic nervous system (from any neural crest element), which results in tumours in the adrenal glands and/or sympathetic ganglia[35]. It is a tumour of early childhood and is the most common malignancy diagnosed in the first year of life, with 90% of tumours arise in children who are <10 years of age, and have a median age at diagnosis of 18 months.

Recently, it was demonstrated that 68Ga-DOTATATE PET could be used to image children with relapsed or primary refractory high-risk NB,[36] and patients with NBL including relapsed or progressive disease showed SSTR2 expression at diagnosis[37] suggesting they could be candidates for TRT therapy with 177Lu-DOTATATE. In a pilot clinical study, Gains and colleagues demonstrated high up-

Table 2.2: Summary data of clinical studies reporting per cycle changes

Reference	No of cycles (patients)	Conclusions on intra-patient variability
[32]	1(n=15), 2(n=9)	Per-cycle kidney: significant positive correlation with per cycle BM (Spearman r = 0.31, P < 0.0001)
	3(n=5), 4(n=5)	Per-cycle tumour: significant correlation with per-cycle kidney (Spearman r =0.16, P=0.04; n =170).
[26]	1(n=3), 2(n=7), 3(n = 10), 4(n=12), 5 (n=1)	Per cycle kidney: mean deviation of all subsequent kidney doses from the first treatment cycle was 1% (range -31% to +47%) for the right kidney and 5% (range -26% to +93%) for the left kidney
[9]	1(n=2), 2(n=4)	Per cycle kidney: The different cycles contributed on average equally to the absorbed dose (within 10%)
	3(n=6), 4(n=9)	Per-cycle tumour: the first 2 cycles make the major contribution to the absorbed dose to the tumor.
[12]	4(n = 30)	Per-cycle kidney: Effective half-life in the kidneys decreased in most of the patients during the therapy Per cycle tumour: Patients with a substantial decrease of tumor burden showed decrease in Teff and increase in 24h uptake value
[33]	3(n = 2), 4 (n =4), 5 (n=7), 6 (n = 5), 7 (n=1), 8 (n=3)	Per cycle kidney: AD/cycle vary between cycles in the same patient
[34]	2(n = 10)	Per cycle kidney: no significant between-cycle difference was observed (p=0.0809) Per cycle tumour: differences of absorbed dose between cycle 1 and 2 were observed, especially for organs very close to, or including tumor cells or metastases.
[10]	2(n=1), 3 (n=6), 4 (n=10), 5 (n=5) , 6(n=2)	Per cycle tumour: The mean ratio between the effective half-lives during cycles 3 (or 5, where applicable) to cycle 1 was 0.98 6 0.12, and the median was 0.98 (range, 0.7–1.3)

take of 68Ga-DOTATATE in 6 out of 8 children[38]. Patients received 2 or 3 cycles of 177Lu-DOTATATE (0.3 GBq/kg; 8.1mCi/kg per dose) at a median interval of 9 weeks and a median administered activity of 7.3 GBq. Five of these patients had stable disease as assessed using the Response Evaluation Criteria in Solid Tumors (RECIST). This study, while limited in the number of patients studied, provided proof-of-principle that children with NBL can be imaged and treated with somatostatin receptor-targeted agents.

2.4 Image-based Adaptation of Dose in 177Lu-DOTATATE Treatment

2.4.1 68Ga-DOTATATE PET/CT Imaging

TRT is known for its relatively narrow therapeutic window. This means that "low" doses may prove ineffective or suboptimal, while "high" doses may cause acute or chronic renal toxicity.Therefore, the optimal dose should be somewhere in between, thereby leading to the best possible treatment, which means yielding maximal therapeutic effect given tolerable and manageable toxicities. Adaptation of injected radioactivity to patient characteristics rather than using dosing from cohort studies relies on the idea that treatment efficacy is partly based on how much gets to the tumour rather than how much is administered. This relationship between uptake and response was observed by Kwekkeboom et al when elevated uptake with the Krenning scale correlated with remission[30] The idea in short is elevated uptake corresponds with higher radiation concentration with high tumour dose and high likelihood of response.

There have been a collection of 68Ga-DOTATATE PET tracer studies highlighting a 'protective' aspect of radiopharmaceuticals that is dependent on the tumour load. The idea is that extensive tumour uptake leads to tumour sequestration of the radiotracer and decreased bioavailability for uptake in critical organs like the kid-

neys. This reduces the accumulation and absorbed radiation dose to critical organs like the kidneys, implying the retention of 68Ga-DOTATATE, and perhaps by extension 177Lu-DOTATATE, in the kidneys is inversely related to the SSTR-positive tumour burden (as indicated by the intensity and extent of uptake in individual lesions). This suggests that patients with a high tumour burden are likely to be undertreated with empirically-based 177Lu-DOTATATE administrations and can safely manage higher activities than the standard prescription. The influence of tumour load on renal and tumour pharmacokinetics is known as the "tumour sink effect". Beauregard et al showed physiological uptake (i.e. renal, splenic and background uptake) tended to decrease with increasing tumour sequestration. [13] This suggest that patients with a high burden of SSTR-positive NET are likely to be undertreated with fixed-dose PRRT. With this is mind, clinics like Peter MacCallum Cancer Centre have developed adaptations to dose prescriptions based on tumour burden measured on 68Ga-octreotate PET/CT. The dose prescription was determined by an empiric formula with 3 dose ranges: 5–6 GBq for patients with a small tumor burden and impaired renal function, 7–8 GBq for small tumor burden and normal renal function or high tumor burden and impaired renal function, and 9–10 GBq for large tumor burden and normal renal function [29].

2.4.2 177Lu-DOTATATE SPECT/CT Imaging

Recently, there has been an emergence of on-going prospective clinical trials that base treatment planning for multi-cycle 177Lu-DOTATATE treatment on delivering a prescribed Maximum Tolerable Absorbed Dose (MTAD) to non target organs at risk to ensure each patient receives the Maximum Tolerable Activity (MTA).

There the idea is to give a set radioactivity for the first cycle based on a standardised prescription then measure the absorbed dose to the critical organ at risk, in most cases the kidney, using post-treatment 177Lu-DOTATATE SPECT/CT images. Using the renal dosimetry measurements from this initial cycle, a patient specific factor (F) is defined estimating mean renal absorbed dose per unit of In-

jected Activity. This factor is used to either adjust the activity per cycle for a set number of cycles [32, 28] or the number of cycles for a set activity per cycle [11, 33] in order to reach the same prescribed renal dose level in each patient. Taken from external beam radiation [39], the threshold to the dose limiting kidneys is a cumulative renal absorbed dose cut off of 23Gy or cumulative renal Biological Effective Dose of 27Gy.

The Uppsala and Lund groups have demonstrated the feasibility and advantage of varying the number of cycles with a fixed injected activity of 7.4GBq to deliver an absorbed dose of 23 Gy or BED of 27 $\pm$ 2 Gy to the kidney. From the Illuminet clinical trial at Lund and Gothenburg, Sundlov et al showed promising interim results of a Phase II trial in personalising the number of cycles for 51 patients to reach the prescribed cumulative renal biological effective dose of 27 $\pm$ 2 Gy in patients with risk factors for renal toxicity and 40 $\pm$ 2 in patients with no risk factors[33]. They found that 20% of patients are overdosed and more than 50% underdosed from the widely used 7.4GBq x 4 protocol and the number of fixed-IA cycles of 7.4GBq that could be tolerated ranged between two and ten (50% of patients being able to tolerate more than four cycles) based on their renal dose. Similar results were demonstrated by Garske et al. with 43.8% of patients safely receiving five to seven cycles of 7.4 GBq, more than the widely-accepted four cycles[11].

In a different approach, Del Prete et al. investigated adapting the activity in each patient's cycle to deliver a set renal dose of 23Gy. [28]. He found the personalised protocol resulted in an average 1.48-fold increase in cumulative maximum tumour absorbed dose compared to empiric 7.4Gy x 4 protocol. The optimum injected activity per therapy cycle ranged from 4.1 GBq to 26.2 GBq, with a median of 9.2 GBq.

These studies observed that image-based dosimetry adaptation of IA is feasible and allowed for safe administration of much higher additional cycles (up to 10) or higher administered activities (up to 9.6GBq) which may improve patient outcome. In a study of 200 NETs patients, Garske-Román et al. highlighted the importance of

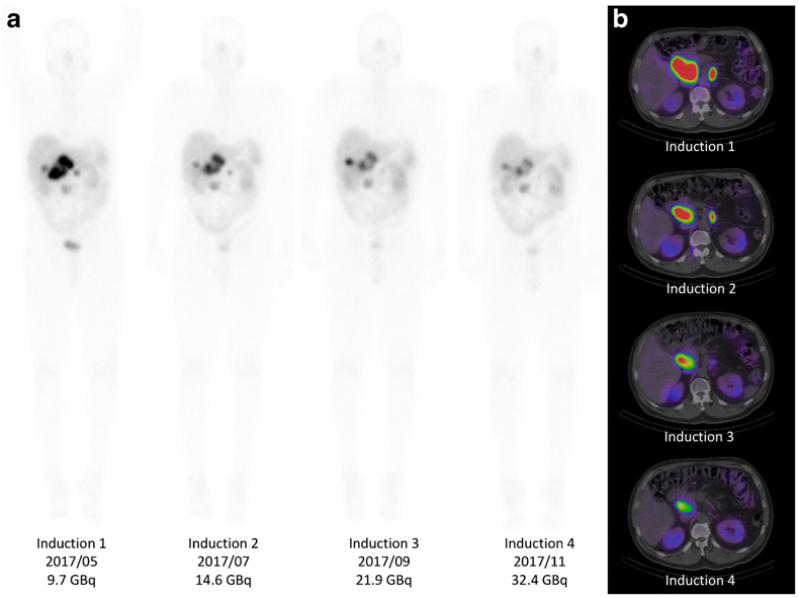

Figure 2.2: Representative image showing heterogeneity and change in uptake per cycle using a personalised dosimetry protocol. Reprinted from Personalized 177 Lu-octreotate peptide receptor radionuclide therapy of neuroendocrine tumours : initial results from the P-PRRT trial, Vol 46, Del Prete, Michela and Buteau, François-Alexandre and Arsenault, Frédéric and Saighi, Nassim and Bouchard, Louis-Olivier and Beaulieu, Alexis and Beauregard, Jean-Mathieu, 728–742, Copyright (2019), with permission from Springer Nature

individualised kidney dosimetry in observing patients in whom the absorbed dose to the kidneys reached 23 Gy had a longer Overall Survival (OS) than those in whom it did not[11].

These authors have shown the feasibility of individualised dosimetry and been able to reduce the high-patient variability in renal dose with the aim to give as much activity per set number of cycle or as many cycles per set activity as possible.

2.5 Variability in Distribution of Pharmacokinetics

The mean residence time, clearance rate and absorbed dose are the most common parameters for prediction of response to therapy using 177Lu-DOTATATE. However, the correlation between these parameters and NETs response for 177Lu-DOTATATE has been inconclusive. Ilan et al study is the only one at the time of writing to

show a significant correlation between the absorbed dose until best response and tumor response in a subset of 24 pancreatic NETs tumors[10] treated with 177Lu-DOTATATE. However, he also noted some lesions received a rather high absorbed dose but showed only minor reduction in size and vice versa. Del Prete notes in 36 measurable NETs lesions in 15 patients, no significant correlation was found between the radiological response and the cumulative lesion absorbed dose three months after the induction course (RECIST, Pearson r =0.19, P=0.27, Fig. 3; SWOG, r =0.08, P = 0.62). Over the follow-up period, no significant correlation was observed between variation of other parameters (e.g., creatinine, eGFR, blood panels) and the renal or BM absorbed dose. [28]. In most studies with post-dosimetry results, none of the absorbed dose parameters (mean, minimum, maximum, uniformity) were found to have a significant correlation with NETs response.

Among other factors like tumor-specific radiosensitivity, interstitial pressure and necrosis, tumor shrinkage is likely to be related to factors potentially influence the heterogeneity in binding affinity and receptor density. Heterogeneity is a major feature of TRT treatment and this heterogeneity is due to the spatial arrangement of receptor expression within a tumour. Theoretical studies have confirmed heterogeneous dose and uptake distributions are less therapeutic than uniform distributions of the same mean dose[40]. Heterogeneous uptake can create situations in which a fraction of cells is under irradiated, while another fraction of cells is "overkilled". These theoretical findings have been confirmed clinically when Sgourus noted a trend towards increased response with increasing uniformity (r = 0.37; P = 0.06). [41]

Recently, tumor heterogeneity was suggested to correspond to SSTR2 expression in NBL SPECT/CT and PET/CT studies. Zhang et al revealed histological colocalisation of SSTR2 and 68Ga-DOTATATE uptake in NBL CHLA-15 tumour xenografts[36]. Werner et al determined baseline intratumoural SSTR heterogeneity as assessed by SSTR-PET (68Ga-DOTATOC) and concluded that the four heterogeneity parameters of Entropy, Correlation, Short Zone Emphasis and Homogeneity outperform conventional PET parameters, such as mean and maximum standard-

ized uptake value SUV mean/max in distinguishing between responders from non-responders in a retrospective cohort of 142 patients[42] . Werner et al. further showed that an intratumoural textural feature (TF) analysis of a baseline SSTR-PET can differentiate high-risk from low-risk groups of patients with pancreatic NET tumours (pNET) scheduled for 177Lu-DOTATATE therapy. [43]. Aside from 68Ga-PET, SPECT scans provide an alternative imaging option. Wetz et al. showed that an 111In-DTPA0 octreotide SPECT scan of the spatial SSRT distribution in NET metastases as quantified by asphericity was predictive of response to 177Lu-DOTATATE [44].

With these recent studies, imaging parameters which quantify the spatial arrangement of the uptake may be clinically useful and contribute to more accurate characterization of patent pharmacokinetics for individualized treatment schedules. In a surprise observation, Hatt and colleagues [45] demonstrated that the predictive value of textural parameters is not affected by partial volume effect and is relatively independent of the method used to delineate the tumor volumes to be analyzed for PET.

Chapter 3

Current practices and technologies in dosimetry

3.1 Quantitative SPECT for 177Lu-DOTATATE

With 177Lu-DOTATATE treatment, it is possible to visualise the distribution and pharmacokinetics over time in 3-dimensions (3D) in different body compartments with the use of SPECT/CT and dedicated software. This process can be summarized as dosimetry. Lutetium-177 (177Lu) decays with low-energy charged particles (β-, Auger and conversion electrons) with a mean energy of approximately 134 keV per decay and a maximum kinetic energy of 177Lu of 498.3 keV [46] and a γ fraction with energies of 113 keV and 208keV emitted in 6.4% and 11.0% of decays, respectively. This γ radiation can be visualised at a set time point with a a SPECT/CT scintigraphic camera positioned outside of the body. Since the physical half-life ($\sim$6.7 days) and biological half life of 177Lu are in the order of days, this image acquisition process has to be done repeatedly in order to follow the process.

Although planar 2D imaging might render sufficient information for an estimate of the absorbed dose for 177Lu-DOTATATE patients, it is known to have inherent limitations regarding the accuracy of activity quantification namely challenges in estimating variations to the thickness or volume of an organ and the uptake in organs

that contain tumour tissue or overlap with tumours due to spill-out of counts from large tumour to nearby organs. SPECT with low-dose CT can circumvent these problems [27].

For the SPECT images to be quantitatively useful, accurate compensation for the interaction of a γ photon with the camera and patient have to be applied. Dead time and Attenuation corrections account for counts which would not have otherwise been imaged and Scatter corrections compensate for counts which would have otherwise been included. The Medical Internal Radiation Dosimetry Committee (MIRD) no 26 pamphlet presents a set of guidelines outlining data acquisition protocols and image reconstruction techniques that are recommended for quantitative 177Lu SPECT imaging[47]. SPECT images are also affected by the reconstruction parameters. Cheng et al found the optimal parameters for kidneys, an organ at risk during 177Lu-DOTATATE, are more iterations and less smoothing up to imaging 24hours post 177Lu-DOTATATE treatment but more smoothing and fewer iterations afterwards [48].

Quantitative estimates of activity using counts in a SPECT image are also hampered by the limited spatial resolution resulting in Partial Volume Effects (PVE) which in most cases can be corrected in clinical practice using experimentally determined recovery coefficients. For a patient, the activity $A_{(ijk)}$ within a voxel at coordinate ijk can be determined from the counts per second CPS_{ijk} by Equation 3.1:

$$A_{ijk} = CPS_{ijk} \times SF \tag{3.1}$$

where SF (cps/MBq) is the sensitivity factor for the SPECT/CT image system

3.2 MIRD Dosimetry Chain for Heterogeneity

Voxel-based dosimetry provides a more detailed description of the characteristically heterogeneous pharmacokinetics and absorbed dose to normal organs and tumours

in 177Lu-DOTATATE therapy.

A voxel is an arbitrary division of volume associated with 3D images - the equivalent of pixels for 2D images - and it is associated with tomographic image acquisitions like SPECT, PET and CT. With the advent of the latest PET/CT and SPECT/CT technologies, quantification of activity distributions can be performed with resolutions adequate for voxel dosimetry, typically of 5 mm or even less. The distribution of therapeutic radiopharmaceuticals in volumes smaller than those that can be fully resolved by the imaging system is usually assumed to be homogeneous which is a limitation as voxels can be the mix of two organs or different parts of an one organ (eg. the medulla and cortex for kidneys).

The MIRD scheme for voxel-based dosimetry is an extension of the one for organ-based dosimetry found in MIRD Pamphlet 21 [49] with the source and target being considered are voxels as shown in Equation 3.2

$$\bar{D}(voxel_{target}) = \sum^{N} \tilde{A}(voxel_{target}) \cdot S(voxel_{target} \leftarrow voxel_{source}) \tag{3.2}$$

In many publications, voxel based dosimetry is based on the MIRD formalism which is described in their Pamphlet no 17 [50]. Similar to organ based dosimetry, voxel dosimetry calculations assume a homogeneous tissue composition and a uniform radionuclide distribution within individual voxels, although authors have indicated heterogeneity exists at sub-voxel dimensions in the kidneys for example [51]. The methodology is summarised in Figure 3.1

When acquiring sequential images over several days, it is impossible to achieve exactly the same patient position at each time of measurement. The registration process ensures one voxel with the same coordinates in every image corresponds to the same anatomical region at different time points. In this process, a CT image is chosen as reference because of the high bony contrast and other CT images are aligned to that image. The corresponding deformation matrix found for a specific CT is applied its contemporaneous SPECT image. This is based on the reasonable assumption that SPECT and the CT acquired together at each time point are

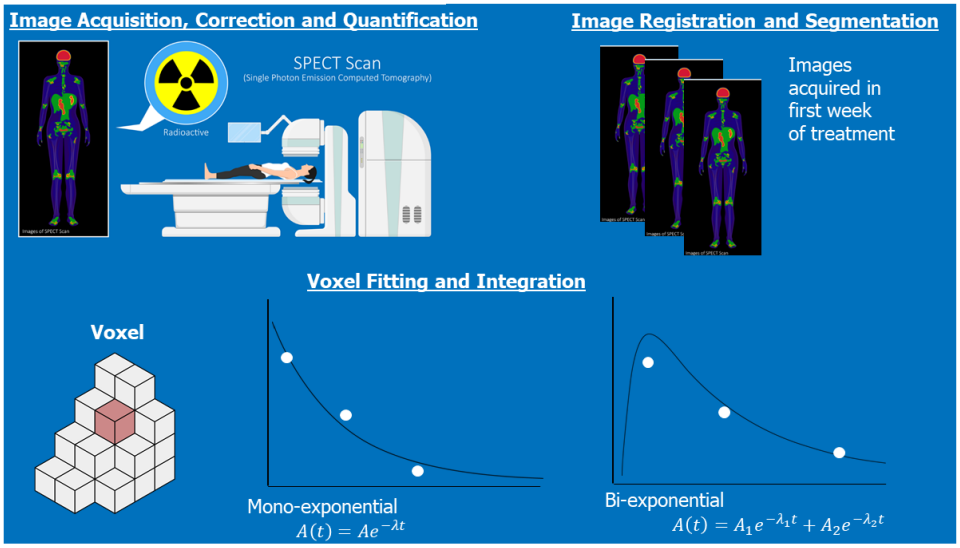

Figure 3.1: Workflow of voxel based dosimetry

already registered.

Patient positioning alone is not sufficient to yield registered images in most cases. Both respiratory motion during a scan and the lack of reproducible patient positioning between scans make it difficult to track the uptake within a particular voxel over time. Unlike External Beam Radiation Therapy (EBRT), TRT patients receiving post treatment longitudinal SPECT/CT are not typically set up in a reproducible manner using immobilisation devices and lasers. Moreover, organs may move in relation to one another in a non-reproducible manner.

There are two main types of registration: rigid and non-rigid, with the latter seen as a more accurate approach as it allows for more degrees of freedom. For voxel dosimetry, CT-based registration of serial SPECT images is preferred to SPECT-SPECT image registration because it avoids problems associated with the coarse SPECT spatial resolution and noise, lack of anatomical information, as well as, temporal changes in the activity distribution. He and colleagues showed that misregistration of volumes of interest (VOI) have a larger impact for small organs (such as the kidneys) and low uptake organs close to high uptake ones (such as lungs). The misregistration produced errors in organ activities that were proportional to VOI shifts ranging from –1 to 1 voxel in three directions.[52]

Investigating rigid and non-rigid registration of 6 or 7 SPECT/CT images acquired over a week, Katarina et al found that the values of the residence time and absorbed dose determined from serial SPECT/CT were within 5% except in the head-neck-shoulder region where non-rigid registration gave improved values [53]. The small difference in the mean and median values of residence time and absorbed dose obtained by rigid and non-rigid registration could be explained by the use of a single numeric such as mean or median to represent the population of voxels within a VOI.

The practice of radiomics involves extraction of quantitative data from images in an effort to perform either diagnosis or planning during treatment and follow up. This technique lends itself to the study of heterogeneity. Traditionally, radiomics studies have been used with CT image datasets with great efficacy. Increasingly, radiomics on functional imagining such as PET has been shown by authors to have value. Recently, radiomics has been done on SPECT imaging due to the improvements in acquisition and it's increasingly quantitative nature.

The bio-kinetics of 177Lu-DOTATATE uptake and clearance in SPECT/CT is heterogeneous and has been traditionally explored through the use of intensity based characterisations which have yet to relate to the response seen in patients. The spatial information contained in these images may be indicative of clinically relevant changes in the tumour and the advanced techniques of analysis traditionally reserved for SPECT/CT studies may prove valuable when applied to calculated image maps of the patient's dose and biokinetics.

The steps and limitations to calculating the pharmacokinetics and absorbed dose in each voxel of an image are discussed in the next sections.

3.3 Clinically feasible Absorbed Dose-Rate Images

The conversion of SPECT images to absorbed dose images can be done through four main methods in increasing complexity: Local Energy Deposition (LED), voxel S values, dose point kernel convolution and the gold standard full Monte Carlo (MC) radiation transport.

The simplest approach for voxel-level dosimetry is to assume that the emitted energy from 177Lu-DOTATATE in a voxel is completely absorbed in that voxel, that is, locally deposited. This approach is essentially a rescaling of the voxel activity value and is thus fast. Such an assumption is valid only for radioactive particles whose maximum range in tissue is equal to or less than the voxel dimensions (typically 4 mm for SPECT) which is the case for 177Lu. Indeed, Ljungberg et al showed almost no difference in the dose-rate volume histograms for 177Lu between the assumption of local energy deposition and the more accurate yet computational intensive Monte Carlo approach[54].

The voxel S value method is convolution-based and uses Voxel Dose Kernels (VDK) to estimate the distribution of energy depositions in nearby voxels from a decay in a single voxel. The VDK was first described in MIRD Pamphlet 17[50] which describes especially the calculation of these VDK which depends on both the radionuclide and voxel size. This pamphlet provides a database VDK for the following 5 radionuclides: Phosphorus32, Strontium89, Yttrium90, Technetium99, Iodine131 and 2 different voxel sizes. Since its publication in 1999, Lanconelli et al [55] has provided a freely available and validated database of VDK that includes 177Lu and 13 different voxel sizes. Due to the voxel size, most of the energy originating from a 177Lu-DOTATATE voxel will be deposited within it and the VDK will consider energy contributions around the source voxel due to the photons. Next step is to convolve the SPECT with an appropriate VDK based on the radionuclide and SPECT resolution to acquire the absorbed dose image at a voxel level. There

are many ways to convolve the VDK with voxels in the SPECT image. While for small regions the VDK can be directly applied, fast fourier transform can be used for larger images to speed up the calculations. In a comparison of voxelised doses for the kidneys calculated by Monte Carlo and the voxel S value technique, Grimes et al showed that the 3D dose distributions produced by the respective methods are nearly identical agreeing within -2.3% $\pm$ 2.4%[56].

As for the difference between calculation methods, Pacilio et al showed the major concern for voxel dosimetry on clinical SPECT images is more strongly represented by image blurring than by differences between LED and VDK with both methods yielding similar dosimetric results[57].

3.4 Incorporation of Radiobiology in Dosimetry

Recently there has been a push to account for the biological impact of different dose rates, the radiosensitivity of tumours and the heterogeneity of uptake and dose distribution into the absorbed dose calculations, arguing that it is more reflective of the response than physical dose [58] . Indeed, the biological relation between the absorbed dose and clinical effect is also dependent on other, partly unknown, factors such as the dose rate, the intracellular distribution of the radionuclide, and the tumour's radiosensitivity[58, 59, 60]

The Linear-Quadratic (LQ) radiobiological model is used to convert the absorbed physical dose to Biological Effective Dose (BED). The BED was coined by Fowler [61] and relates absorbed dose and dose-rate with radiosensitivity and repair of radiation damage to take into account TRT dose rates and NBL radiosensitivity. The radiosensitivity is encapsulated in α (the radiosensitivity per unit dose) and β (radiosensitivity per unit dose squared) parameters which aim to provide a numerical figure that correlates to single and double strand breaks - the two main mechanisms of damage to cells from radiation. The finally parameter is μ for the repair rate assuming an exponential repair process. BED has shown to correlate with renal toxicity with a similar beta-emitter Y90-DOTATOC. These parameters are obtained

either from literature or clonogenic assays quantifying cell survival.

In NETs patient, BED, instead of absorbed dose, has been considered for possible correlation with renal damage [58, 60]. BED values for the kidneys used in these calculations according to the LQ model were $\frac{\alpha}{\beta} = 2.5$ Gy and μ (repair half-life) of 2.8 h.

In addition to the BED, Equivalent Uniform Biological Effective Dose (EUBED) (3.3) of the distribution data allows for accounting for the impact on treatment outcome of the heterogeneous nature of uptake and subsequent dose deposition of the radiopharmaceutical - inherently difficult to capture with summary metrics like mean.

$$EUBED = \frac{1}{\alpha} \ln \left(\frac{\sum_{i=1}^{N} e^{-\alpha BED_{ijk}}}{N} \right) \tag{3.3}$$

where BED_{ijk} is the BED of voxel at coordinates (ijk) and N is the total number of voxels

3.5 Clinically feasible Pharmacokinetic Modelling

Zhao also looked at the connection between the fitting and the absorbed dose and found even if the deviation in effective half-life estimation is similar to that calculated using M3, the deviation in absorbed dose calculated by M2 can go up to 50% for monoexponentials. He showed trap-monoexponential hybrid gave the same results as biexponential[62] .

Once the images are registered, the amount and rates of 177Lu-DOTATATE uptake and excretion need to be determined.

In order to extrapolate the renal and tumour doserate-time curve for a voxel or region, several experimental data points are collected as SPECT images acquired during the first week after 177Lu-DOTATATE therapy. The pattern of accumulation and excretion of radiopharmaceuticals is governed by passive and active physiological mechanisms, such as receptors. These biological processes are generally assumed

to be characterised by a single- or two-step phase, the first with an early peak lasting about 24 hours after injection related to an initial fast phase of extravasation and excretion of 177Lu-DOTATATE, followed by a slower phase of renal uptake and washout [63, 64]. The bi-phasic process can be described as either a sum of exponentials with different rates where the number of exponentials summed (typically two) is limited by the number of images available[65] or a hybrid definition with a linear function for the initial phase and a single exponential for the renal uptake and washout. Simpler analyses have focused on characterising only the slower second phase with a monoexponential as 70%-75% of the AUC occurs after approximately 24 h meaning the uncertainty in the curve-fitting contribution will to a large extent be governed by the estimation of pharmacokinetics in this phase [66, 67].

The most commonly reported pharmacokinetic parameter in dosimetry is area under the dose rate curve AUC which is a measure of the cumulative exposure or dose to the voxel or region from time of injection to infinity. While a physiologically based pharmacokinetic (PBPK) model has been developed for 177Lu-DOTATATE treatments which takes into consideration multiple organs at once [68], the majority of studies determine AUC through integrating the doserate-time curve either analytically, numerically or a hybrid of the two. Choice of integration method depends on how the doserate-time curve was constructed. For a hybrid model, numerical integration using trapezoids is done up to the last image time point and integration beyond the last data point is generally performed by analytically integrating a monoexponential function. If the decay-corrected exponential rate is positive or zero, indicating uptake of activity over time in a particular voxel, then the physical decay rate of 177Lu-DOTATATE is used in the analytic expression. For a curve only constructed of exponentials, analytical integration is performed.

Guerriero et al found that a careful choice of the method (excluding trapezoidal methods) results in negligible importance (differences smaller than 10%) when data reach two radionuclide effective half-lives [66] and Zhao et al showed the simpler trap-monoexponential hybrid gave similar results to more elaborate biexponential[62].

Recently, more advanced analyses have shown it is feasible to do a systematic testing of different curve shapes and determining which model fits the data best using a statistically-based criterion, such as the Akaike or F-test [69, 70]. Due to a potentially high level of noise in 177Lu-DOTATATE images, voxel-by-voxel fitting and integration introduces additional challenges due to image noise and noise propagation. In general, if the number of imaging time points is ≤ 5, a numeric integration may prove more accurate than elaborate fits with exponentials.

The European Association of Nuclear Medicine (EANM) guidelines suggest a minimum of three measurements per kinetic phase are required to enable error estimation [71] which will lead to a minimum of six acquisitions per patient for the uptake and clearance phase of the kidneys. This mathematically optimal sampling represents a barrier to having the necessary information in routine clinical care about pharmacokinetics in 177Lu-DOTATATE patients owing to practical difficulties such as non-clinically feasible sampling points (eg. after hours), labor intensive for the therapeutic team of technologists, physicists and physicians, somewhat uncomfortable for the patients involved and resource demanding on nuclear medicine departments.

To avoid repeated SPECT/CT acquistions at every treatment cycle, efforts have been investigated in the last three years to reduce SPECT/CT acquisitions across multiple cycles within the same patient without substantially affecting the estimated AUC. These approaches are based on the idea that AUC depends mainly on the area under after 1 to 1.5 times the effective half life which is $\approx$ 42h for 177Lu-DOTATATE.

Zhao et al showed a monoeponential fit with a single SPECT/CT performed at around 48-72h post injection coupled with a population mean half-life of 45h resulted in renal absorbed dose deviations within 10% of a three time point calculation, provided the organs or tumours biokinetics can be approximated by a monoexponential [62]. This approximation may introduce errors in the AUC, especially when the effective half-life of a particular patient is very different from the population mean. Using a late data point minimizes the impact of deviations in

effective half-life. Sundlov et al suggested one SPECT/CT at 96h after each cycle gives sufficiently reliable dosimetric results to base individualize planning on [8]. If these single measurements are to be made then they should be done at later times which is consistent with a paper published by Haenschieid and colleagues where they made a theoretical motivation that one single measurement after four days is adequate to calculate the AUC[6]. The total absorbed dose $D(r_s)$ to a tissue under consideration r_s after time t_1 is Equation 3.4

$$D(r_s) = D(r_s, t_1) \times \frac{2 \times t_1}{ln2} \tag{3.4}$$

where $D(r_s, t_1)$ is the doserate from a single measurement at t_1

While this single time point approach after each cycle is appealing, Del Prete et al found a hybrid method of imaging at two time points in the first cycle and a single time on day three in the non-initial cycles slightly improved accuracy for the kidneys and max dose in the tumour[7]. Of important note, both Del Prete and Sundlov did not recommend extrapolating pharmacokinetics from the first cycle to subsequent cycles. Del Prete noted this method having a relative error of 16% and -7.1% for the tumour and kidneys respectively compared to a trapezoidal-monoexponential fit to data acquired in each cycle [7]. Sundlov also noted a constant underestimation of the actual dose delivered to the kidneys in non-initial cycles when estimated from pharmacokinetics in the first cycle whether that estimation is done using SPECT alone (errors of -2 $\pm$ 39%) or hybrid of planar and SPECT/CT (errors -3 $\pm$ 36%) [8]. A summary of the fitting methods discussed can be found in Table 3.1.

In a pragmatic effort to increase clinical implementation of dosimetry, there is an assumption of stable (or sufficiently similar) patient pharmacokinetics between cycles. The idea is to completely characterise the doserate-time curve in the initial cycle with multiple image acquisitions and characterise subsequent cycles using a single acquisition. The rate of clearance and uptake in a subsequent cycle is considered invariable from the first cycle and the amplitude for the AUC is adjusted for the single measurement using Equation 3.5. This method is seen as a compromise when

Table 3.1: Description of most common fitting methods used in clinics

Initial Cycle	Non-initial cycles	Description	Difficulty in Clinical Implementation
Bi- exponential	Bi-exponential	Bi-exponential from time of administration to infinity	High
Linear + Mono-exponential	Linear + Mono-exponential	Trapezoidal function from the injection time until the 24-h time point followed by a monoexponential biological decay function	Average
Mono-exponential	Mono-exponential	Mono-exponential biological decay from time of administration to infinity, except in cases of biological accumulation of activity, only physical decay	Average
2TP Monoexponential	1TP method based on the day 3 data	From day 1 to day 3, monoexponential biological decay except in cases of biological accumulation of activity, only physical decay scans. Single-time point method	Low
1TP	1TP	Single-time point method	Low

it is not possible to perform multiple SPECT/CT studies due to time constraints. Garske et al was the first to propose it is a valid approximation to assume unchanged effective half-life [12] with the caveat that patients at risk for kidney dysfunction or with large change of tumor volume need to be monitored in more detail.

$$D_n(r_s) = D_i(r_s) \times \frac{D(r_s, t_s)_n}{D(r_s, t_s)_i} \tag{3.5}$$

where D_i and $D(t_s)_i$ are the dose and doserate measured in the initial cycle, $D(t_s)_n$ is the dose rate measured in a non-initial cycle, D_n is the dose in the non-initial cycle, t_s is the time of spect acquisition and r_s is the tissue under consideration.

For delineating VOI for pharmacokinetics, Sandstrom and colleagues showed good agreement (less than 5% difference) between contouring the entire kidney on the CT and simpler methods of scaling the calculations using activity contained in a small VOI of 4 ml on the SPECT or thresholding the SPECT at either 42%, 50%, 60% or 70% of the maximum activity[72]. These measures reduced calculation times from 3 to 5 hour for the left and right kidney to between 15 and 45 minutes.

Chapter 4

Software for simplified modelling methods

4.1 Introduction

There is growing evidence of variable per-cycle tumour and renal pharmacokinetics in a patient. However, the range of available clinical methods for modelling normal organ and tumour pharmacokinetics makes comparison of single center inter-cycle pharmacokinetic results challenging. Given the relatively small patient cases for 177Lu-based treatments, harmonisation of tools and software would be an important step forward to enable comparison of single-center results and facilitate multi-center randomised controlled trials. The landscape of methods used for modelling intra-cycle pharmacokinetics and dose of NETs patients in the clinic is very fragmented. The variety of fitting methods published by groups in nuclear medicine centers over the last 8 years is summarised in Figure 4.1.

There is no option among the currently available methods that is open source and capable of incorporating the range of available fittings. Additionally, there has not been a study comparing results using the range of currently available options in Table 3.1.

In an effort to boost the harmonisation of multiple single-center reports by inves-

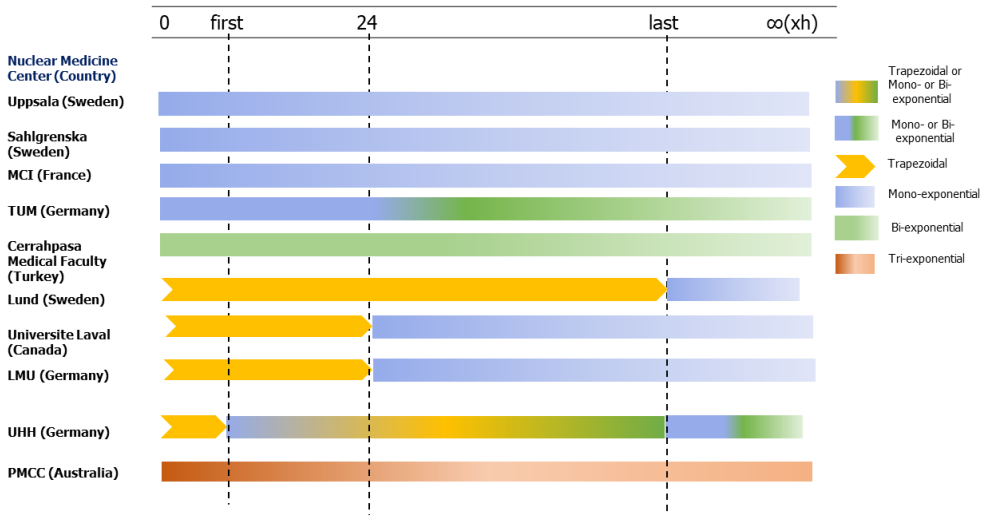

Figure 4.1: Most common fitting strategies used by nuclear medicine centers around the world

tigators characterising normal organ and tumour kinetics, this chapter presents the main characteristics of a multi-platform software package dedicated to performing conventional and simplified fitting methods for sequential dose rate images derived from SPECT/CT at the voxel level. Additionally, two use cases are presented at the end of the chapter.

4.2 Overall Features

XINDA is a free open-source platform I wrote in the Python 3.6 open source programming language for pharmacokinetic modelling and dosimetry calculations based on longitudinal SPECT/CT image. It can exist within the framework of a clinical nuclear medicine dosimetry workflow as shown in Figure 4.2 and does not rely on any commercial library and is implemented for Windows, Linux, and Mac operating systems. It uses the SimpleITK open-source, cross-platform library system that provides developers with an extensive suite of software tools for image analysis distributed under the Apache 2.0 license. Its installation is straightforward from the hosted repository.

I designed the platform so each patient is given a subdirectory within the main

project directory where the data is locally transferred. For each cycle, the series of longitudinal SPECT DICOM data and corresponding contoured structure RT-Structure Set (RT-STRUCT) file of a cycle is subsequently read and stored as a 4-dimensional numpy array with the available patient metadata such as time of administration and activity in a plain text file (.txt file). The contour coordinates of the RT-STRUCT file in the xyz dimensions are transformed into the image space through matrix calculations. It was assumed that the analyzed SPECT images were calibrated, that is, voxel values were expressed in becquerel (Bq). The images were considered as registered, in such a way that they form a 3D+t sequence of activity image A(x,t),

The RT-STRUCT data is converted to a binary mask for each VOI with the same dimensions as the primary SPECT image set. After each entry in the project setup workspace has been imported and converted to the desired format, dosimetric and image feature analysis can proceed. The workflow for the calculation of different fits are shown in Figure 4.2.

I coded the elementary modules of XINDA to perform the following functionalities:

- Support for the RT-STRUCT objects. This makes it possible to read VOI that have been created and stored using commercial nuclear medicine treatment planning platforms. This RT-STRUCT file can include multiple VOI.
- The measurement of overlap of VOI contours on sequential SPECT/CT images using the Sorenson-Dice coefficient (DICE)
- Storage of VDK for voxel sizes ranging from 4 to 13 mm for 177Lu
- Conversion of doserate-images into radiobiological maps at the voxel level. BED values for the kidneys used in these calculations according to the LQ model were done with $\frac{\alpha}{\beta} = 2.5$ Gy and μ (repair half-life) of 2.8 h [58, 60].
- This software uses the MIRD formalism for doserate calculation and employs convolution VDK of each voxel of the SPECT with the VDKs for177Lu freely

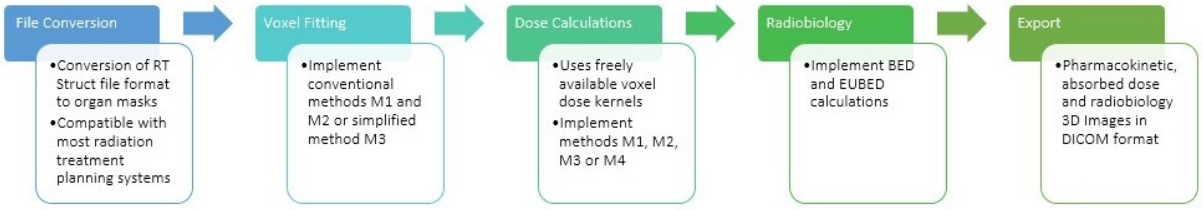

Figure 4.2: Workflow of the dosimetry process in which XINDA can be involved

available online at http://www.medphys.it/down_svoxel.htm for the calculation of absorbed dose rate.

- Registration of images at the voxel level to ensure a voxel has the same x,y,z location to enable quantification of the retention and clearance within a voxel.

4.3 Registration Module

For post registration analysis, I developed a custom module using the Python 3.6 programming language (Python Software Foundation) and based on the open source image analysis SimpleITK framework [73]. With this custom module, I was able to evaluate the accuracy of the registration of the longitudinal SPECT/CT scans using a quantitative metric rather than only through visual inspection using imaging tools like checkerboards. I contoured the kidneys, spine and tumour volumes on the reference scan (2h time point) and redefined these volumes on each of the serial scans to be registered to the first scan. The percentage of spatial overlap between the pre- and post- registration volumes was determined quantitatively using the Sorensen Dice similarity coefficient (DSC), that is a number between 0 and 1 [74]. Figure 4.3 shows the increase in the spatial overlap after registration of the kidney and spine volumes defined on the non initial scans (4, 24, 48h) to the reference (2h) as measured by the DSC.

I developed a Python 3.6 module based on the SimpleITK registration framework which supports several types of optimisers, similarity metrics and interpolators. By

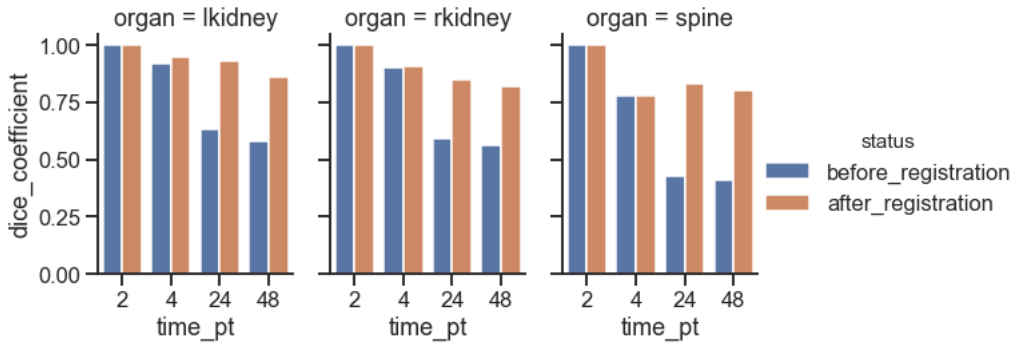

Figure 4.3: Improvement in DSC score before and after deformable registration

building a custom registration module instead of using clinically available commercial software, I was able to take advantage of the large number of settings available in the command-line interface of the SimpleITK framework. I designed the module to focus registration in the contoured regions rather than on the whole body (as is typical of commercial software) to improve the accuracy of the registration and reduce the calculation time. Using this module, CT-CT rigid registration was performed choosing the data set from the first time point to be the reference image. The CT images from each time was registered to the reference image using 3D rigid transformation. Select parameters for the 3D rigid registration are shown in Table 4.1. The resulting transformation matrix was applied to the corresponding SPECT images.

Table 4.1: Select parameters used in the python module for the 3D rigid registration

Parameter	Value
Similarity Metric	Mattes Mutual Information
Number of histogram bins	50
Interpolator	Nearest Neighbour
Optimiser	Gradient Descent
Number of Iterations	100
Learning Rate	1
Sampling Strategy	Random
Sampling Percentage	1%

4.4 Pharmacokinetic Modelling Module

4.4.1 Fitting and Model Selection

I coded a class that uses the NumPy v1.17 open source Python library for large multi-dimensional arrays to store and manipulate the dose values within the kidneys and tumours for each patient. The date and time from each SPECT scan was read directly from the DICOM header using the Datetime v2.3 module found in the standard Python Library and the Pydicom Python package. Using the date-time stamp read from each SPECT scan, the time post injection was calculated by reading in the time of administration from a text file. This program design allows the time post injection to be calculated automatically from the DICOM data without the user having to input the values manually. Values for a particular voxel at different time points were stored in a 4D numpy matrix with the same dimensions as the SPECT image (128x128x128) and a fourth dimension equal to the number of imaging time points. Finally, the values were fitted using various integration functions defined within the SciPy v1.2.3 scientific computing and technical computing open-source Python library. The three types of doserate-time fittings performed in the code (M1, M2 and M3) are defined in Table 4.2. The respective equations that guided the coding are defined in Table 4.3.

4.5 Use Cases

4.5.1 NBL patients receiving 177Lu-DOTATATE

Here, I describe the procedure for applying multiple pharmacological modelling methods to SPECT/CT imaging after the first cycle of 177Lu-DOTATATE administered to children with NBL using the XINDA tools. The imaging data shown in Figure 4.4a was obtained as part of a collaboration with University College London Hospital (UCLH) where there was a recently completed clinical trial described in more detail in the next Chapter. In brief, these children were administered activities

Table 4.2: Doserate-Time modelling methods. The non-linear least-squares method was used in monoexponential curve fitting

Name of fitting method	Initial Cycle	Non-initial cycles	Type	Description
M1	Linear + Mono-exponential	Linear + Mono-exponential	Conventional	Trapezoidal function from the injection time until the time point on day 1 followed by a monoexponential biological decay function. This method is applied after each treatment.
M2	4TP Mono-exponential	4TP Mono-exponential	Conventional	Mono-exponential biological decay function using all SPECT/CT time points. Physical decay is assumed in cases of biological accumulation of activity. This method is applied after each treatment cycle.
M3	2TP Mono-exponential	1TP method based on the day 3 data	Simplified	Mono-exponential biological decay function using SPECT/CT time point on day 1 and day 3 is applied after the initial cycle. The single-time point method is applied in non-initial cycle.
M4*	1TP method	1TP method	Simplified	Dose determined from SPECT/CT measured on day 3

TP = time point
* Method was excluded from doserate-curve fitting as it uses only a single time point

based on a weight adjusted protocol of 75MBq/kg for the first cycle and 100MBq/kg for the subsequent cycles if the whole body dose of the initial cycle was less than 0.5Gy [75]. Images were acquired at the nominal times of 4, 24, 48 or 72h post administration. I manually defined the VOIs of both kidneys and the tumour by delineation from the CT and SPECT respectively. This delineation was checked and adjusted where necessary by a nuclear medicine radiologist. The absorbed-dose rate images are calculated from the quantitative SPECT image using a 4.42x4.42x4.42 voxel S-value kernel. After conversion, the mean absorbed doses within the VOIs are calculated by using three published curve fitting methods outlined in Table 4.2

The deviations in absorbed dose (AD) calculation (ΔAD)were calculated using

Fitting Method		Mathematical Representation
Name	Reference	
M1	[9, 32, 28, 8]	$\begin{cases} a_1 t & \text{for } 0 \leq t < t_i \\ a_1(t_i) + a_2(t - t_i) & \text{for } t_i \leq t < t_{24} \\ A\exp(-\lambda_{(x,y,z)} - \lambda_{\text{phys}})\ t) & \text{for } t > t_{24h} \end{cases}$
M2,M3	[12, 34, 26, 10, 11]	$A\exp(-\lambda_{(x,y,z)} - \lambda_{\text{phys}})\ t$
M4	[6]	$D(r_s) = D(r_s, t_1) \times \frac{2 \times t_1}{ln2}$

Table 4.3: Most common fitting methods used in published clinical studies

the formula 4.1:

$$\Delta\text{AD} = \frac{\text{dose}_{\text{M2,M3,M4}} - \text{dose}_{\text{M1}}}{\text{dose}_{\text{M1}}} \tag{4.1}$$

where $\text{dose}_{\text{M2,M3,M4}}$ is the dose calculated using clinical protocols M2, M3 or M4.

The use case shows large differences in the calculated absorbed dose to the kidneys between method M1 and M3. The results thus stress the importance of nuclear medicine centers describing the method to calculate the absorbed dose and a tool for inter-method comparison of results from single-center clinical studies. The comparison of deviations in absorbed dose estimations between the clinical methods M1, M2, M3 and M4 were analysed using the Bland-Altman method to identify any systematic difference between the measurements or outliers[76]. In brief, 95% Limits of Agreement (LOA) for each comparison tells us how far apart measurements between 2 methods are likely to be. If a measurement falls out of this limit then it could indicate a possible outlier or systematic difference.

Methods M1 and M2 created doserate-time curves fitting all four data points while method M3 employed a simpler approach with only two points as shown in Figure 4.4. The dose rate-time was plotted instead of activity-time as this is the recommended workflow for converting SPECT images to absorbed dose images as outlined in MIRD Pamphlet 23 [77]. Additionally, there is anecdoctal evidence that changes in dose rate may be more clinically relevant than change in activity.

Next, the per-cycle renal absorbed doses calculated using M2, M3 and M4 were

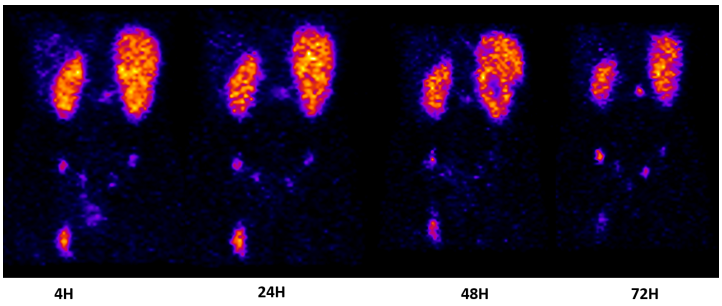

(a) Serial SPECT/CT scans of representative patient after receiving the first cycle of 177Lu-DOTATATE

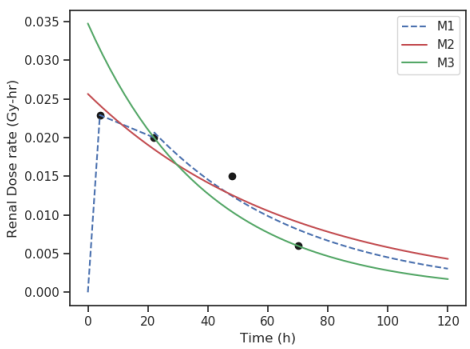

(b) Comparison of fits for renal dose rates (Gy-hr)

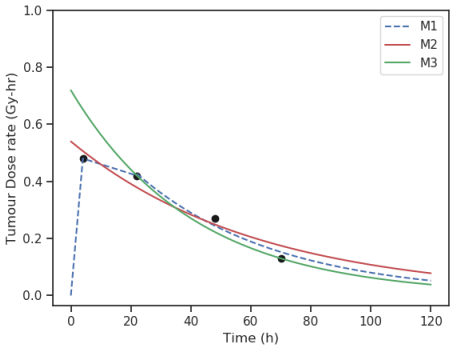

(c) Comparison of fits for tumour dose rates (Gy-hr)

Figure 4.4: Longitudinal SPECT/CT scans of a patient 4.4a. Illustration of the three modelling methods for the doserate-time curves of the kidney 4.4b and tumour 4.4c used by XINDA for the patient case. Both M1 (gold standard) and M2 use all points while the simplified M3 uses the data on day 1 and day 3

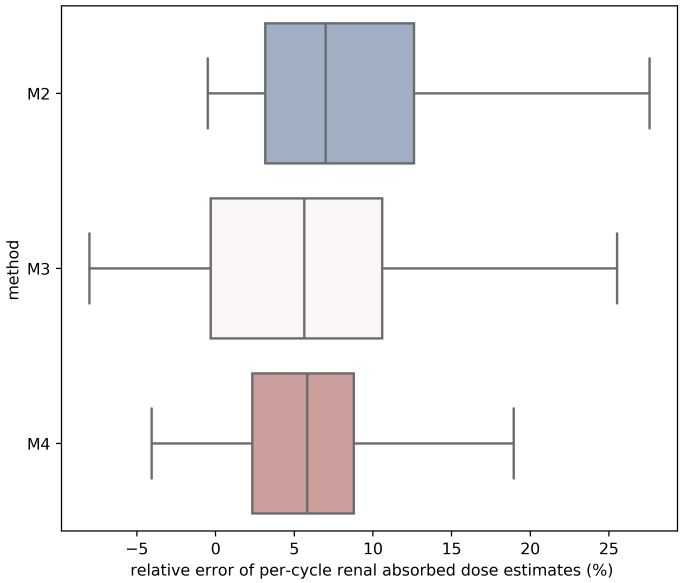

Figure 4.5: Box plots comparing the deviations of kidney absorbed doses per unit injected activity estimated by methods M2, M3 and M4 relative to M1. Boxes represent the interquartile range, and whiskers the interdecile range

compared to those calculated with the gold standard (M1). The corresponding relative deviations are presented in Figure 4.5. The simplified single time point method (M4) was found to be the most accurate when compared to M1 on a per-cycle basis. The interdecile ranges of relative error were largest for M3 (-7% to 25%) followed by M2 (0.9% to 28%) while M4 had the smallest deviation (-4% to 18%).

The results of the Bland-Altman (Difference plot) analysis of the per-cycle renal absorbed dose for M2, M3, M4 relative to M1 is shown in Figure 4.6. The Bland-Altman compares two measurements of the same metric, in this case per-cycle dose, to understand how repeatable are the measurements. From the Bland-Altman plot analysis, none of the methods resulted in marked systematic differences in the mean per cycle renal dose indicating differences in the per-cycle renal dose measured by M1, M2, M3 and M4 are within the limits of agreement. An average absorbed dose difference of 4% was found between the methods. Method M4 yields the smallest mean difference of 0.08 followed by M3 then M2.

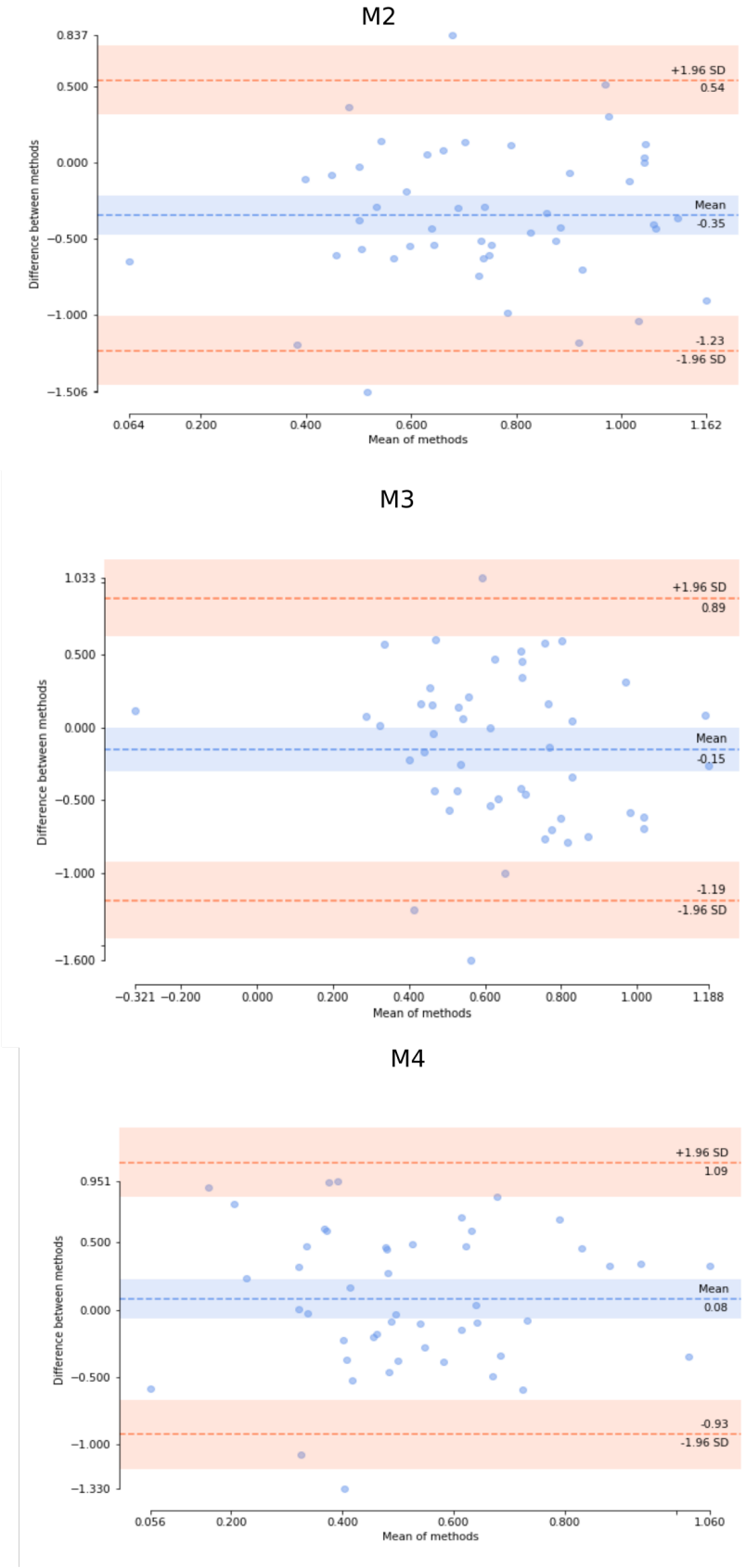

Figure 4.6: Pairwise quantification of the difference in absorbed dose estimates relative to M1 (hybrid of linear and Monoexponential) using Bland-Altman analysis. Method M2 uses 4 time points, Method M3 uses 2 time point and simplified Method M4 uses a single time point. The red region and red dotted line represent 95% Limits of Agreement for each comparison. The blue dotted line and shaded region represent the mean of the difference between the methods

4.5.2 NBL xenografts receiving 131I-mIBG

The second use case is the fitting of a time-activity curve generated for an in-vivo study exploring the impact of External Beam Radiation Therapy (EBRT) on the uptake of Iodine-131 meta-iodobenzylguanidine (131I-mIBG) in a BALB/c mouse NBL model. My program was used as part of a bigger study to observe changes in the uptake of 131I-mIBG in a NBL tumour due to pre-radiation with External Beam Radiation Therapy. The hypothesis was there would be enhanced accumulation of 131I-mIBG if EBRT was given prior to TRT as a result of increased vessel permeability following EBRT. In this application the tumour uptake of 131I-mIBG in NBL xenografts case is sampled by gamma counter radioactivity measurements at 2, 4, 24, 48 and 72h post injection and fitted using a modified version of M1 with trapezoidal integration to the final time point and assuming physical decay thereafter in Figure 4.7a. The percentage of injected 131I-mIBG dose per gram of tumour tissue (%ID/g) was slightly but not statistically significantly increased at the 2 and 4 h p.i. in the EBRT + 131I-mIBG group (where 131I-mIBG administration was preceded by EBRT 24 h earlier) in comparison to the 131I-mIBG only group. 131I-mIBG uptake was significantly greater in the EBRT + 131I-mIBG group at 24 h ($p< 0.01$), 48 h ($p< 0.001$) and 72 h ($p< 0.05$) compared to the 131I-mIBG only group. Autoradiography was performed on two tumours that were excised 24 h after administration of 131I-mIBG, one each from the EBRT + 131I-mIBG and 131I-mIBG groups. Figure 4.7b verifies the increased uptake of 131I-mIBG at 24 hour as seen in the fitting done by XINDA. The autoradiography showed a marked increase in tumour-associated 131I-mIBG uptake when EBRT was administered prior to 131I-mIBG compared to 131I-mIBG alone. Overall, the combined treatment led to a more than two fold increase in 131I-mIBG uptake and radiation absorbed dose than that attributable to 131I-mIBG only (8.03 and 3.61 Gy with or without EBRT beforehand)[1].

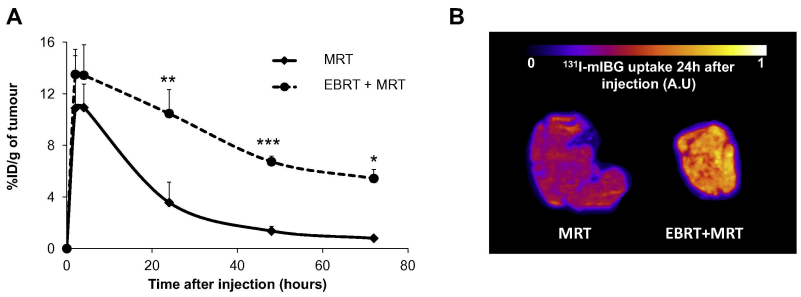

Figure 4.7: Use case showing (a) 131I-mIBG uptake with or without EBRT pretreatment at 2 h, 4 h, 24 h, 48 h and 72 h after 131I-mIBG injection(b) Autoradiography showing differential 131I-mIBG uptake in tumour 24 h after EBRT treatment compared to without.

4.6 Summary

We were able to successful code and implement an open source solution for analysis of per-cycle changes in pharmacokinetics that can incorporate protocols across multiple centers.

In order to validate XINDA, the 3D dose and effective half-life of the initial cycle of patient 001 from the cohort of patients analysed from the LuDO trial were calculated using method M1. The results were compared to results calculated using MIM SurePlan MRT (MIM Software Inc, Cleveland Ohio). A specialised workflow was designed in collaboration with engineer David Mirando from MIM Software for the 3D comparison of the renal and tumour kinetics and dose. The kidneys and tumour were defined within MIM on the first time point and these contours were applied to the later images in the time series. The MIM RTSTRUCT files for the image series were imported to XINDA from MIM. The RTSTRUCT files were converted into renal and tumour binary masks within XINDA and the doses within these masks were calculated using voxel-kernel convolution. The relative difference between XINDA and MIM calculated doses was calculated using the following formula:

$$\text{Relative difference} = \frac{\text{XINDA}_{\text{dose}} - \text{MIM}_{\text{dose}}}{\text{MIM}_{\text{dose}}} \tag{4.2}$$

where $\text{XINDA}_{\text{dose}}$ is the dose calculated from XINDA and MIM_{dose} is the dose calculated from MIM SurePlan MRT

The mean renal dose calculated by XINDA was higher than the MIM dose, but the difference between the two was small at +6.2%. For the tumour dose, the relative difference between MIM and XINDA was always less than 7.3% except for a few voxels at the boundary of the tumour where the statistical uncertainty seems higher.

Given the computational resource needed for voxel-level dosimetry with the number of voxels in the 10^6, optimisations were included such as matrix calculations for the calculations of image coordinates within the contours of VOI. This solution provides vendor neutral quantification by reading in DICOM-RTSTRUCT files.

The flexibility of the software represents a step forward in harmonisation but is restricted by the specialised knowledge needed to run the script. We are currently exploring implementing or porting the code to Amazon Web Services for a cloud based solution. Unlike in the more traditional approach, the dose will be calculated using an integration of dose-rate images as opposed to an integration of activity images to allow for the analysis of changes in the dose rate immediately after treatment and a reduction in noise. This method assumes that the rate of change in activity is close to the rate of change of doserate which can be seen as a reasonable assumption.

Although various commercial and research software programs that enable the fitting of doserate-time curves have been developed (examples in Table 4.4), multi-platform software that can easily interface with the RT-STRUCT and perform radiobiology calculations is not yet widely available.

To strengthen validation and encourage reproducible research practices the Python source code will be publicly provided at https://github.com/javianmalcolm for download. This code can be used in its current state or extended to incorporate new functionality as dosimetry research progresses. Currently, the script can only be used by someone with knowledge of running Python scripts. To increase accessibility of the scripts, it is hoped to develop a Graphical User Interface (GUI) that would not require any specialised knowledge to use. Currently, there are multiple single-centre

Table 4.4: Comparison of a sample of software used in published dosimetry studies for 177Lu-DOTATATE

Name of Software	Used by	Accessibility		Fitting Functionality		Voxel based	Radiobiology	Ref
		Commercial	Available to the Public	Exponentials	Trapezoids and Exponentials			
GE Dosimetry Toolkit	MCI [4], Uppsala	yes	yes	yes	no	no	no	[34]
Hermes/Olinda EXM v.2.0	TUM[1]	yes	yes	yes	yes	no	no	[78]
OLINDA v1.0	CMF[5]	no	yes	yes	no	no	no	[79]
VRAK [6]	PCC[7]	no	no	yes	no	yes	no	[16]
Lunadose	Lund University	no	no	yes	yes	no	yes	[33]
Matlab	UHH [2], LMU[3]	no	no	yes	yes	no	no	[80, 63]
MIM SurePlan MRT	Academics	yes	no	yes	yes	yes	no	[81]
XINDA	This study	yes	yes	yes	yes	yes	yes	

[1] TUM Technical University of Munich
[2] UHH University Hospital Heidelberg
[3] LMU Ludwig-Maximilians-University of Munich
[4] MCI Montpellier Cancer Institute
[5] CMF Cerrahpasa Medical Faculty
[6] VRAK Voxelized Registration and Kinetics
[7] PCC Peter Callum Cancer Center

61

trials being conducted to investigate TRT treatments, however, there is a paucity of large Randomised Controlled Trials (RCT) because of the few patients that are being treated. It is hoped that individual centers would be able to use XINDA to perform centralised dosimetry using their centre specific protocols and dosimetry results can be converted and compared across centres.

Chapter 5

Per-cycle changes in pharmacokinetics

5.1 Introduction

Paediatric cases represent a vulnerable population for pharmacokinetic changes between repeated cycles of 177Lu-DOTATATE. This chapter aims to identify quantitative changes in tumour and kidney biokinetics measured as mean effective half life and dose measured as absorbed dose and BED (Δ parameters) during a four-cycle course of 177Lu-DOTATATE treatment. A secondary aim is to investigate the potential to predict patient response from these changes.

Here, using data on six children with neuroblastoma who were imaged with 68Ga-DOTATATE PET/CT and subsequently received intra-cycle SPECT/CT after 177Lu-DOTATATE, it is possible to explore the per-cycle variability and relationships in the parameters of effective half life and absorbed dose of NETs in response to a course of 177Lu-DOTATATE treatment.

5.2 Methods

5.2.1 Patients and Therapy

The 177Lu-DOTATATE (LuDO) trial is a phase IIa, single centre, two-stage clinical trial registered in the European Clinical Trials Database (EudraCT number 2012-000510-10) and in the International Standard Randomized Controlled Trials Number Registry (ISRCTN98918118) to evaluate the safety and activity of 177Lu-DOTATATE in metastatic high-risk relapsed or refractory Neuroblastoma (NBL)[75]. Of the 21 patients registered for the trial, 20 received treatment with 177Lu-DOTATATE. Only 8 of these 20 patients were given four cycles of treatment with the remaining 12 receiving either one (n = 10) or two (n=2) cycles. Therefore, the analysis of per-cycle changes was restricted to the 8 patients who received four cycles; however we were only able to collect clinical and imaging data for 6 of the 8 patients due to logistical issues. We retrospectively identified six children (mean age of 5 years, range 2 to 5 years) treated with 177Lu-DOTATATE between February 2014 and May 2016 as part of this trial. Each child received a mean per-cycle activity of 2.9GBq (range 1.45GBq to 4.71GBq). These cycles were given at 8 to 10 week intervals. All children were imaged with 68Ga-DOTATATE PET/CT according to the local protocol[82] on a Discovery STE PET/CT system (GE Healthcare). A detailed description of the patient characteristics and actual delivered activities are shown in Table 5.1. The parents or guardian, as well as comforters and caregivers, of each patient gave written informed consent for treatment and the work was undertaken at UCLH.

At the time of writing, the baseline tumour volumes for the 6 patients analysed were not available or reported in the main trial results. However, prior to commencing trial treatment, all patients had a baseline tracer uptake in their tumour deposit at least as high as in their livers as measured by SUV_{max} on 68Ga-DOTATATE. Baseline disease assessments included 123I-mIBG SPECT/CT scans which were scored according to SIOPEN criteria[83]. Patients undergoing treatment with any

Table 5.1: Summary of patient characteristics and actual delivered activities during177Lu-DOTATATE therapy for the 6 analysed patients

Patient	Age (years)	Sex	Primary site	Metastases at baseline	GFR (mL/min)	Weight (kg)	Actual Per Cycle Activity (GBq)
1	7	f	adrenal	bone	144	37.2	2.86/ 3.67/ 4.68/ 4.25
2	4	f	adrenal	bone	77	21.4	1.45/ 2.16/ 2.57/ 2.86
3	6	m	adrenal	bone	115	21.4	1.54 /2.00 /2.07 /2.15
4	10	f	adrenal	bone	122	33.2	2.55/ 3.61/ 3.54/ 3.60
5	8	m	adrenal	brain	83	19.4	1.55/ 2.08/ 2.04/ 2.39
6	5	m	adrenal	bone	122	34.5	3.05/ 4.11/ 3.70/ 4.71

anti-tumour agents or who had prior treatment with radiolabelled somatostatin analogues were excluded from the trial.

The administered activity was planned on a weight-adjusted clinical protocol of either 75MBq/kg or 100MBq/kg with a per cycle whole body dose limit of 0.5Gy as follows:

$$\text{Personalised IA (GBq)} = 75/100\frac{\text{MBq}}{\text{kg}} \times \text{Weight(kg)} \tag{5.1}$$

To reduce the radiation dose to the kidneys, an intravenous infusion of amino acids (2.5% L-lysine HCl and 2.5% L-arginine in water for injection) at the rate of 1 L over 4 h was commenced 30 min before the administration of the radiopharmaceutical. The 177Lu-DOTATATE was then administered intravenously via a second pump over 30 min. After administration of 177Lu-DOTATATE, SPECT/CTs were acquired at nominal times of 4, 24, 48 and 72h over the upper abdomen including the entire organs at risk (kidneys, liver and spleen) to map the pharmacokinetic uptake and clearance. The acquisition parameters are summarized in Table 5.2. Imaging was performed on a GE BrightSpeed (GE Healthcare, Waukesha, USA) dual-headed gamma camera equipped with 3/8" thick NaI(Tl)-crystals with medium energy general purpose collimators. The SPECT data acquired was reconstructed iteratively using Ordered Subsets Expectation Maximization (OSEM)(20subsets) with CT-based correction for attenuation using the low- dose CT (20 mA, 120 kV, 1.25 mm slice thickness). Imaging data were evaluated using a dedicated workstation (Xeleris-Workstation, GE Healthcare, Waukesha, USA) at standard clinical

Table 5.2: Summary of the key specifications of the SPECT/CT regarding the image acquisition. Medium-energy general purpose collimators were employed and an energy window centered over the 208-keV photo peak.

Acquisition Parameters	Value
SPECT Matrix size(pixels)	128 x 128
Pizel size(mm)	4.46 x 4.46
Acquisition time	60 projections x 30s
Energy window centered at 208keV	20.00%
System sensitivity in 208 keV window (cps/MBq)	13
Crystal thickness (inches)	8/8
Slice Thickness (mm)	4.46
kVp	120
Tube current(mA)	20
Focal Spot Size (cm)	0.70
Filter Type	BODY FILTER
Convolution Kernel	STANDARD
Patient Position	FFS

settings.

5.2.2 Per cycle deviations in dose and effective half life

XINDA, the module of python scripts developed in the previous chapter, was used to convert each SPECT image to an absorbed dose rate image using the kernel convolution method. The per cycle effective life was determined from fitting a curve to the longitudinal dose rate images using method M1 (see Table 4.2) and calculating the area under this curve for dose. XINDA was designed to import reconstructed DICOM images from the GE Xeleris workstation with VOI contours stored in RT-STRUCT files.

We defined $\Delta(c_{later}, c_{earlier})$ as the deviation between values measured at earlier and subsequent cycles were defined as: 5.2

$$\Delta\text{parameter} = \frac{\text{pvalue}_{\text{later}} - \text{pvalue}_{\text{earlier}}}{\text{pvalue}_{\text{earlier}}} \tag{5.2}$$

where p value is either the value of the dose or effective halflife at a later or earlier cycle.

The following four pairs of deviation were examined: Overall: $\Delta(c4, c1)$, Early:

$\Delta(c2, c1)$, Middle: $\Delta(c3, c2)$ and Late:$\Delta(c4, c3)$

5.2.3 Dose Effect Relationship

In individual tumour lesions, radiological response was evaluated by the variation in lesion size on CT one month after the fourth cycle according to the International Neuroblastoma Response Criteria (INRC). The various correlations between the per-cycle changes in renal and tumour effective half life and dose and response were evaluated.

5.2.4 Statistics

Univariable analysis was performed for dose and effective half life from the total kidney and tumour volume in the four deviation categories. A Wilcoxon-Mann-Whitney signed rank test was utilized to determine whether there was a significant difference in parameter value from a later cycle relative to the immediately previous cycle or initial cycle value. Additionally, univariable logistic regression was performed with the absolute difference in each feature relative to baseline and the considered endpoint (tumour response) to assess the association between feature change and outcome. All p-values were adjusted using Benjamin & Hochberg false discovery rate to account for multiple comparisons. All statistical analyses were performed using Excel and p values $p<0.05$ considered statistically significant

5.3 Results

The following sections summarizes the renal and tumour Δdose and Δhalflife analysis for 24 cycles using SPECT image data (Figure 5.1)

5.3.1 Per-cycle kinetics

From these images, the per cycle mean ($\pm$SD) effective half life in six representative lesions was 97 $\pm$ 3 h, 98 $\pm$ 29 h, 78 $\pm$ 21 h and 66 $\pm$ 34 h for cycles 1, 2, 3 and 4

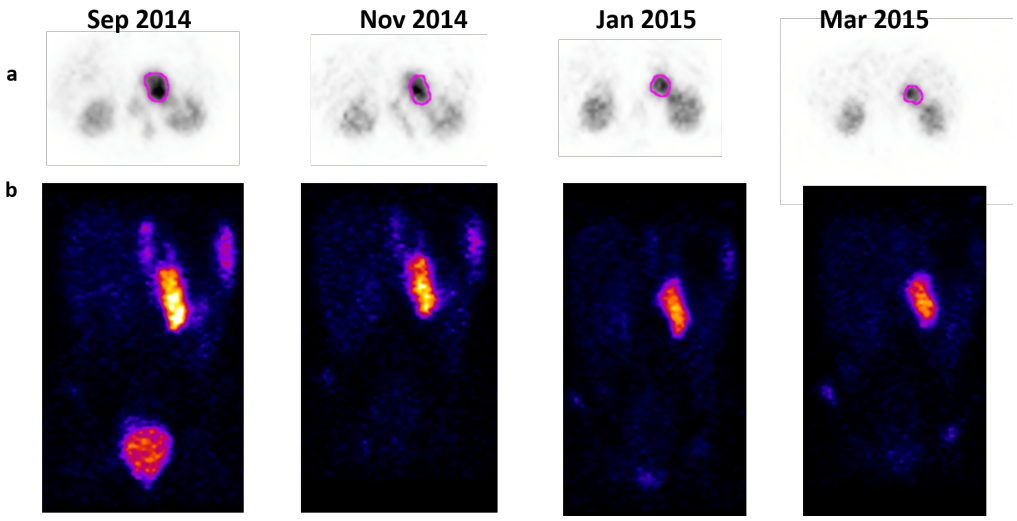

Figure 5.1: Longitudinal SPECT/CT at 24h after each cycle of 177Lu-DOTATATE showing reduction in max uptake of lesion for patient 001. Patient 001 showed Stable Disease. She had a stable response during the treatment course as seen on a) coronal and b) axis SPECT slices

respectively. The per cycle mean (±SD) absorbed dose was 7.5 ± 1.4 Gy/GBq, 5.4 ± 1.4 Gy/GBq, 3.1 ± 2.5 Gy/GBq and 1.2 ± 34 Gy/GBq for cycles 1, 2, 3 and 4 respectively. The medians and standard deviations of these changes in mean dose, effective half life and BED for the kidneys and tumours are presented in Table 5.3.

The per-cycle measurements for each patient's renal and tumour absorbed dose and effective half life are presented in Figure 5.2 and Figure 5.3 respectively.

All six patients showed a decreasing trend in renal effective half life with patient 1 and 3 having the greatest deviation of -52.57% and -73.32% relative to the first cycle. A variable per cycle tumour absorbed dose and effective half life was also noted across patients as treatment continued; although there was no clear trend.

The maximum observed absorbed dose in tumours was 9.32 Gy/GBq in the first cycle. The contribution from the different therapy cycles to the accumulated absorbed dose to the tumour is shown in Figure 5.4. In all six patients, the first 2 therapy cycles contributed more than 50% (range 54.67 - 78.72) to the accumulated tumour dose. The third cycle contributed less than the previous two cycles in 4/6 patients. In patients 5 and 6, more than 75% of the accumulated dose to the tumour was achieved during the first two cycles (75.1% and 78.2% respectively). In

Table 5.3: Summary of per-cycle deviations in absorbed dose (Gy/GBq), effective half life (h) and BED (Gy/Gbq)

					Relative error vs C1 (%)			Correlation vs C1		
	C1	C2	C3	C4	C2	C3	C4	C2	C3	C4
Dose (Gy/GBq)										
kidney	0.68 (0.21)	0.58 (0.35)	0.70 (0.32)	0.76 (0.17)	-13 (53)	22 (67)	23 (39)	0.26	-0.53	0.35
tumour[a]	7.5 (1.4)	5.4 (1.4)	3.1 (2.5)	1.2 (2.4)	-24 (22)	-61 (29)	-84 (40)	0.22	0.67	-0.82
Effective Half life (h)										
kidney	51 (9.0)	41 (4.7)	25 (3.9)	32 (4.3)	-16 (14)	-50 (9.7)	-34 (17)	0.48	0.44	0.05
tumour[a]	97 (37)	97 (29)	78 (21)	66 (34)	18 (53)	-40 (65)	-28 (40)	0.20	0.03	0.66
BED (Gy/GBq)										
kidney	0.74 (0.20)	0.61 (0.35)	0.7(0.32)	0.82(0.18)	-18 (47)	20 (60)	16 (32)	0.31	-0.51	0.39

Data is presented as median (standard deviation)

[a] Where there were multiple tumours, the tumour with the maximum uptake was chosen

69

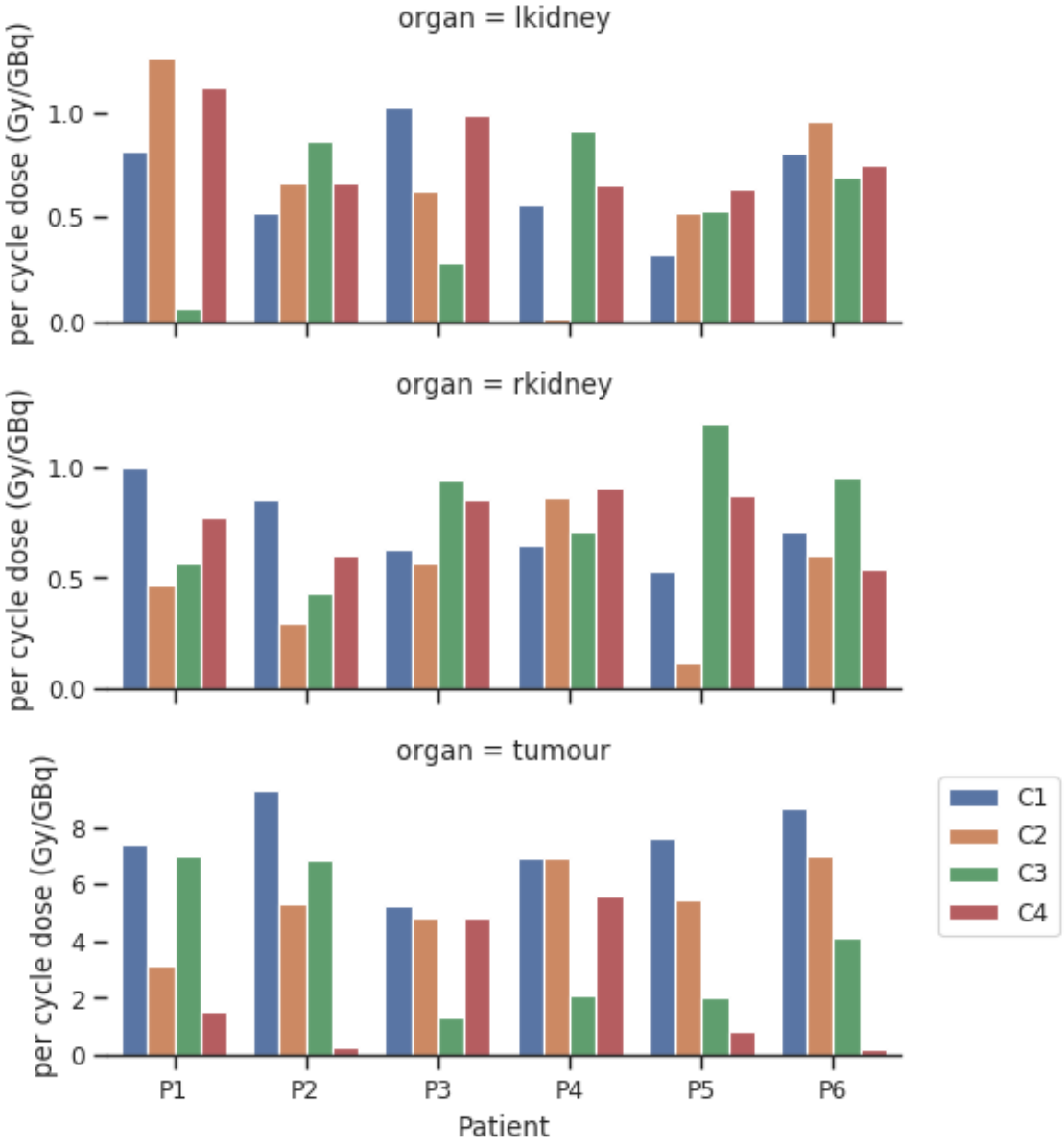

Figure 5.2: Absolute per cycle change in the renal and tumour absorbed dose for each of the six patients

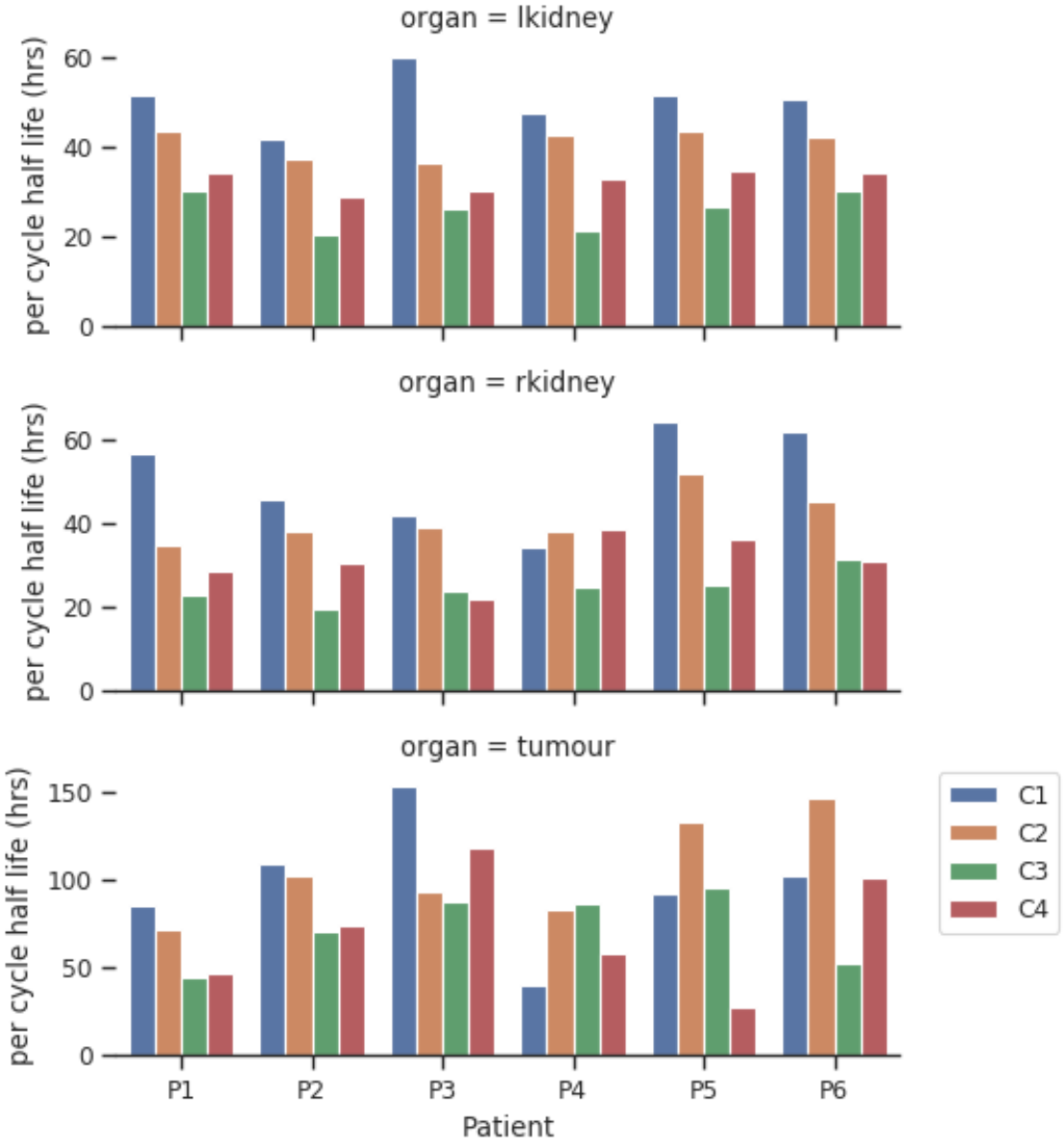

Figure 5.3: Absolute per cycle change in the renal and tumour effective half life for each of the six patients

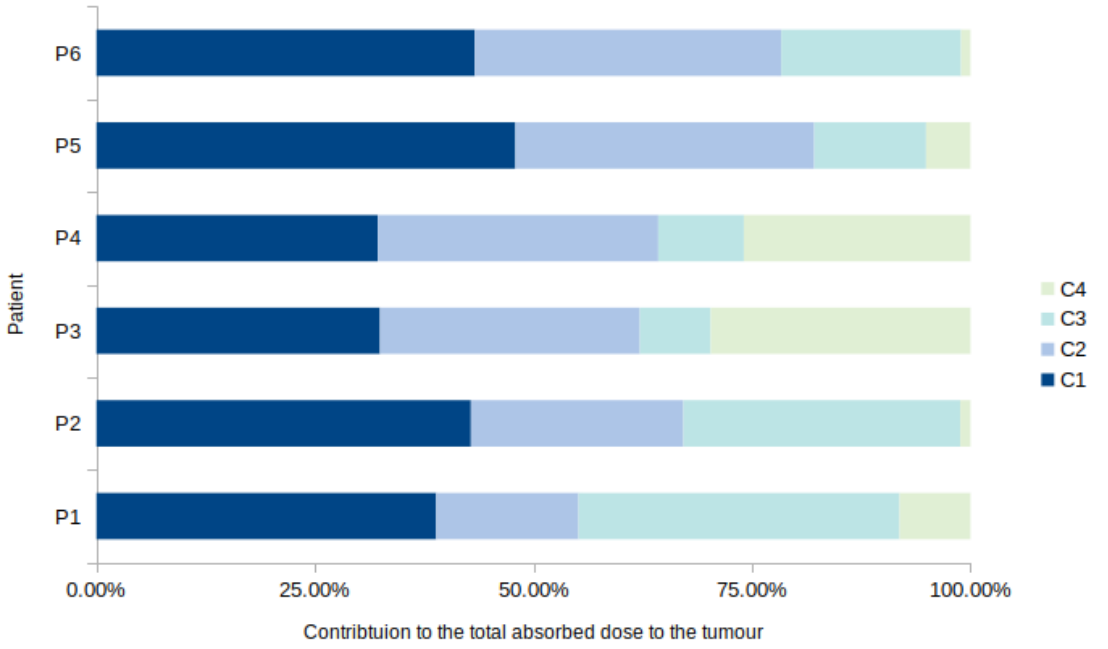

Figure 5.4: The contribution to the cumulative absorbed dose to the tumour from each cycle of therapy for each patient

patients 1, 2, 3 and 4 the contribution to the total dose from the first two cycles was 55.2%, 68.1%, 62.5% and 64.1% respectively. The third and fourth cycles of all patients contributed a mean of 19.1% (range 5% - 37%) and 14.7% (range 1% - 28%) respectively to the total tumour dose.

5.3.2 Dose-Dose and Kinetic-Kinetic correlation

Table 5.3 shows the p-value results from the Wilkinson test quantifying the significance of changes in per-cycle dose and effective half life within the same organ in the four categories of "Overall", "Early", "Middle" and "Late". The difference in renal effective half life in the 'Overall', 'Middle' and 'Late' stages of the course of treatment were considered significant using a $p<0.001$ criteria.

While it is important to characterise changes in the renal and tumour per-cycle biokinetics and dose as treatment continues, it is equally important to be able to predict when these changes might occur. One way of doing this is to perform linear regression on pairs of cycles to see if the biokinetics and dose of a cycle can be predicted by the biokinetics and dose of the previous cycle. Figure 5.5

Table 5.4: Results of two-tailed t-test regarding differences between cycles. p<0.001 is considered significant

		Early $\Delta(C2, C1)$	Overall $\Delta(C4, C1)$	Middle $\Delta(C3, C2)$	Final $\Delta(C4, C3)$
Kidney	Half life	p=0.0015	**p<0.001**	**p<0.001**	**p<0.001**
	Dose	p=0.254	p=0.252	p=0.571	p=0.43
Tumour	Half life	p=0.675	p=0.081	p=0.071	p=0.912
	Dose	p=0.034	p=0.0155	p=0.329	p=0.386

highlights linear regression analysis on dose relationships in the Early (5.5a), Middle (5.5b) and Late sections (5.5c) of a course of 177Lu-DOTATATE treatment. The correlation between per-cycle dose across all organs was highest in the middle section of treatment with $\rho = 0.58$ and weakest in the early section of treatment with $\rho = 0.14$.

Figure 5.6 highlights linear regression analysis on effective half life relationships in the Early, Middle and Late sections of a course of 177Lu-DOTATATE treatment. The correlation between cycles was positive across all sections with an increase in correlation with cycle pairs later in the cycle than earlier. The effective half life ratio between the initial and last cycle for all organs compared resulted in a mean ratio slightly lower than one. It should be noted in the 'Late' section of treatment that the tumours effective half life showed a negative correlation while the kidneys displayed a positive correlation.

Interestingly, a moderate, negative correlation was found between the per-cycle renal and tumour doses using all therapy cycle data (Figure 5.7a). However within-cycle fits (Figure 5.7b) showed no clear relationship visually with some cycle having positive, negative and relatively little change. The trend between the per cycle tumour dose and per cycle renal dose shifts from a negative correlation in the earlier cycles to positive in the later cycles.

A moderate negative correlation was also found when comparing the per-cycle renal and tumour effective half lives (h) using all therapy cycle data (Figure 5.8a) and this relationship was maintained when the correlation was broken down into individual cycles (Figure 5.8b)

5.3.3 Dose-Response Relationship

Stable disease was observed in 3 of 6 patients (50%) and Progressive disease was observed in the remaining three. No objective response was seen in these patients. Tumor response according to INRC criteria and the calculated per cycle changes in the tumour pharmacokinetics and dose are presented in Table 5.5.

Table 5.5: Objective responses according to INRC measured 1 month after the fourth cycle and changes between the first and subsequent cycles in tumour effective half life and dose (n=6)

		ΔTumour Effective Half life(h) relative to C1			ΔTumour dose (Gy/GBq) relative to C1		
Patient	RECIST	C2	C3	C4	C2	C3	C4
1	SD	-16.60	-48.83	-45.03	1.55	-58.08	-5.56
2	PD	-6.81	-36.21	-32.94	0.25	-43.21	-26.12
3	PD	-39.01	-42.58	-22.62	4.83	-8.31	-75.03
4	SD	107.03	117.89	45.28	5.57	-0.36	-69.58
5	PD	44.88	3.56	-70.65	0.81	-28.65	-73.32
6	SD	42.57	-49.29	-1.88	0.21	-19.02	-52.47

SD, stable disease; PD, progressive disease

The deviations from all cycle pairings in both the kidney and tumour of these six patients was not able to differentiate patients with stable disease and progressive disease (Figure 5.9).

At the time of writing, the symptom response, tumour volume changes and tumour marker changes of the patients analysed in this chapter were not available. Table 5.6 is a summary of the response, safety and toxicity reported in the main trial results. Haematological toxicity was assessed according to Common Terminology Criteria for Adverse Events (CTCAE) version 4.0. It is worth noting that the response and toxicity of the six patients analysed in this chapter are likely not representative of the broader patient population in the LuDO trial. This is particularly because the six analysed patients managed four courses of treatment while the majority of patients enrolled in the trial tolerated either one (n = 10) or two (n=2) courses. This suggests the analysed patients were healthier at the start of the trial and/or had a better overall response.

Table 5.6: INRC response criteria and CTCAE v4.0 toxicities reported in the main LuDO trial

Response	
Death before primary outcome assessment at 1 month	6/20
Alive at primary outcome assessment	14/20
Progressed	8/14
Non-responder	6/14
Safety and Toxicity	
Number of treated patients	20
Number of adverse Events	151
Grade 1 events	5/20
Grade 3 events	12/20
Grade 4 events	2/20

In view of the responses observed in the first stage, the trial was closed and did not move on to the second stage.

5.4 Discussion

To optimise repeated 177Lu-DOTATATE cycles in NBL patients, an understanding of the intra-cycle variability of the renal and tumour pharmacokinetics is needed. In this small cohort, the effective half life of the tumour changed from the baseline value at the first cycle while the effective half life of the kidneys remained relatively constant over treatment. The range of deviations was greater in the tumour compared to the deviations in the kidney.

Reports of per-cycle changes for tumour mean absorbed doses have been reported previously for NETs receiving 177Lu-DOTATATE therapy by numerous authors. in Table 2.2 [12, 27, 29, 84]. In contrast, evidence for the variability in per-cycle absorbed dose to the kidneys has been inconclusive with groups at the Lund University [9], Montpellier Cancer Institute [34] and Sahlgrenska Cancer Center [26] observing no intra-cycle differences and Garske and colleagues reporting a tendency that the effective half life in the kidney decreased during therapy in the largest patient cohort (n=30) at Uppsala University Hospital [12]. In agreement with Garske, a moderate decrease in per-cycle renal dose was observed in this study as a function

of the treatment cycles, however it was not statistically significant. This analysis should be repeated in a larger sample size to power the statistics to pick up subtle effects. One explanation for the difference in observations between this study and the observations from the Lund, Montpellier and Sahlgrenska groups could be the number of cycle investigated. These three groups only investigated the first two cycles of treatment which only showed no significant deviation in our study. The mean renal effective half life in this study was 50.97 ± 9.01 which compares well to the effective half lives of 45h [85, 86] and 52h [12] reported by other authors for NETs patient receiving Lutetium-177 (177Lu)-DOTA-TATE (177Lu-DOTATATE).

With our sample, we noticed a moderate negative correlation between per-cycle renal and tumour dose ($\rho = -0.53$, n =24). This relationship is in contrast to the positive correlation reported by Del Prete and colleagues ($\rho = 0.16$, n = 170) in the interim results of a phase II clinical trial of 177Lu-DOTATATE in adult NETs patients[32]. This difference between the results from our study and Del Prete highlights a recognition that our sample might be undersized which limits the robustness of the observations to other datasets and warrants repeat in a larger sample. Not withstanding, our study expands on the knowledge provided by Del Prete by highlighting a variability in the relationship between per-cycle renal and tumour dose as treatment continues with the relationship shifting from a negative correlation at the initial cycle to a positive on at the final cycle. Looking at the confidence interval between our negative correlation, there is a small overlay with the positive correlation of per-cycle renal and tumour dose reported by Del Prete. If the negative correlation in this study is true then one hypothesis is this could indicate an abundance of unbounded tracer in the blood stream. This could be tested by using a compartmental model over the course of treatment and seeing what parameters change.

Interestingly, we did not observe a variability in tumour uptake as a function of treatment cycle and tumour burden as expected based on clinical reports for adult NETs from several single center studies. These studies are summarised in Table 2.2.

This lack of variability could be a direct result of the lack of objective response in these six patients implying no variability in tumour burden. We hypothesise this could also be a factor in the observation of no differentiation between per cycle deviations in the children who showed progressive disease versus stable disease.

This study had limitations. Aside from the small sample size, these SPECT-derived voxelised effective half life and dose maps contain noise that is inherent in the acquisition process that could be transferred in the entire process. Specific aspects of uncertainty within the dosimetry chain can be reduced through phantom studies and uncertainty propagation schema[87].

Another implication of this study is a decrease in the per-cycle contribution to the total dose of the tumour with the major contributions occurring in the first two cycles. The decrease in tumour uptake and dose may have a clinical impact on patient response. Because NBL is considered to generally be radioresistant, these results indicate it may be appropriate to base therapy on an increased administered activity in the first two cycles for some patients rather than an evenly distributed administered activity across four cycles. If the uptake and dose per administered activity of the tumour gradually decreases after each cycle then cancer cells surviving at later cycles are in effect receiving smaller therapeutic doses. These surviving cancer cells may in fact need greater radiation doses for cell death. In a fixed per-cycle activity regimen, the final two cycles of a four cycle treatment may be less effective due to the reduced tumour uptake per injected activity. If the administered activity in the first two cycles were increased relative to the final two cycles then one may capitalise on the higher dose per injected activity of the earlier cycles. These higher per-cycle administrations during the initial two cycles may compensate for the decreasing tumour uptake during the later sections of treatment. Additionally, a higher dose per injected activity in the earlier cycles could mean less cumulated activity is needed to reach a set dose level in the tumour.

By using a more aggressive therapy approach during the earlier stage of the 177Lu-DOTATATE treatment, it may take advantage of the therapeutic window

when uptake and retention by the tumour is at its highest. We, therefore, raise the question of whether the standard planning strategy of equal per-cycle absorbed dose contributions to the kidney within a limit of 23Gy should always be used.

During treatment planning based on kidney limits, it is assumed that the kidney pharmacokinetics is invariable between treatment. This assumption allows for a reduction in the number of treatment cycles that need to be verified with resource intensive post-treatment SPECT/CT. These results hint that this assumption of invariable kinetic effective half life might not be valid in all patient groups treated with 177Lu-DOTATATE especially children.

Early response assessment during a course of treatment could potentially allow response-adapted therapy (i.e., biologically adaptive radiation therapy), which may improve clinical outcomes. For example, the radiation dose could be escalated to nonresponding tumors without increasing the dose to normal tissues through adapting the treatment plan to changing pharmacokinetics.

5.5 Conclusion

In this study, we demonstrated a decrease in the kidney effective half life during treatment as well as a changing relationship between the per-cycle renal and tumour effective half life as treatment cycle increased. A decreasing per cycle contribution to the cumulative tumour dose as treatment cycle continues was also demonstrated. This could be of interest in making a case for the reduction of the number of cycles from the standard of four and an increase in the per-cycle activity of the first two cycles. This decreasing contribution could mean that tumours are receiving less dose as the course of treatment increases despite the per-cycle kidney dose being fairly constant. Alternatively, the portion of tumour remaining at later stages in the treatment may be more radioresistant and need more radiation and not less. Finally, we were not able to find a correlation between deviations in the 'Early', 'Middle' or 'Late' sections of a course of treatment and patient response.

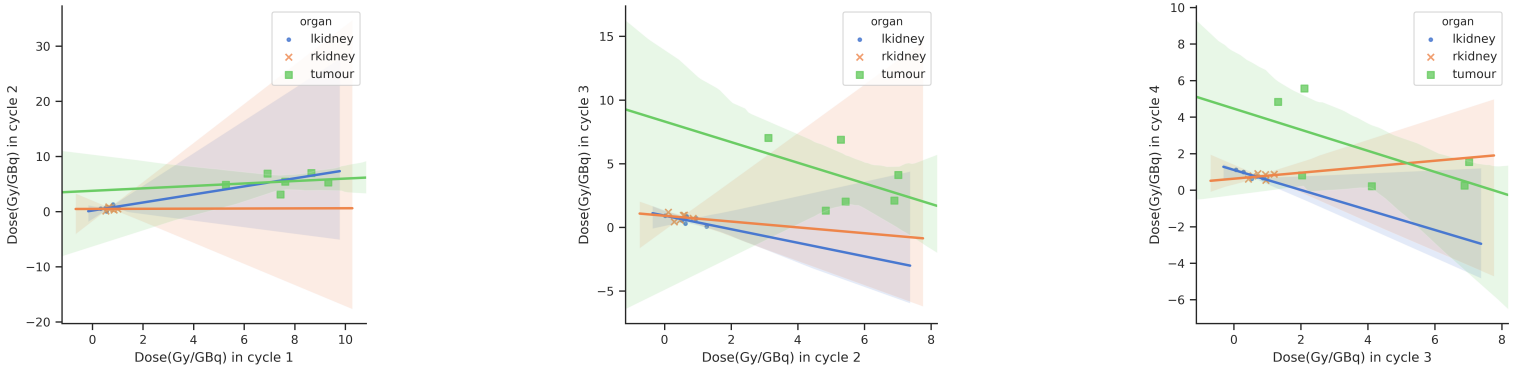

(a) Early: Correlation between organs doses from first therapy cycle and second therapy cycle.The tissue doses were weakly correlated with $\rho = 0.14$

(b) Middle: Correlation between organ doses from second therapy cycle and third cycle. Across all tissues, there was a moderate negative correlation between doses $\rho = -0.58$

(c) Late: Correlation between organ doses from third therapy cycle and forth cycle. Across all tissues, there was a moderate negative correlation between doses $\rho = -0.49$

Figure 5.5: Inter-cycle relationships between doses in the kidneys and tumour in the 'Early', 'Middle' and 'Late' stages of the treatment (n=18, left kidney (blue circle), right kidney (orange cross) and tumour (green square)

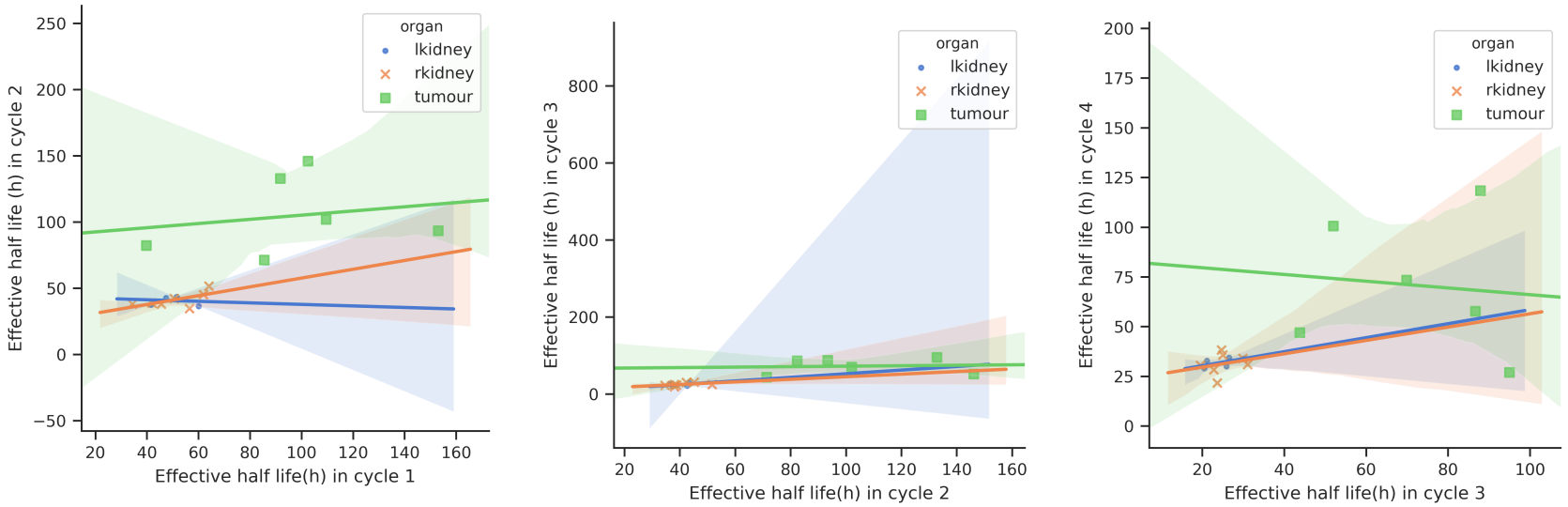

(a) Early: Correlation between organ half lives from first therapy cycle and second therapy cycle. Across all tissues, there was a very weak positive correlation between half lives $\rho = 0.12$

(b) Middle: Correlation between organ doses from second therapy cycle and third cycle. Across all tissues, there was a weak positive correlation between half lives $\rho = 0.24$

(c) Late: Correlation between organ doses from third therapy cycle and forth cycle. Across all tissues, there was a weak positive correlation between half lives $\rho = 0.37$

Figure 5.6: Inter-cycle relationships between half life in the kidneys and tumour in the 'Early', 'Middle' and 'Late' stages of the treatment (n=18, left kidney (blue circle), right kidney (orange cross) and tumour (green square)

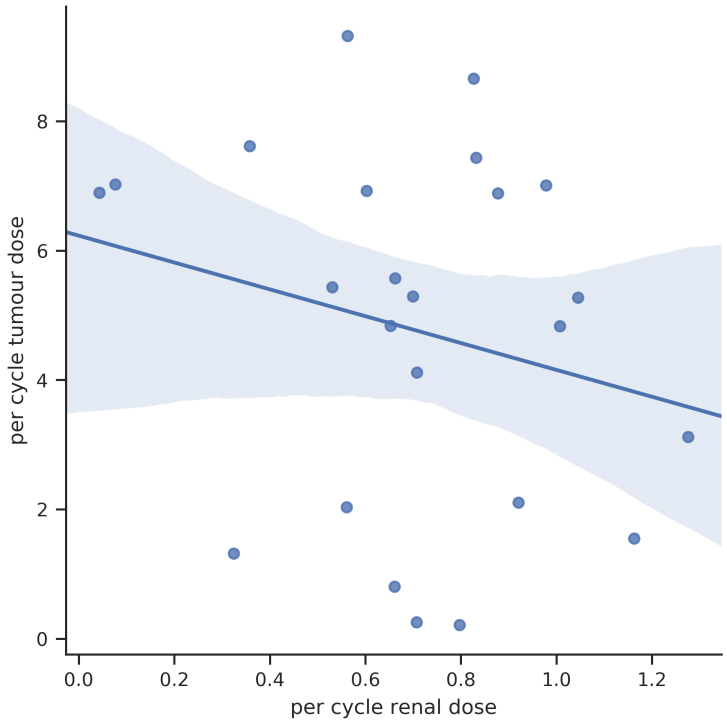

(a) There was a moderate correlation between the per cycle renal and tumour absorbed dose across all cycles (ρ = -0.53, p<0.05, n = 24).The shaded region is a 95% confidence interval.

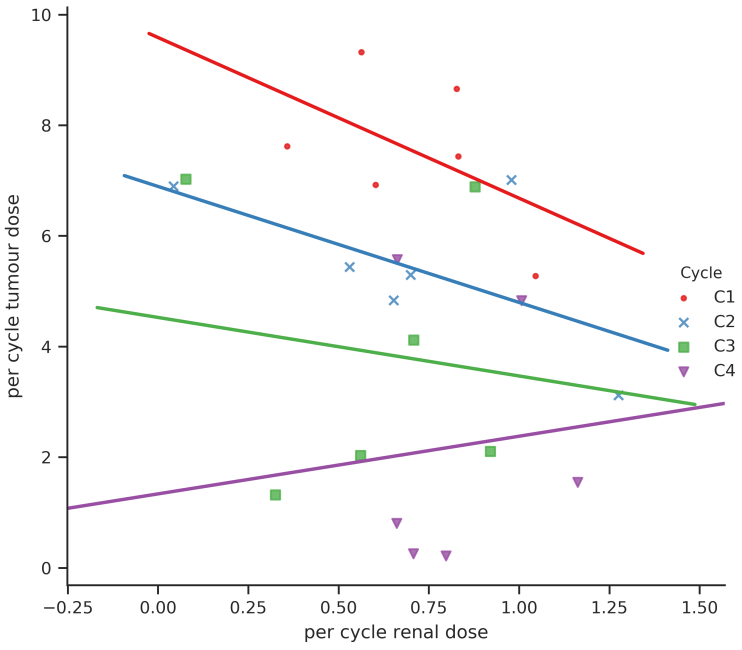

(b) Individual trends in the tumour and renal absorbed dose as a function of treatment cycle. Visual inspection shows a changing relationship with cycle number. The sample size (n=6) was too small for a meaningful statistical test

Figure 5.7: Correlation between the tumour and renal absorbed dose (Gy/GBq)

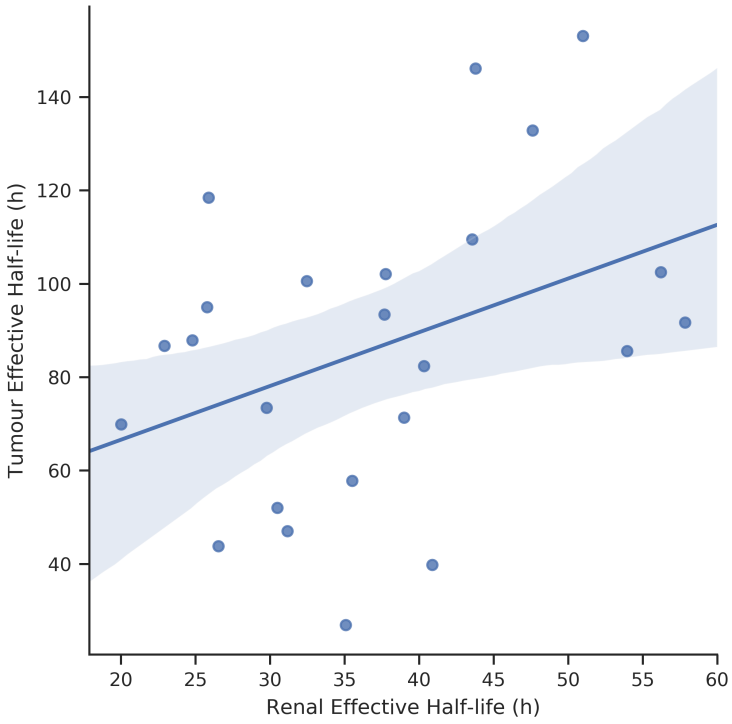

(a) There was a moderate correlation between the per cycle renal and tumour effective half lives using data from all cycles (ρ = 0.46, p<0.05, n = 24).The shaded region is a 95% confidence interval.

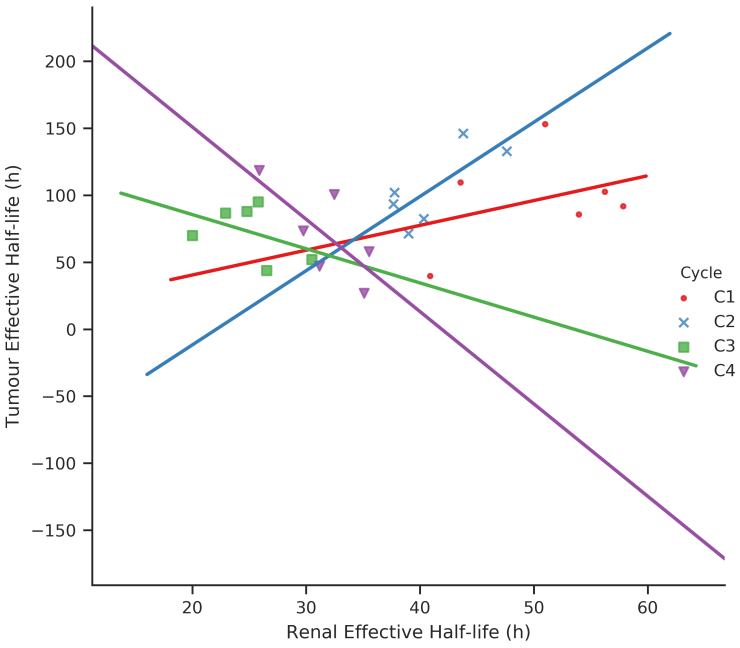

(b) Individual trends in the per cycle renal and tumour effective half lives for each cycle. Sample size (n=6) was too small for statistical test between cycle but visual inspection shows a cycle dependent variation in the correlation

Figure 5.8: Correlation between the tumour and renal effective half life (h)

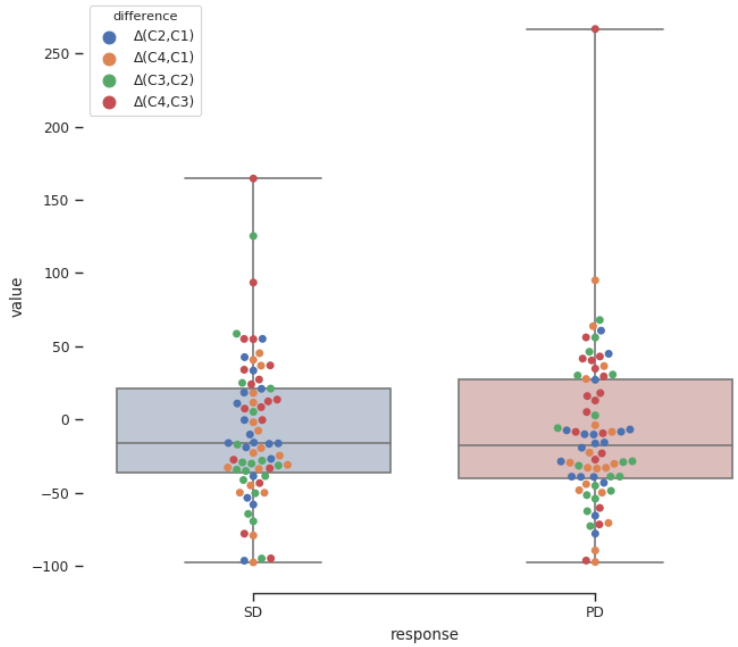

Figure 5.9: Comparison of deviation in dose and half life in relation to response

Chapter 6

Temporal changes in the heterogeneity of the pharmacokinetics

6.1 Introduction

In the context of image analysis, a histogram is a graphical representation of the voxel values. In the previous chapter, the changes in kidney and tumour uptake, dose and radiobiology was characterised using the conventional parameters of mean dose, mean effective half-life and mean BED. The heterogeneous nature of 177Lu-DOTATATE uptake may be of clinical significance, however, the spatial arrangement of voxel values is not reflected by histogram-derived indices. Characterising the different heterogeneous uptake patterns in addition to the conventional dosimetry metrics of mean and median may prove clinically relevant.

This chapter aims to determine whether the magnitude of the changes in the heterogeneity of the pharmacokinetics, physical and radiobiological dose of NETs (ΔParameters)is significant over the course of 177Lu-DOTATATE treatment and to investigate the relationship between response and the longitudinal differences in heterogeneity parameters. As a secondary analysis, the radiobiological impact

of temporal changes in the uptake heterogeneity during treatment was explored through the radiobiological metric: EUBED.

Recently, two groups have shown the utility of the heterogeneity parameters Entropy, Correlation, Homogeneity and Asphericity derived from pre-treatment somatostatin receptor Ga68-DOTATATE PET/CT [42] and intra-treatment 177Lu-DOTATATE SPECT [44] of the tumour in predicting Progression Free Survival (PFS), Overall Survival (OS) and response for NETs patients treated with 177Lu-DOTATATE. These parameters derived from the Ga68-DOTATATE PET/CT reflect the spatial arrangement of the tumour uptake.

6.2 Method

6.2.1 Patient Characteristics and Imaging Acquisitions

Details of the patient characteristics and SPECT/CT acquisition methods have been previously described in Chapter 5. Briefly, six children with relapsed or primary refractory neuroblastoma who were enrolled in a single center Phase II clinical trial at University College London Hospital were retrospectively analysed.

All children were imaged with 68Ga-DOTATATE PET/CT according to the local protocol [82] on a Discovery STE PET/CT system (GE Healthcare). Patients were injected intravenously with at least 100 MBq for adequate image quality. Imaging took place at least 45 min but no longer than 1 h after injection. A low-dose scout projection (120 kVp; 10 mA; pitch, 1.75) was used to localize the region of head to thigh for transmission and emission imaging. CT was performed at 140 kVp and 40 mA for paediatrics. PET was performed in 3-dimensional mode with 4 min per bed position. Iterative reconstruction with 21 subsets (2 iterations) was performed with attenuation correction. If disease sites showed avid uptake of 68Ga-DOTATATE that was greater than uptake in the liver, then the child was considered eligible for therapy.

6.2.2 Radiobiological Experiments and Calculations

Clongenic Assay

Due to the non-standard clinical combination of 177Lu-DOTATATE with NBL, the radiobiological sensitivity of this particular tumour treatment-disease combination was explored with a colony formation assay rather than using α and β values from literature as was done for calculating the kidney BED in the previous chapter.

Two cell lines were chosen to reproduce the range of levels of the 177Lu-DOTATATE target, SSTR, in NETs. The neuroblastoma cell line CHLA-15 was obtained from the Childrens Oncology Group and maintained in Iscove Modified Dulbecco's medium supplemented with 2 mM L-glutamine, 1% (v/v) insulin, 1% (v/v) transferrin, 1% (v/v) selenium and 20% (v/v) foetal bovine serum (FBS, Autogen Bioclear, UK) at 37° C in a 5% CO_2 atmosphere. The neuroblastoma cell lines SK-N-BE(2)C was obtained from the American Tissue Culture Collection. SK-N-BE(2)C cells were maintained in Dulbecco Modified Eagle medium (DMEM) supplemented with 15% (v/v) FBS, 2 mM L-glutamine and 1% (v/v) non-essential amino acids at 37 ° C in a 5% CO_2 atmosphere. Cells were seeded for 24 hours in medium and then treated the following day with increasing concentrations of 0, 1.0, 1.5, 2.0, 2.5, 3.0 MBq for 4 hours. Cells were thenwashed and left to grow colonies over 12 days.

Internalisation Assay

To generate the radiobiology parameters, alpha (α) and beta (β), the cell absorbed dose during irradiation and the 12 day incubation period of the colony formation assay should be expressed as a function of absorbed dose in Gy instead of administered activity in the medium in MBq. To do this, the percentage of cell uptake or the amount of radioligand bound to the receptors at the cell membrane and internalised into the cell from the medium at 4 hr was determined using an internalisation assay. Additionally, for the conversion of activity in MBq to Gy, an S factor of 0.67 (mGy/MBq.s) was used for converting cumulated activity of 177Lu-DOTATATE to dose in a NBL cell[88]. Cells were incubated for 4 hours with 0.5MBq of 177Lu-

DOTATATE. The final macroscopic mean absorbed dose $\bar{D_{cell}}$ to the cells over a period of 12 days was calculated using the following integration after the 4h incubation using Equation 6.1

$$\bar{D_{\text{cell}}} = S_{\text{factor}} \times \int_{T_0=4}^{\infty} A_{\text{cell}} \exp(-\lambda_{\text{phys}} t) \tag{6.1}$$

where $\bar{D_{\text{cell}}}$ is the mean dose to the cell during the 12d incubation, A_{cell} is the internalised activity in the cell at 4h and λ_{phys} is the physical half life and the S_{factor} was 0.67 mGy/MBq.s

Using the mean of the experimentally determined α and β values for cells with high and low SSTR receptor density, the radiobiological impact of the heterogeneity within the per-cycle absorbed dose images was determined using the EUBED with the following equation:

$$EUBED = \frac{1}{\alpha} \ln \left(\frac{\sum_{i=1}^{N} e^{-\alpha BED_{ijk}}}{N} \right) \tag{6.2}$$

where BED_{ijk} is the BED of voxel at coordinates (ijk) and N is the total number of voxels

6.2.3 Heterogeneity Quantification

Additional non-standard quantification of the heterogeneity was extracted from the dosimetric and biokinetic 3D maps of the tumour VOIs using the freely available LIFEx 5.10 for Linux operating system [89]. Using this platform, the features of heterogeneity and their definitions in Table 6.1 were considered for each intra-cycle SPECT and pre-treatment Ga68-DOTATATE PET/CT scan. Further description of the calculated features and their formulae as proposed by the Image Biomarker Standardization Initiative is provided in the Appendices.

Inspired by the Uppsala group, 42 percent of the maximum in the tumour on the per-cycle physical dose and effective half life images was used to define the tumour sub-volume for heterogeneity extraction. The 42% threshold was previously shown

to most closely resemble the true functional volume [72] .

Table 6.1: Full description of the selected features across the 42% threshold tumour subvolumes. No image processing method was applied

Parameter	Description	Derived from	Parameter Image	Feature Abbreviations
Entropy	Measures randomness of distribution e.g. a homogenous matrix demonstrates low Entropy	The gray-level co-occurrence matrix reflects the probability of observing a pair of values in voxels at a given distance in a given direction	Dose, Kinetic, PET/CT	DOSEentropy, KINentropy, PETentropy
Homogeneity	A measure for continuous areas of same or similar voxel values in an image or voxel of interest (VOI).	The gray-level co-occurrence matrix reflects the probability of observing a pair of values in voxels at a given distance in a given direction	Dose, Kinetics, PET/CT	DOSEhomogeneity, KINhomogeneity, PEThomogeneity
Correlation	A measure of intensity linear-dependencies.	The gray-level co-occurrence matrix reflects the probability of observing a pair of values in voxels at a given distance in a given direction	Dose, Kinetics, PET/CT	DOSEcorrelation, KINcorrelation, PETcorrelation
EUBED	A measure accounting for the biology of non-uniform tumour absorbed dose distributions on tumour control	Radiobiology parameters applied to the physical dose image	Dose	DOSEeubed
Asphericity	Asphericity is a quantitative measure of shape irregularity. for example, asphericity of 0.5 means that the surface of the lesion is 50% larger than the surface of a sphere with the same volume.	Surface and volume of the tumour	Dose, Kinetics, PET/CT	DOSEasphericity, KINasphericity, PETasphericity

6.2.4 Delta Parameters

The typical approach to quantify the significance of per-cycle changes compared to a difference of 0 would involve univariate analysis performed using a single-sample Wilkinson T-test. However, in this study, the limited number of samples (n = 6 patients) due to the rarity of the disease relative to the number of heterogeneity parameters (n = 13) limits the usefulness of p-value statistics test. Alternatively, the Concordance Correlation Coefficient (CCC) was used to determine the agreement between parameters of each cycle. This coefficient accounts for the fact that per-cycle measurements are obtained from the same patient. CCC as a measure of

agreement describes the correlation between two measurements that fall on a 45deg line passing through the origin and is defined as:

$$CCC = \frac{2\rho\sigma_x\sigma_y}{\sigma_x^2 + \sigma_y^2 + (\mu_x - \mu_y)^2} \tag{6.3}$$

where μ_x,μ_y, σ_x, σ_y are the mean and variance of two measurements x and y respectively, and ρ is the Pearson's Correlation Coefficient between x and y [90]. CCC is scaled between ± 1 where a value of one indicates perfect measurement agreement.

The net change in heterogeneity parameters relative to their baseline values was determined using Equation 6.4

$$\Delta\text{change} = \frac{\text{Parameter}_{\text{subsequent cycle}} - \text{Parameter}_{\text{initial cycle}}}{\text{Parameter}_{\text{initial cycle}}} \tag{6.4}$$

Here, $\text{Parameter}_{\text{subsequent cycle}}$ was the value at the end of a non-initial cycle and $\text{Parameter}_{\text{initial cycle}}$ was the value after the first cycle for each patient.

Additionally, changes between the heterogeneity in the pre-treatment 68Ga-DOTATATE PET/CT and SPECT/CT of the first cycle were defined in the form equation 6.5

$$\Delta\text{change} = \frac{\text{Parameter}_{\text{initial cycle}} - \text{Parameter}_{\text{PET}}}{\text{Parameter}_{\text{PET}}} \tag{6.5}$$

Here, $\text{Parameter}_{\text{PET}}$ was the value measured on the pre-treatment 68Ga-DOTATATE PET/CT and $\text{Parameter}_{\text{initial cycle}}$ was the value after the first cycle for each patient.

6.2.5 Delta Parameter Response Relationship

In individual tumour lesions, radiological response was evaluated by the variation in lesion size on CT one month after the fourth cycle according to the International Neuroblastoma Response Criteria (INRC). The various correlations between intra-cycle changes in the pharmacokinetic and dose heterogeneity in the tumour and tumour response were explored.

6.3 Results

Figure 6.1 is a representative image of the pre-treatment PET/CT and the post-treatment SPECT/CT used in this analysis.

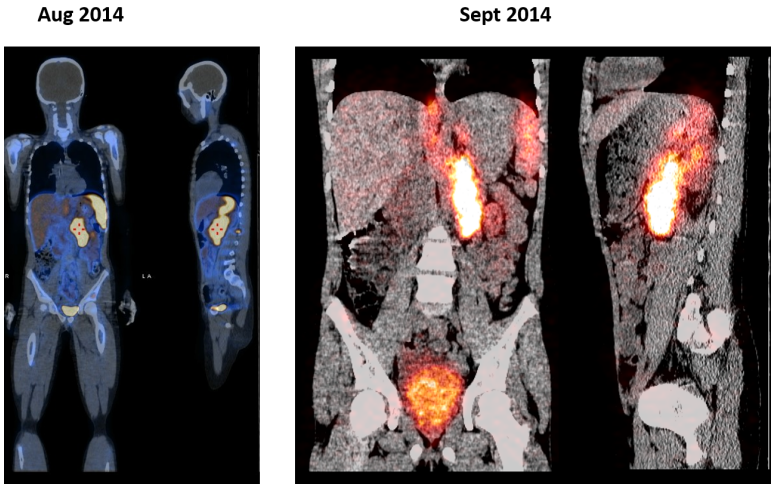

(a) Intense uptake (SUVmax 13.8) can be detected in the left adrenal gland (at the center cursor) on both the PET/CT and SPECT/CT images.

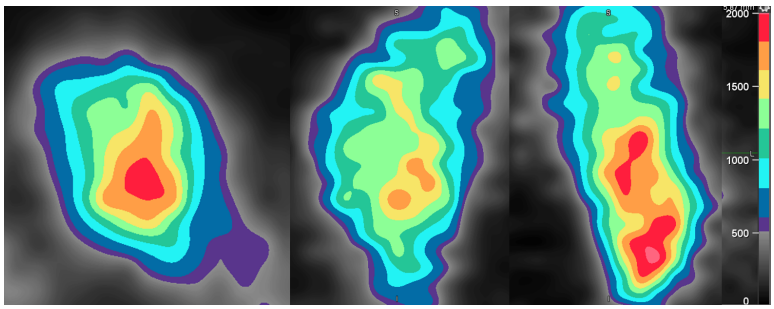

(b) Illustration of heterogeneity within 42% functional volume of tumour in 3 dimensions

Figure 6.1: llustration of heterogeneity in the tumour region of patient 1 on both the pre-treatment 68Ga-DOTATATE PET/CT acquired on August 2014 and the 177Lu-DOTATATE SPECT image acquired on September 2014

A comparison of SPECT/CT voxel values within the 42% tumour subvolume at the same post injection time points for different cycle highlights a wide variation in values.

6.3.1 Radiobiology

The uptake in both cell lines was found to be relatively low with 0.65% of the radioactivity internalised in the SK-N-BE(2)C cell line compared to 0.31% for CHLA-15.

The survival of SK-N-BE(2)C and CHLA-15 cells after exposure to escalating absorbed radiation doses from 177Lu-DOTATATE is shown in Figure 6.3, as well as photos of the surviving colonies after 12 days for the CHLA-15 cells Figure 6.4a and SK-N-BE(2)C cells Figure 6.4b . The CHLA-15 cells showed to be more radio resistant than SK-N-BE(2)C with both showing increased cytotoxic effect with an increasing dose. Curves according to the LQ model were fitted with high correlation coefficients (R^2 = 0.92 and 0.97, respectively). The α and β values obtained from the LQ model are shown in Table 6.2. The $\frac{\alpha}{\beta}$ ratio was found to be 0.09 for SK-N-BE(2)C and 1.41 for CHLA-15.

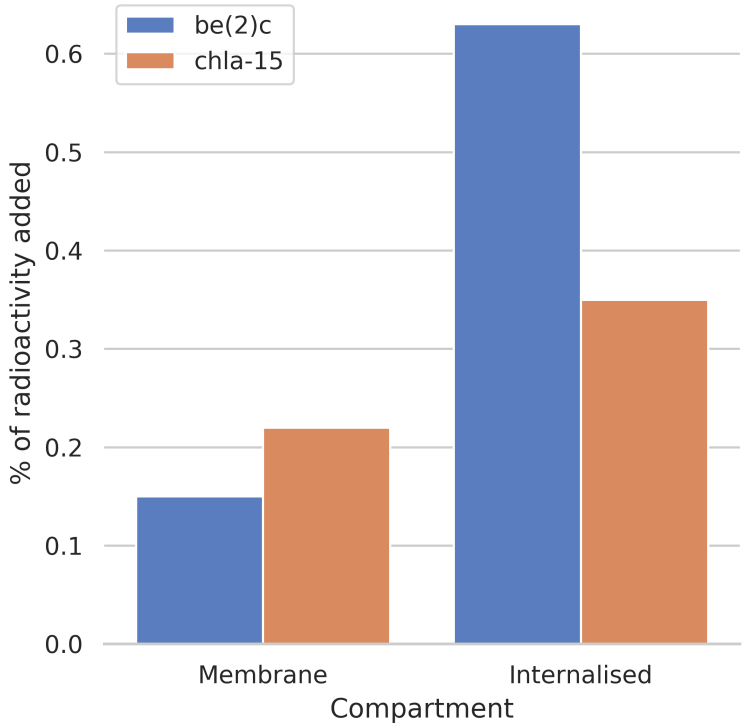

Figure 6.2: SSTR-mediated uptake of 177Lu-DOTATATE by SK-N-BE(2)C and CHLA-15 cells. The uptake was measured 4 h after incubation with 0.5MBq of 177Lu-DOTATATE

Table 6.2: Comparison of alpha beta values for cells SK-BE(2)C and CHLA-15 derived from colony formation assays

Cell line	Receptor density	Alpha, $\alpha(Gy^{-1})$	Beta, $\beta(Gy^{-2})$
SK-N-BE(2)C	high	0.041 ± 0.266	0.429 ± 0.209
CHLA-15	low	0.551 ± 0.139	0.391 ±0.09

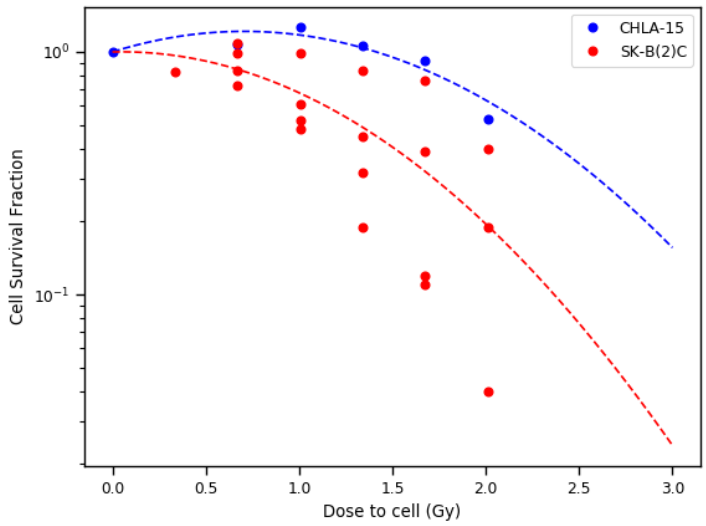

Figure 6.3: Survival curves of neuroblastoma cell lines SK-N-BE(2)C (n=3) and CHLA-15 (n=1) obtained after exposure at different doses of 177Lu-DOTATATE. The x-axis is expressed in dose (Gy) and the y axis in survival fraction. The curves were fitted with the LQ model

6.3.2 Delta parameters

Figure 6.5 demonstrate the relative change in DOSEcorrelation, DOSEeubed, KINasphericity and KINentropy in each patient as a function of cycle number. The relative change in features at subsequent cycles (C2-C4) relative to the first cycle (C1) varied substantially from as little as a mean of 0.25 ± 9% for all six patients for the radiobiological metric EUBED to a maximum difference of -525% between C1 and C4 for DOSEcorrelation in patient 6. The results show some features appear to have a cycle dependent change like DOSEcorrelation and KINasphericiy while other heterogeneity parameters like DOSEeubed and KINentropy were invariable across all parameters. Individual patient plots in Figure 6.5 highlight differences in feature values between cycles with the tumour, however with no clear trend with some patients having a considerable increase in KINasphericity at the final cycle compared to the initial cycle like patient 6 while some showing relatively little variability for the same parameter like patient 3.

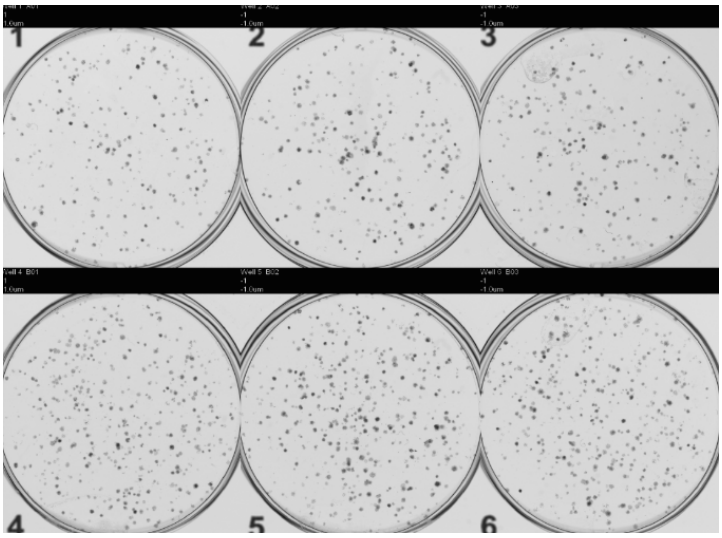

(a) Photo of CHLA-15 colonies

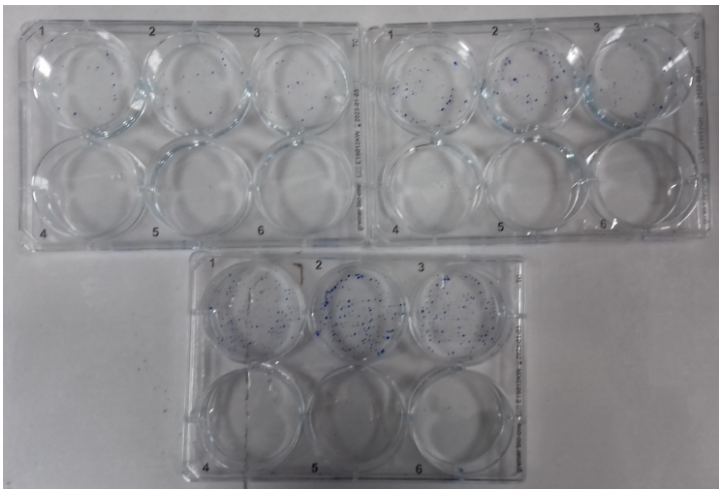

(b) Photo of SK-N-BE2 colonies

Figure 6.4: Photos of stained SK-N-BE(2)C and CHLA-15 colonies after increasing activities of 177Lu-DOTATATE

Change in heterogeneity parameters over time

Figure 6.6 summarises the pair-wise correlations between heterogeneity parameters measured from the pre-treatment PET and the effective half-life image map calculated from longitudinal SPECT images acquired after the first cycle. The mean | CCC | across the same heterogeneity parameters was 0.25 ± 0.37 (Figure 6.6). However, the CCC for homogeneity calculated in both the pre-treatment PET and intra-cycle SPECT exceeded 0.80. It is worth noting that a strong correlation (CCC $\geq$ 80) was observed between KINCorrelation and PEThomogeneity. All other pairs of heterogeneity parameters had a | CCC | $<$ 0.70.

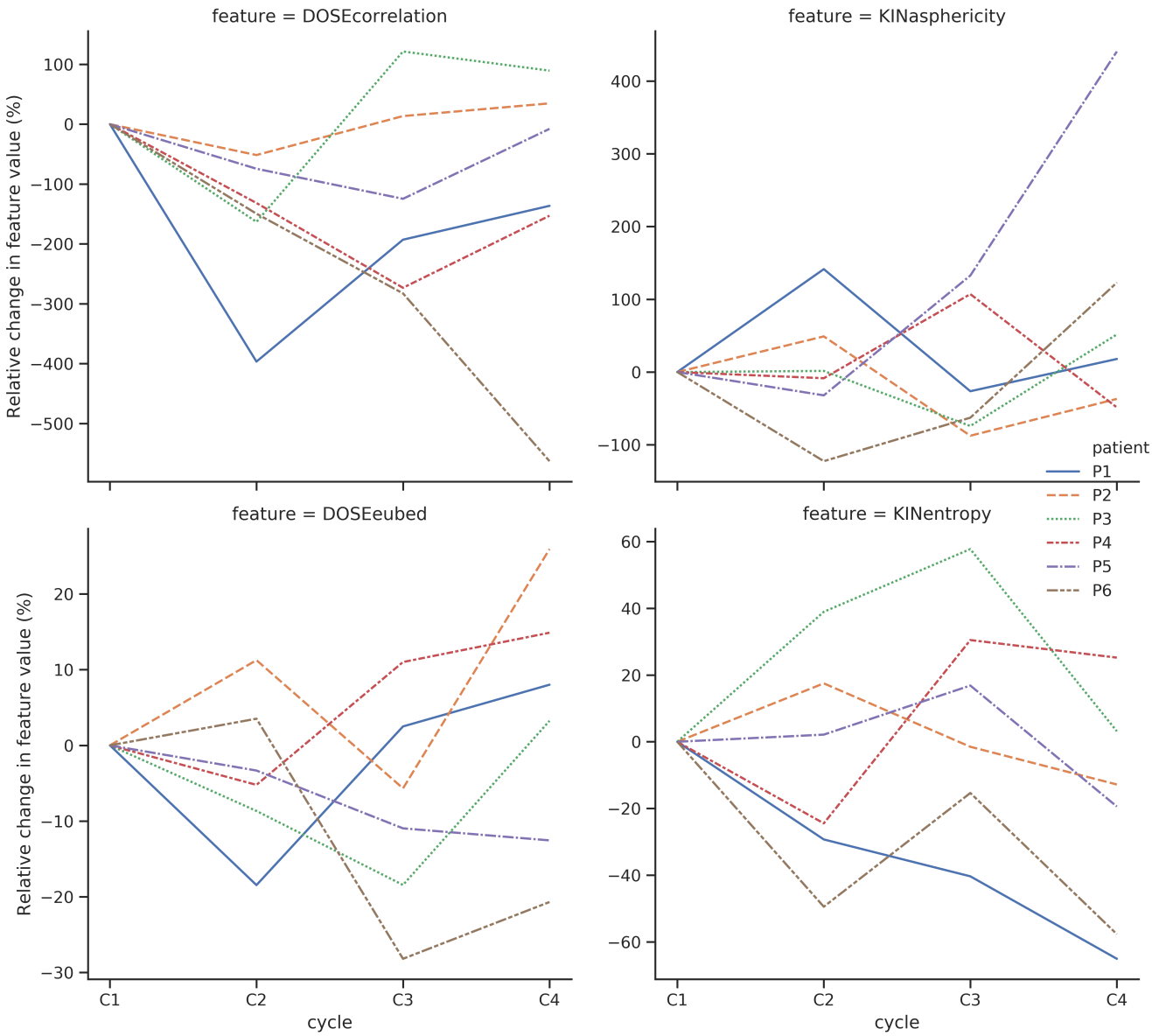

Figure 6.5: Percent change in value (relative to the initial cycle) as a function of treatment cycle for four different features

In addition to comparing the heterogeneity in the pre-treatment PET and effective half life image of the first cycle, a cluster analysis on the correlation between the heterogeneity parameters calculated from the pre-treatment PET and the SPECT/CT-based absorbed dose image of the first cycle was generated (Figure 6.7). This clustered heat map enabled exploration of which heterogeneity parameters from the pre-treatment PET/CT could predict heterogeneity parameters in the absorbed dose of the initial cycle. The PET and DOSE heterogeneity parameters are normalised and compared for all six patients. Each row shows the eight

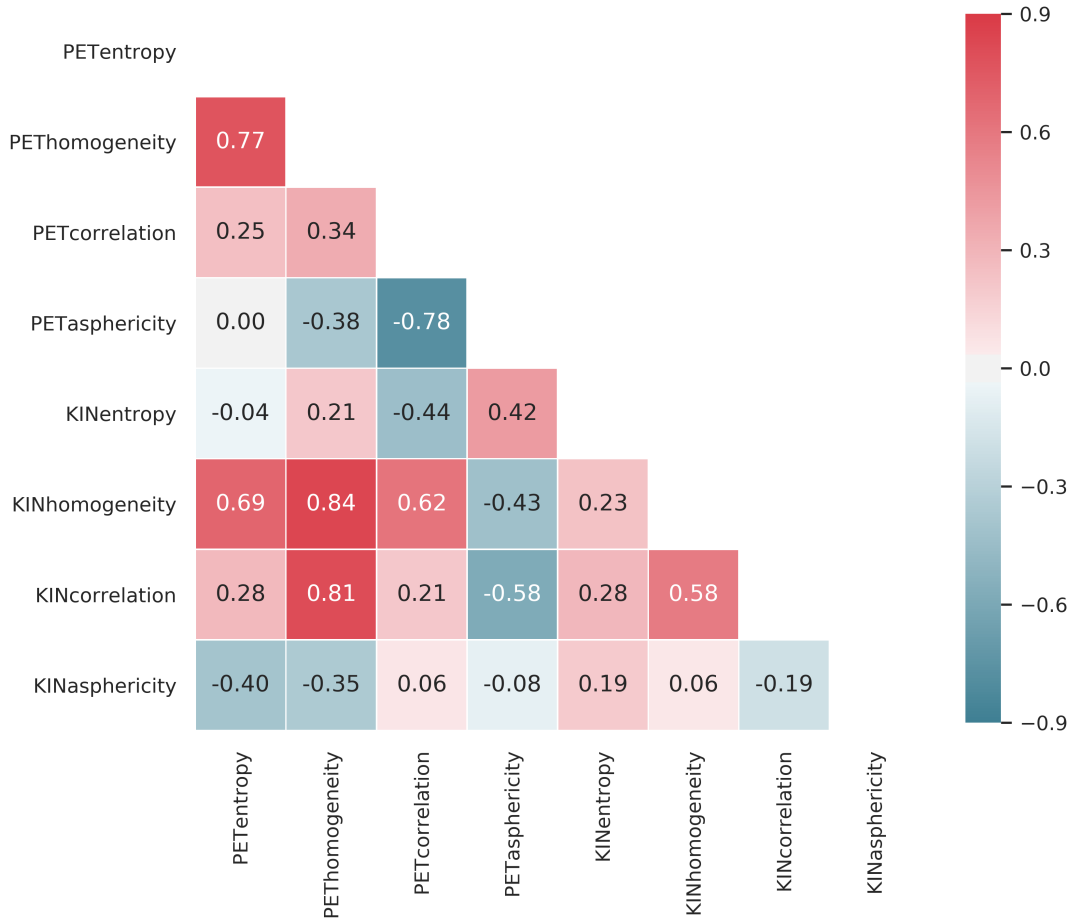

Figure 6.6: Correlation matrix of the 4 heterogeneity parameters derived from both the pre-treatment Ga68-DOTATATE PET/CT and the SPECT/CT-based effective halflife map of the initial cycle

normalised heterogeneity parameters for a particular patient. The rows are clustered according to patient ID using a Euclidean distance metric and the columns are clustered according to the CCC. The heterogeneity parameters are joined based on the strength of their correlation and the height of the clustered heatmap indicates the order in which the clusters were joined. The cluster analysis shows the strongest correlations between the pairs of DOSEentropy and DOSEcorrelation and PETentropy and PEThomogeneity. These pair-wise correlations were strong | CCC | >0.80 in patient 1 and patient 3 respectively. The strongest correlation between the heterogeneity parameters of the DOSE and PET images was the homogeneity of the DOSE image and the asphericity of the PET image.

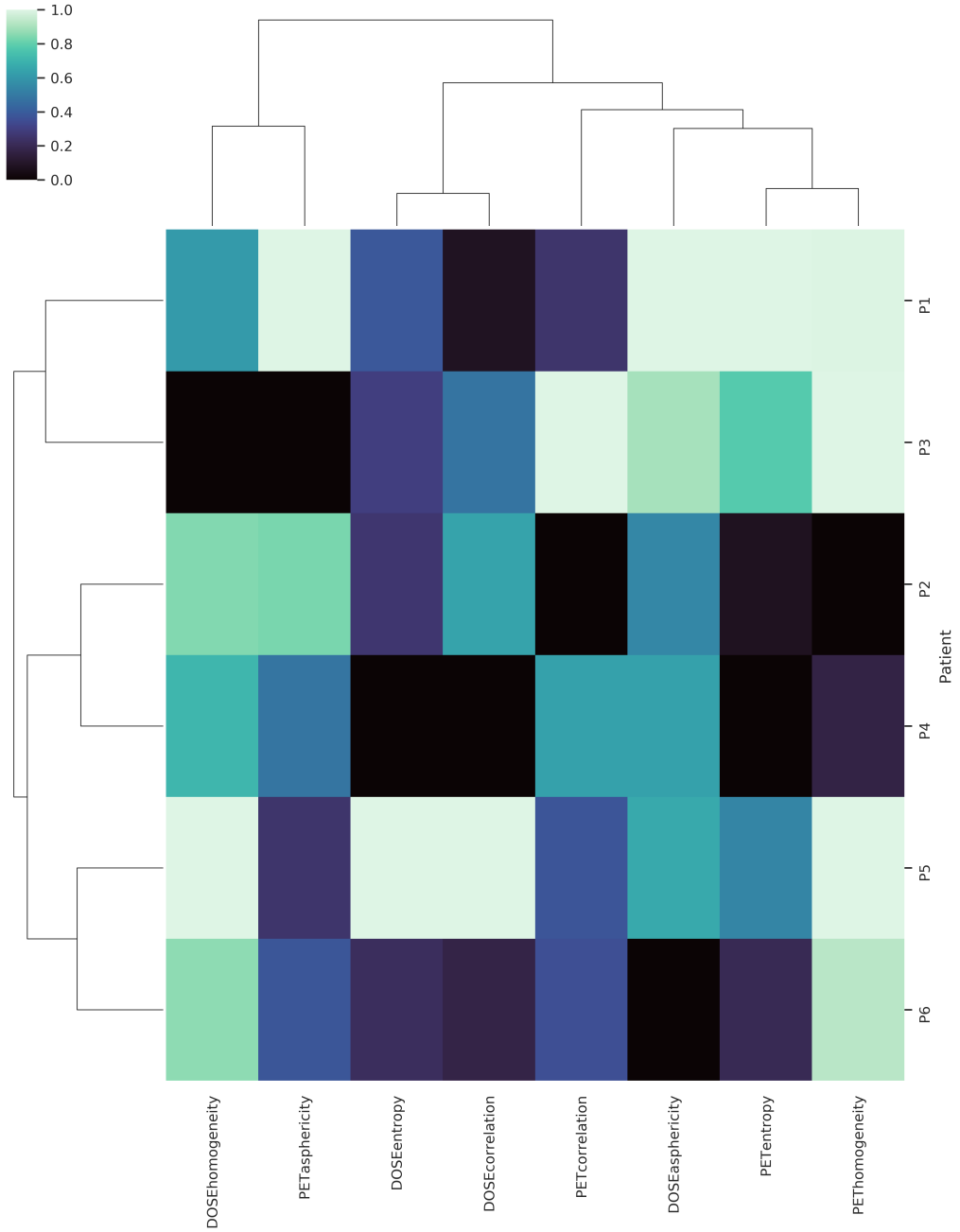

Figure 6.7: Clustered heatmap depicting the results of cluster analysis based on correlation between pre-treatment Ga68-DOTATATE PET/CT and Lu177-DOTATATE-based dose image of the initial cycle. The rows are clustered according to patient ID using a Euclidean distance metric and the columns are clustered according to the CCC

6.3.3 Correlation of heterogeneity parameters with patient response

Stable disease was observed in 3 of 6 patients (50%) and Progressive disease was observed in the remaining three. Due to the small sample size relative to the parame-

ters, regression models would have limited usefulness. Qualitatively, the relationship between changes in heterogeneity features categorised by dose-based and kinetics-based was visually explored (Figure 6.8). There was no clear relationship between RECIST response and intra-cycle changes (Δ) in Homogeneity, Asphericity, Correlation and Entropy derived from either the absorbed dose or effective halflife images. It is worth noting though that there was a differential response between dose-derived and kinetic-derived Correlation in the Stable Disease patients with KINcorrelation generally increaseing and DOSEcorrelation generally decreasing.

6.4 Discussion

This study aimed for characterisation of the variation of heterogeneity in pharmacokinetics and radiobiology with response in PET and SPECT based parameters extracted from a sub-volume of the tumour of children treated with 177Lu-DOTATATE. To our knowledge, this study is the first of its kind to investigate intra-cycle changes in heterogeneity of the tumour.

Homogeneity demonstrated superior correlation between the pre-treatment PET and first cycle SPECT time points. Additionally, dose-derived and kinetic-derived heterogeneity parameters Correlation showed a general increase and decrease trend respectively in patients who showed SD at one month. Despite the small sample, this observation is in line with the finding of Werner and colleagues who also demonstrated the ability of correlation measured at a single time point to differentiate between responders and non-responders[42].

Though we anticipated changes in regional (as opposed to total) tumour features may better demonstrate prediction of response compared to clinical parameters, this was not observed. In an study with NBL xenograft models, Zhang et al demonstrated that SSTR expression levels are associated with 68Ga-DOTATATE PET/CT uptake and antitumour efficacy of 177Lu-DOTATATE[36]. With this finding, it could be hypothesized that changes in SSTR spatial expression during treatment due to cell kill in previous cycles or receptor overexpression might be a predictor of response.

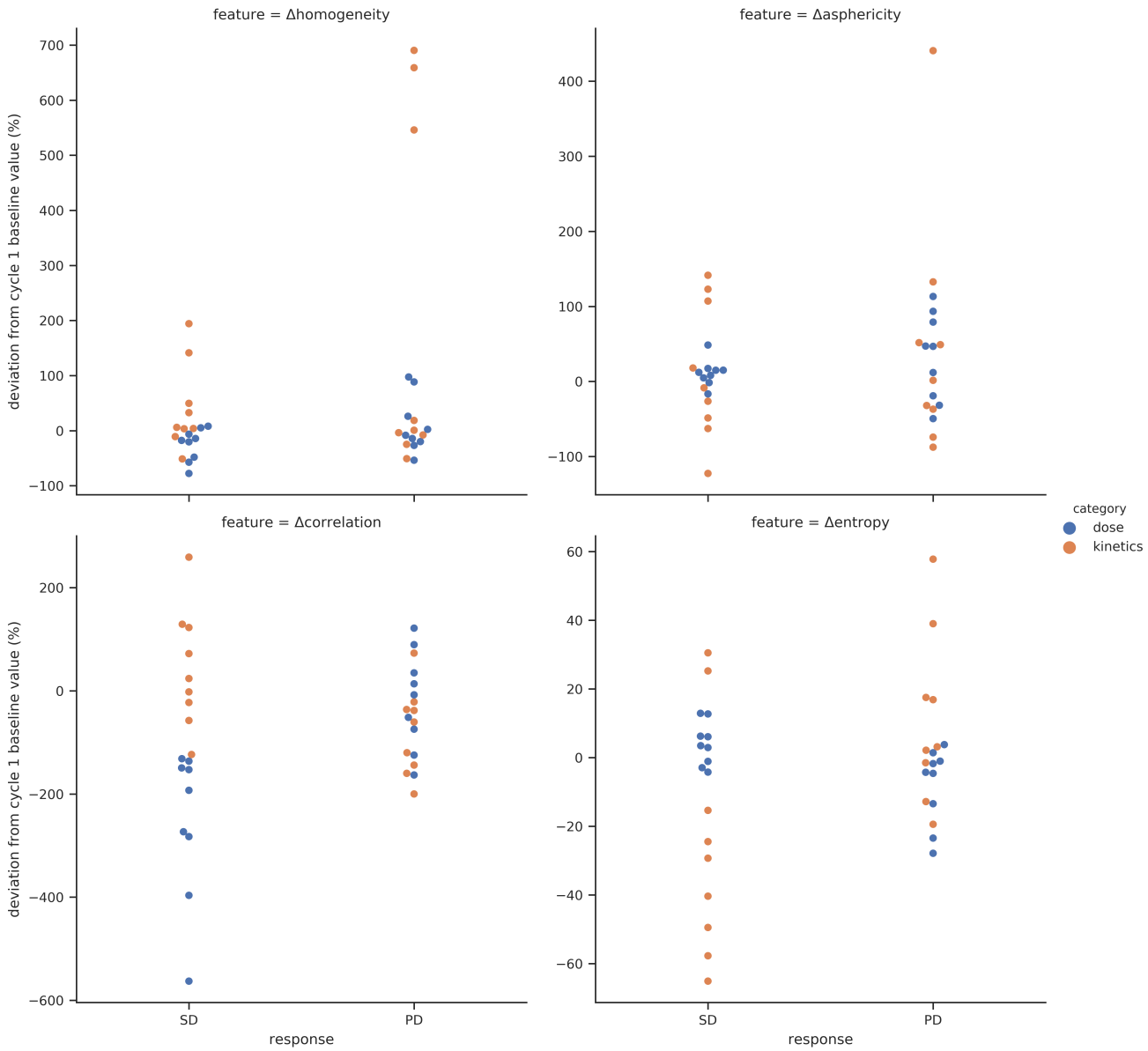

Figure 6.8: Plot of change in heterogeneity of somastatin receptor SPECT parameters (n=18) and patient response groups . Visual inspection appears to show no significant difference in changes in heterogeneity in the patients reaching stable disease (SD) or progressive disease (PD)

However, this was not observed in this cohort.

It has been suggested that radiobiological dose has a stronger correlation to response than physical dose. In a landmark clinical study, Sundlov showed the utility of radiobiology in the clinic for absorbed dose individualisation based on renal BED limits of 32 Gy to limit nephrotoxicity. By tracking the radiobiological dose in each patient per cycle, they were able to increase the number of cycles from 4 to a median of 7 cycles (range 5-8).The higher uptake of 177Lu-DOTATATE in

SK-N-BE(2)c compared to CHLA-15 corroborates with other studies suggesting a higher SSTR expression in SK-N-BE(2)c compared to CHLA-15[91].

While Entropy and Homogeneity measured on 68Ga-DOTATATE PET/CT did not correlate with response in this cohort of patients treated with 177Lu-DOTATATE, Khurshid and colleagues showed Entropy and Homogeneity measured on baseline Ga68-PSMA PET prior to Lu177-PSMA therapy had a negative ($\rho = -0.327$)and positive ($\rho = 0.315$) correlation with pre and post therapy PSMA levels [92]. One biological hypothesis for the observed differences is in contradistinction to pre-treatment 68Ga-DOTA-peptide imaging of NETs, where the uptake level in the tumour correlates with tumour differentiation, the uptake level in prostate cancer on pre-treatment 68Ga-PSMA PET/CT reflects the expression of prostate specific membrane antigen (PSMA).

This study has three main limitations. Emission tomographic images, particular SPECT, is characterised by noise due in part to the physical limitations of the collimator and the image reconstruction process. This leads to blurring termed as the Partial Volume Effect. PVE results in inaccuracies in the estimation of voxel values which in turn may be a source of error for quantification of the spatial heterogeneity of said voxel values. In addition to the smoothing with a 3-dimensional Butterworth filter performed during reconstruction of the SPECT images at UCLH, I performed additional smoothing with a Laplacian of a Gaussian kernel before analysing the heterogeneity in the 177Lu-DOTATATE scans. This smoothing is sensitive to areas with rapidly changing intensities, enhancing edges and reducing overall noise in the images. This additional smoothing also allowed for more realistic data points for the analytical fitting of the voxel values and reduced unrealistic clearance rates i.e clearance rates slower than the physical decay. However, Hatt and colleagues demonstrated that the predictive value of textural parameters is not affected by partial volume effect and is relatively independent of the method used to delineate the tumor volumes to be analyzed [45].

The analysis of heterogeneity can also be limited by the size of the lesion. For

small metastatic bone lesions observed in some of the patients, the analysis of heterogeneity may be challenging. In our study, the smallest lesion was 16x20 mm which is about 100 voxels. A second point that needs further investigation is the influence of reconstruction parameters on tissue heterogeneity. SPECT/CT reconstruction algorithms require smoothing of the raw image data which could influence the assessment of heterogeneity.

Multiple hypotheses were tested to explore correlations between different heterogeneity parameters taken from the KINETIC, PET and DOSE images. One impact of testing multiple hypotheses with an alpha of 0.05 to signify significance is that there is a chance of observing at least one significant result, even if all of the tests are actually not significant. Methods for dealing with multiple testing frequently call for adjusting alpha in some way, so that the probability of observing at least one significant result due to chance remains below the desired significance level. Such methods include using the Bonferroni Correction which tends to be a bit conservative or a False Discovery Rate.

Standard protocol in studies using features from tomographic imaging to characterise spatial heterogeneity in tumours involves a starting step of exploring the repeatability of the values of these features on different imaging systems. Given these images were acquired with the intent for diagnostic assessment of SSTR expression in the case of PET and physiological uptake in the case of SPECT, it was not possible to investigate the robustness of these features across various imaging systems to improve the generalisation of the results. Additionally, these images were reconstructed using standard protocols in clinical routine at our collaborator institution at University College London Hospital (UCLH) and were not necessarily acquired with optimal parameters of differing reconstruction parameters at different time points [48].

6.5 Conclusion

In this pilot study, we showed the feasibility of leveraging the intra-cycle SPECT data conventionally reserved for dosimetry to quantify temporal changes in the heterogeneity parameters - Entropy, Homogeneity, Correlation and Asphericity - in radiobiological dose, physical dose and effective half life of NBL patient receiving 177Lu-DOTATATE. We also showed the feasibility of a workflow to incorporate radiobiological in-vitro experiments into image analysis. Homogeneity demonstrated superior correlation between the pre-treatment PET and first cycle SPECT time points. Additionally, dose-derived and kinetic-derived heterogeneity parameters Correlation showed a general increase and decrease trend respectively in patients who showed SD at one month. Delta heterogeneity parameters however failed to identify responders.

Chapter 7

Conclusion and Outlook

To our knowledge, these are the first studies looking at the temporal and spatial patterns in the dose and biokinetics of lesions and kidneys of NBL patients receiving 177Lu-DOTATATE. This thesis attempts a paradigm shift from looking at a course of four cycles of 177Lu-DOTATATE as a single treatment made of largely independent cycles to a perception of the course of 177Lu-DOTATATE being a series of individual treatments which are interrelated.

To accomplish the project goals, the first step was to build a framework for modelling and extracting lesion and tumour pharmacokinetics and dosimetric data using various clinical protocols (Chapter 4). Accordingly, we developed a Python-based script named XINDA, which has implemented multiple nuclear medicine clinical protocols for modelling pharmacokinetics and provides physical dosimetric and radiobiological calculations. This was fundamental to subsequent analysis of the temporal response of the kidneys and tumour of children with NBL during 177Lu-DOTATATE treatment (Specific Aim 2) and investigation of the spatial variation of the lesion physical dose, radiobiological dose and pharmacokinetics (Specific Aim 3 and 4). All aims ultimately, to improve differentiation of responders from non-responders.

This chapter provides a complement to the complete discussions provided at the end of each chapter. The goal of Specific Aim 2 was to determine if we could utilize temporal variations in conventional metrics of mean dose and effective half-life in the kidneys and tumour during treatment to identify NBL patients who would respond

to 177Lu-DOTATATE treatment. In Chapter 5, we demonstrated the cycle-related variation in renal effective half life and the changing relationship between per-cycle renal and tumour effective half-life using longitudinal SPECT/CT image sets.

The reasons for intra-cycle variability were not examined in the study and still remains unclear in the literature. For variation in per-cycle renal kinetics and dose, it may be that blood pressure and degree of hydration, and thus renal perfusion, varied between cycles secondarily affecting the residence time in the kidneys and therefore the dose. The intra-cycle lesion variability is a complex issue. As discussed in Chapter 5, the relative radioresistance of NBL means the intra-cycle variability over a course of treatment is less likely to be explained by a rapid reduction of size so that saturation or down-regulation of SSTR is a more plausible explanation.

In Chapter 6 we analysed changes in the spatial pattern of effective half life, physical dose and EUBED during 177Lu-DOTATATE treatment in the same cohort of patients. An additional heterogeneity investigation was performed on each patient's pre-treatment 68Ga-DOTATATE PET/CT scan. The goal was to identify a time variation of four heterogeneity metrics - Homogeneity, Asphericity, Correlation and Entropy - in pre- and intra- treatment images that might be useful for response prediction prior to or during treatment. However, using linear regression analysis, we failed to identify a significant heterogeneity metric with demonstrated association to treatment response.

Our preliminary findings across all three chapters could be significant to the field in three ways. There has been a growing adoption of pharmacokinetics-based strategies to improve the effectiveness of 177Lu-DOTATATE therapy in NETs by increasing the retention time within the tumour through the use of antagonists like 177Lu-OPS201 (177Lu-DOTA-JR11)[93, 94]. Somatostatin receptor (SSTR) agonists, like 177Lu-DOTATATE, have successfully targeted SSTR-2 for both imaging and therapy in NET patients for over 20 years. In general, an agonist binds to a receptor and produces an effect within the cell. SSTR-2 agonists like 177Lu-DOTATATE are internalised by the cells. A relatively new development in the field

of SSTR targeting is the use of SSTR antagonists, which seem to confer greater specificity, more favourable pharmacokinetics and better tumour visualization than agonists [93]. An antagonist may bind to the same receptor, but does not produce a response, instead blocking that receptor to a natural agonist. These radiolabelled antagonists seem to recognise more receptor-binding sites than agonist radioligands. These agents can improve outcomes through higher tumour uptake and longer tumour residence times (1.7 - 10.6 times higher doses compared to 177Lu-DOTATATE) and tumour-to-kidney ratios up to 6.2 times higher than for the agonists [94]. Additionally, clinical studies with new radiopharmaceuticals like 177Lu-PSMA617 for the treatment of prostate cancer have also been reporting reduction in tumour size and improvement in quality of life as early as the second cycle[95, 23, 29].

As treatments are becoming increasingly more sophisticated and dependent on pharmacokinetics, a systematic characterisation could add valuable insight for patient prescription individualisation.

A next step for personalised dosimetry is to prove its clinically relevant additional benefits over the currently well-established empirical dosing methods using fixed-activity concepts in all patients or some with particular risk factors. Ideally, individualised approaches to dosimetry would be tested in prospective RCTs with adequate methodology for a direct comparison of outcomes in patient cohorts treated with a fixed-activity approach compared to a personalised dosimetry approach. Data from RCTs of this nature may clearly and unequivocally establish that the benefits achieved from a personalised dosimetry-approach are directly from optimisation of the treatment and may avoid underdosing and/or overdosing.

In the LuDO trial, 177Lu-DOTATATE monotherapy was found to not be effective in NBL patients and the trial was discontinued. Future trials with combination treatments may potentially improve outcomes. One approach to improve the effectiveness of future clinical trials of 177Lu-DOTATATE in NBL patients is to explore combination treatments of 177Lu-DOTATATE and 131I-mIBG. 131I-mIBG is routinely used to treat high-risk NBL patients and is delivered to the cells through

the norepinephrine transporter as opposed to through receptors as is the case for 177Lu-DOTATATE. The differing transport mechanisms may potentially overcome the limitations of a single agent of 177Lu-DOTATATE.

The lethality of 177Lu-DOTATATE therapy in possible future trials may also be increased by the use of radiopharmaceuticals with high linear energy transfer (LET) like Actinium-225 and Bismuth-213. For example, 213Bi-DOTATOC has been reported to result in a high number of long-lasting antitumour responses, including one complete remission, in patients who developed resistance against therapies with beta emitters like 90Y/177Lu-DOTATOC[96]. 225Ac-DOTATOC in NETs has also demonstrated promising treatment efficacy with long-lasting responses observed in several patients.

Combination regimens of 177Lu-DOTATATE with radiosensitisers may also improve the efficacy of treatment and is standard in some centres around the world. The addition of radiosensitising drugs can influence the ability of tumour cells to respond to radiation and further increase the efficacy of the therapy, e.g., by influencing DNA damage and repair mechanisms. Two proposed approaches for potentiating the therapeutic response of 177Lu-DOTATATE through radiosensitisation are combinations with the HSP90 inhibitor Onalespib or chemotherapeutic agent Capecitabine. In an in-vivo therapy study, Onalespib and 177Lu-DOTATATE demonstrated significant effects on tumour growth as monotherapies, delaying tumour doubling time from 4.8 days in untreated controls to 5.3 and 6.4 days respectively. However, the most pronounced effects were seen in the combination group, where tumour doubling time was extended to 8.3 days [97]. Furthermore, there is a non-randomised Phase I/II trial (NCT04086485), slated to start on April 23, 2020 will specifically look at the radiosensitisation effects of PARP inhibitor Olaparib with 177Lu-DOTATATE in adult NET patients. By enhancing the effectiveness of 177Lu-DOTATATE, radiosensitisers can lower the dose of radiation necessary for tumour control and potentially mitigate the side effects.

Targeted agents like 177Lu-DOTATATE are usually more cytostatic than cyto-

cidal and tend to induce necrosis and cystic change in solid tumours without necessarily producing tumour shrinkage as measured by anatomical CT/MRI. Therefore, anatomical imaging alone may have major limitations in predicting response, particularly in assessing targeted agents like 177Lu-DOTATATE that stabilise the tumour and provide other important aspects of response such as symptom control or improvements in quality of life. In that context, changes in the tumour's SUV from serial functional PET images with 68Ga-DOTATATE or 18F-fluorodeoxyglucose (FDG) may be a better predictor of response.

PET with FDG has been widely adopted as a tool for evaluating metabolic activity in tumours. FDG can allow the measurement of tumour response even in the absence of anatomical changes. Recently, the PET Response Criteria in Solid Tumours (PERCIST) [98] was proposed as a new method for the quantitative assessment of metabolic changes in solid tumours. While the RECIST method is used as an evaluation of change in physical volume or size, PERCIST may be more appropriate for response assessment of NBL/NET given the slow growing nature of these tumours and could provide clinicians with more accurate information of therapeutic response at an earlier stage of treatment.

Amino acid infusion was utilised for each patient receiving 177Lu-DOTATATE in the LuDO trial. Glomerular cells are relatively radiosensitive and not able to regenerate; therefore all radio-labelled therapies bear a high nephrotoxic potential. Renal irradiation is not SSTR mediated, but related primarily to the very rapid clearance of the small radiopeptides that are filtered through the glomeruli and reabsorbed by the tubular cells with subsequent radiation to the glomeruli, which leads to the nephrotoxicity. Co-infusion of amino acids inhibit tubular reabsorption of 177Lu-DOTATATE and reduce off target uptake in the kidneys. The use of amino acids allows higher activities to be administered to the patient resulting in a higher tumour dose with a smaller increase in off-target renal dose, reducing the possibility of acute nephrotoxicity.

The established dose limit of 23 Gy for kidneys for 177Lu-DOTATATE is de-

rived from EBRT data for bilateral kidney irradiation indicating a 5% risk of renal dysfunction at 5 years ($TD_{5/5}$) at a mean absorbed dose of 18-23 Gy[99]. The appropriateness of directly applying this renal dose limit derived from EBRT to TRT is worth considering, especially with the limited nephrotoxicity reported in clinical trials using this 23 Gy threshold. While CT can be used for relatively straightforward calculation of the absorbed dose in EBRT, in TRT the spatial and temporal distribution of radiation during the decay time of the isotope is extremely complex, depending on a highly dynamic interplay of pharmacokinetics (such as perfusion, metabolism, target expression heterogeneity, transmembrane cellular uptake, intracellular degradation, radionuclide release, and excretion), repair mechanisms, and radiobiological phenomena (low and continuously decreasing dose rate). The differing dose rates, differing fractionation schemes and the markedly more heterogeneous renal absorbed dose distribution of TRT may result in varying toxicity for the same renal physical dose delivered by both EBRT and TRT.

Typically, the prescription of 177Lu-DOTATATE is focused on achieving the maximum tolerable dose which means concentrating on the dose to off-target organs at risk like the kidneys. It may be worth concentrating on the dose to the tumour as the basis for prescription as we ultimately want to treat the tumour. While this may be an intuitive approach, it does face technical challenges. Since the tumours typically treated by 177Lu-DOTATATE are small compared to the typical SPECT voxel dimensions, calculations for tumour dosimetry are particularly susceptible to partial volume effects. This increases the uncertainty in verifying that any prescribed tumour dose is achieved. Additionally, unlike EBRT, it is difficult to determine the amount of activity to administer to achieve a set dose to the tumour as this is based on a complex interplay of patient-specific pharmacokinetics. The results from this thesis indicate that understanding this interplay for the initial cycle does not automatically translate to understanding the interplay for later cycles as tumour uptake is variable across multi-cycle treatments. The use of tumour dose prescriptions similar to EBRT would require a more accurate characterisation of the

relationship between administered activity and tumour dose and the change in that relationship over time. Concentrating on the dose to the kidney also suffers from the unknown relationship between administered activity and renal dose, however the larger volume and relative constancy in shape and volume of the kidney throughout treatment reduce the uncertainty in calculating the delivered renal dose.

In addition to the specific technical limitations mentioned in the individual discussions of each chapter, one of the main difficulties encountered in this study was acquisition of a large enough patient sample to investigate the changes during multi-cycle 177Lu-DOTATATE. Serial SPECT scans after each cycle of treatment – termed "full dosimetry" - is generally considered resource intensive in terms of clinical staff hours and scanner time. As a result, patients typically receive "full dosimetry" for the initial cycle and simplified dosimetry for subsequent cycles in clinical practice. Therefore, research relying on "full dosimetry" after each cycle of treatment to explore spatial and temporal changes is limited by patient numbers. This is compounded by NBL being a relatively rare cancer accounting for about 6% of all cancers in children.

Moreover, the specialised knowledge and experience required to perform accurate dosimetry studies is not available in many clinical centres. Therefore, many clinical studies with 177Lu-DOTATATE have omitted dosimetry, instead using blanket fixed activities or fixed activities adapted to patient characteristics, limiting the available data to compare the results of this research. Historically, interpretation and comparison of dosimetry data and ultimately dose-response relationships have generated confusion because of the lack of standardisation. Finally, patient cohorts treated with 177Lu-DOTATATE are typically clinically heterogeneous, heavily pre-treated and have treatment resistant tumours. This makes it difficult to generalise findings from this research to a broader population.

Inter-patient per-cycle variability could have an impact on clinical practice. While not every patient is likely to benefit, patients that are in higher risk groups with poor renal function as measured by GFR or high disease burden as measured

by PET may benefit from improved monitoring over the course of their multi-cycle 177Lu-DOTATATE therapy. Given the technical improvements in simplifying dosimetry to single time points, it may be possible to perform dosimetry at a single intermediary cycle and adjust the activity determined at the initial cycle to reach a set safety dose threshold. Also, current optimisation of a patient's prescribed administered activity using a dosimetry approach uses the rate of retention and clearance measured from the initial cycle to determine the activity needed to achieve a set per-cycle renal dose in the subsequent cycles. If the dose and effective half-life per injected activity for non-initial cycles vary significantly from the first cycle measurements then patients may be exposed to higher per-cycle renal doses than expected.

One of the achievements of this thesis was the creation of a series of freely available Python-based packages for SPECT/CT-based per-cycle renal and tumour kinetics and dose calculations named XINDA. With these packages, nuclear medicine physicists have access to four published dosimetry methods used across ten nuclear medicine centres in six countries. In a 2015 survey of European nuclear medicine centres distributed over 26 countries, 16% of respondents reported "limited access to dedicated software" as a factor limiting the implementation of patient-specific dosimetry in their centre[4]. XINDA represents a novel approach for cross-centre freely available code that is extendable and can potentially allow for centralised analysis.

Conventionally, a course of multi-cycle 177Lu-DOTATATE is viewed as a single treatment evenly divided into fractions or cycles. This thesis takes an unconventional approach of exploring multi-cycle 177Lu-DOTATATE as a series of independent treatments where earlier cycles may affect later ones. This forms the foundation for exploration of the impact of per-cycle changes on the cumulative dose and biokinetics of multi-cycle 177Lu-DOTATATE.

In addition, this thesis leverages existing three-dimensional imaging data in a novel way to understand spatial changes in the 177Lu-DOTATATE distribution

within the tumour during treatment. TRT represents one of the few systemic therapies where it is possible to visually track changes in both the spatial and temporal distribution of the radiolabelled drug in organs of interest. The conventional practice in dosimetry studies is to collapse the available three-dimensional data and report mean dose or dose-volume histograms for the tumours and kidneys. The method of analysis used in this thesis connects in a novel way conventional heterogeneity analysis reserved for anatomical images of tumour morphology like CT/MRI to post-treatment three-dimensional SPECT/CT-based kinetics and dose parameter maps.

Appendices

Formulae for Heterogeneity Paramaters

Correlation

$$Correlation = \frac{\sum_{i=1}^{N_g}\sum_{j=1}^{N_g} p(i,j)ij - \mu_x\mu_y}{\sigma_x(i)\sigma_y(j)} \tag{7.1}$$

Homogeneity

$$Homogeneity = \sum_{k=0}^{N_g-1} \frac{p_{x-y}(k)}{1+k^2} \tag{7.2}$$

Entropy

$$Entropy = -\sum_{i=1}^{N_g}\sum_{j=1}^{N_g} p(i,j)log_2(p(i,j)+\epsilon) \tag{7.3}$$

Asphericity

$$Asphericity = -\sqrt[3]{H-1} with H = \frac{1}{36\times\pi}\frac{S^2}{V^2} \tag{7.4}$$

Formulae for Modelling Patient Pharmacokinetics

Single Time Point
$$D(r_s, t_1) \times \frac{2 \times t_1}{\ln 2} \tag{7.5}$$

Monoexponential
$$A \exp(-\lambda_{x,y,z})\ t \tag{7.6a}$$

Biexponential
$$A_1 \exp(-\lambda_{1,x,y,z})\ t + A_2 \exp(-\lambda_{2,x,y,z})\ t \tag{7.6b}$$

Hybrid
$$\begin{cases} a_1 t & \text{for } 0 \leq t < t_{\text{initial}} \\ a_1(t_{\text{initial}}) + a_2(t - t_{\text{initial}}) & \text{for } t_{\text{initial}} \leq t < t_{24} \\ A \exp(-\lambda_{(x,y,z)} t) & \text{for } t > t_{24h} \end{cases} \tag{7.7}$$

Bibliography

[1] Aurélien Corroyer-Dulmont, Nadia Falzone, Veerle Kersemans, James Thompson, Danny P. Allen, Sarah Able, Christiana Kartsonaki, Javian Malcolm, Paul Kinchesh, Mark A. Hill, Boris Vojnovic, Sean C. Smart, Mark N. Gaze, and Katherine A. Vallis. Improved outcome of 131 i-mIBG treatment through combination with external beam radiotherapy in the SK-n-SH mouse model of neuroblastoma. *Radiotherapy and Oncology*, 124(3):488–495, sep 2017.

[2] Javian Malcolm, Nadia Falzone, Boon Lee, and Katherine Vallis. Targeted radionuclide therapy: New advances for improvement of patient management and response. *Cancers*, 11(2):268, feb 2019.

[3] Nadia Falzone, Boon Quan Lee, Sarah Able, Javian Malcolm, Samantha Terry, Yasir Alayed, and Katherine A. Vallis. Targeting micrometastases: The effect of heterogeneous radionuclide distribution on tumor control probability. *Journal of Nuclear Medicine*, 60(2):250–258, jun 2018.

[4] Katarina Sjögreen Gleisner, Emiliano Spezi, Pavel Solny, Pablo Minguez Gabina, Francesco Cicone, Caroline Stokke, Carlo Chiesa, Maria Paphiti, Boudewijn Brans, Mattias Sandström, Jill Tipping, Mark Konijnenberg, and Glenn Flux. Variations in the practice of molecular radiotherapy and implementation of dosimetry: results from a european survey. *EJNMMI Physics*, 4(1):28, dec 2017.

[5] Sally L George, Nadia Falzone, Sarah Chittenden, Stephanie J Kirk, Donna Lancaster, Sucheta J Vaidya, Henry Mandeville, Frank Saran, Andrew D.J.

Pearson, Yong Du, Simon T Meller, Ana M. Denis-Bacelar, and Glenn D Flux. Individualized 131I-mIBG therapy in the management of refractory and relapsed neuroblastoma. *Nuclear Medicine Communications*, 37(5):466–472, 2016.

[6] Heribert Hänscheid, Constantin Lapa, Andreas K. Buck, Michael Lassmann, and Rudolf A. Werner. Dose mapping after endoradiotherapy with177lu-DOTATATE/DOTATOC by a single measurement after 4 days. *Journal of Nuclear Medicine*, 59(1):75–81, jun 2017.

[7] Michela Del Prete, Frédéric Arsenault, Nassim Saighi, Wei Zhao, François-Alexandre Buteau, Anna Celler, and Jean-Mathieu Beauregard. Accuracy and reproducibility of simplified QSPECT dosimetry for personalized 177lu-octreotate PRRT. *EJNMMI Physics*, 5(1), oct 2018.

[8] Anna Sundlöv, Johan Gustafsson, Gustav Brolin, Nadja Mortensen, Rebecca Hermann, Peter Bernhardt, Johanna Svensson, Michael Ljungberg, Jan Tennvall, and Katarina Sjögreen Gleisner. Feasibility of simplifying renal dosimetry in 177lu peptide receptor radionuclide therapy. *EJNMMI Physics*, 5(1), jul 2018.

[9] Michael Garkavij, Mattias Nickel, Katarina Sjogreen-Gleisner, Michael Ljungberg, Tomas Ohlsson, Karin Wingårdh, Sven-Erik Strand, and Jan Tennvall. 177lu-[DOTA0,tyr3] octreotate therapy in patients with disseminated neuroendocrine tumors: Analysis of dosimetry with impact on future therapeutic strategy. *Cancer*, 116(S4):1084–1092, feb 2010.

[10] E. Ilan, M. Sandstrom, C. Wassberg, A. Sundin, U. Garske-Roman, B. Eriksson, D. Granberg, and M. Lubberink. Dose response of pancreatic neuroendocrine tumors treated with peptide receptor radionuclide therapy using 177lu-DOTATATE. *Journal of Nuclear Medicine*, 56(2):177–182, jan 2015.

[11] Ulrike Garske-Román, Mattias Sandström, Katarzyna Fröss Baron, Lars Lundin, Per Hellman, Staffan Welin, Silvia Johansson, Tanweera Khan, Hans Lundqvist, Barbro Eriksson, Anders Sundin, and Dan Granberg. Prospective observational study of 177lu-DOTA-octreotate therapy in 200 patients with advanced metastasized neuroendocrine tumours (NETs): feasibility and impact of a dosimetry-guided study protocol on outcome and toxicity. *European Journal of Nuclear Medicine and Molecular Imaging*, 45(6):970–988, mar 2018.

[12] Ulrike Garske, Mattias Sandström, Silvia Johansson, Anders Sundin, Dan Granberg, Barbro Eriksson, and Hans Lundqvist. Minor changes in effective half-life during fractionated177lu-octreotate therapy. *Acta Oncologica*, 51(1):86–96, oct 2011.

[13] Jean-Mathieu Beauregard, Michael S. Hofman, Grace Kong, and Rodney J. Hicks. The tumour sink effect on the biodistribution of 68ga-DOTA-octreotate: implications for peptide receptor radionuclide therapy. *European Journal of Nuclear Medicine and Molecular Imaging*, 39(1):50–56, sep 2011.

[14] Florian C. Gaertner, Khalil Halabi, Hojjat Ahmadzadehfar, Stefan Kürpig, Elisabeth Eppard, Charalambos Kotsikopoulos, Nikolaos Liakos, Ralph A. Bundschuh, Holger Strunk, and Markus Essler. Uptake of PSMA-ligands in normal tissues is dependent on tumor load in patients with prostate cancer. *Oncotarget*, 8(33), jul 2017.

[15] Nusrat J. Begum, Anne Thieme, Nina Eberhardt, Robert Tauber, Calogero D'Alessandria, Ambros J. Beer, Gerhard Glatting, Matthias Eiber, and Peter Kletting. The Effect of Total Tumor Volume on the Biologically Effective Dose to Tumor and Kidneys for 177 Lu-Labeled PSMA Peptides. *Journal of Nuclear Medicine*, 59(6):929–933, feb 2018.

[16] John Violet, Price Jackson, Justin Ferdinandus, Shahneen Sandhu, Tim Akhurst, Amir Iravani, Grace Kong, Aravind Ravi Kumar, Sue Ping Thang,

Peter Eu, Mark Scalzo, Declan Murphy, Scott Williams, Rodney J. Hicks, and Michael S. Hofman. Dosimetry of 177lu-PSMA-617 in metastatic castration-resistant prostate cancer: Correlations between pretherapeutic imaging and whole-body tumor dosimetry with treatment outcomes. *Journal of Nuclear Medicine*, 60(4):517–523, oct 2018.

[17] Wolfgang P. Fendler, Svenja Reinhardt, Harun Ilhan, Andreas Delker, Guido Böning, Franz J. Gildehaus, Christian Stief, Peter Bartenstein, Christian Gratzke, Sebastian Lehner, and Axel Rominger. Preliminary experience with dosimetry, response and patient reported outcome after lu-PSMA-617 therapy for metastatic castration-resistant prostate cancer. *Oncotarget*, 8(2), sep 2016.

[18] John Violet, Shahneen Sandhu, Amir Iravani, Justin Ferdinandus, Sue Ping Thang, Grace Kong, Aravind Ravi Kumar, Tim Akhurst, David A. Pattison, Alexis Beaulieu, Jennifer Mooi, Christina Guo, Victor Kalff, Declan G Murphy, Price Jackson, Peter Eu, Mark Scalzo, Scott Williams, Rod J Hicks, and Michael S Hofman. Long term follow-up and outcomes of re-treatment in an expanded 50 patient single-center phase II prospective trial of lutetium-177 (177lu) PSMA-617 theranostics in metastatic castrate-resistant prostate cancer. *Journal of Nuclear Medicine*, page jnumed.119.236414, nov 2019.

[19] Jonathan R. Strosberg, Edward M. Wolin, Beth Chasen, Matthew H. Kulke, David L Bushnell, Martyn E. Caplin, Richard P. Baum, Pamela L. Kunz, Timothy J. Hobday, Andrew Eugene Hendifar, Kjell E. Oberg, Maribel Lopera Sierra, Dik J. Kwekkeboom, Philippe B. Ruszniewski, and Eric Krenning. NETTER-1 phase III: Progression-free survival, radiographic response, and preliminary overall survival results in patients with midgut neuroendocrine tumors treated with 177-lu-dotatate. *Journal of Clinical Oncology*, 34(4_suppl):194–194, feb 2016.

[20] Lidia Strigari, Rosa Sciuto, Sandra Rea, Livio Carpanese, Giuseppe Pizzi, Antonella Soriani, Giuseppe Iaccarino, Marcello Benassi, Giuseppe Maria Ettorre,

and Carlo Ludovico Maini. Efficacy and toxicity related to treatment of hepatocellular carcinoma with 90y-sir spheres: radiobiologic considerations. *Journal of nuclear medicine : official publication, Society of Nuclear Medicine*, 51:1377–1385, September 2010.

[21] Mark N Gaze, Yen-Ch'ing Chang, Glenn D Flux, Rob J Mairs, Frank H Saran, and Simon T Meller. Feasibility of dosimetry-based high-dose 131i-meta-iodobenzylguanidine with topotecan as a radiosensitizer in children with metastatic neuroblastoma. *Cancer biotherapy & radiopharmaceuticals*, 20:195–199, April 2005.

[22] Anna Imhof, Philippe Brunner, Nicolas Marincek, Matthias Briel, Christian Schindler, Helmut Rasch, Helmut R Mäcke, Christoph Rochlitz, Jan Müller-Brand, and Martin A Walter. Response, survival, and long-term toxicity after therapy with the radiolabeled somatostatin analogue [90y-dota]-toc in metastasized neuroendocrine cancers. *Journal of clinical oncology : official journal of the American Society of Clinical Oncology*, 29:2416–2423, June 2011.

[23] C. Kratochwil, F. L. Giesel, M. Stefanova, M. Bene ova, M. Bronzel, A. Afshar-Oromieh, W. Mier, M. Eder, K. Kopka, and U. Haberkorn. PSMA-targeted radionuclide therapy of metastatic castration-resistant prostate cancer with 177lu-labeled PSMA-617. *Journal of Nuclear Medicine*, 57(8):1170–1176, mar 2016.

[24] Richard P Baum, Harshad R Kulkarni, Christiane Schuchardt, Aviral Singh, Martina Wirtz, Stefan Wiessalla, Margret Schottelius, Dirk Mueller, Ingo Klette, and Hans-Jürgen Wester. 177lu-labeled prostate-specific membrane antigen radioligand therapy of metastatic castration-resistant prostate cancer: Safety and efficacy. *Journal of nuclear medicine : official publication, Society of Nuclear Medicine*, 57:1006–1013, July 2016.

[25] Thorsten D Poeppel, Daria Handkiewicz-Junak, Michael Andreeff, Alexander Becherer, Andreas Bockisch, Eva Fricke, Lilli Geworski, Alexander Heinzel,

Bernd J Krause, Thomas Krause, Markus Mitterhauser, Wilfried Sonnenschein, Lisa Bodei, Roberto C Delgado-Bolton, and Michael Gabriel. Eanm guideline for radionuclide therapy with radium-223 of metastatic castration-resistant prostate cancer. *European journal of nuclear medicine and molecular imaging*, 45:824–845, May 2018.

[26] Maria Larsson, Peter Bernhardt, Johanna B Svensson, Bo Wängberg, Håkan Ahlman, and Eva Forssell-Aronsson. Estimation of absorbed dose to the kidneys in patients after treatment with 177Lu-octreotate: comparison between methods based on planar scintigraphy. *EJNMMI Research*, 2(1):49, sep 2012.

[27] M. Sandstrom, U. Garske-Roman, D. Granberg, S. Johansson, C. Widstrom, B. Eriksson, A. Sundin, H. Lundqvist, and M. Lubberink. Individualized dosimetry of kidney and bone marrow in patients undergoing 177lu-DOTA-octreotate treatment. *Journal of Nuclear Medicine*, 54(1):33–41, dec 2012.

[28] Michela Del Prete, François-Alexandre Buteau, and Jean-Mathieu Beauregard. Personalized 177lu-octreotate peptide receptor radionuclide therapy of neuroendocrine tumours: a simulation study. *European Journal of Nuclear Medicine and Molecular Imaging*, 44(9):1490–1500, mar 2017.

[29] D. Denoyer, P. Lobachevsky, P. Jackson, M. Thompson, O. A. Martin, and R. J. Hicks. Analysis of 177lu-DOTA-octreotate therapy-induced DNA damage in peripheral blood lymphocytes of patients with neuroendocrine tumors. *Journal of Nuclear Medicine*, 56(4):505–511, feb 2015.

[30] Dik J Kwekkeboom, Boen L Kam, Martijn van Essen, Jaap J M Teunissen, Casper H J van Eijck, Roelf Valkema, Marion de Jong, Wouter W de Herder, and Eric P Krenning. Somatostatin receptor-based imaging and therapy of gastroenteropancreatic neuroendocrine tumors. *Endocrine-Related Cancer*, 17(1):R53–R73, mar 2010.

[31] A. R. Haug, C. J. Auernhammer, B. Wangler, G. P. Schmidt, C. Uebleis, B. Goke, P. Cumming, P. Bartenstein, R. Tiling, and M. Hacker. 68ga-DOTATATE PET/CT for the early prediction of response to somatostatin receptor-mediated radionuclide therapy in patients with well-differentiated neuroendocrine tumors. *Journal of Nuclear Medicine*, 51(9):1349–1356, aug 2010.

[32] Michela Del Prete, François-Alexandre Buteau, Frédéric Arsenault, Nassim Saighi, Louis-Olivier Bouchard, Alexis Beaulieu, and Jean-Mathieu Beauregard. Personalized 177lu-octreotate peptide receptor radionuclide therapy of neuroendocrine tumours: initial results from the p-prrt trial. *European journal of nuclear medicine and molecular imaging*, 46:728–742, March 2019.

[33] Anna Sundlöv, Katarina Sjögreen-Gleisner, Johanna Svensson, Michael Ljungberg, Tomas Olsson, Peter Bernhardt, and Jan Tennvall. Individualised 177lu-DOTATATE treatment of neuroendocrine tumours based on kidney dosimetry. *European Journal of Nuclear Medicine and Molecular Imaging*, 44(9):1480–1489, mar 2017.

[34] Lore Santoro, Erick Mora-Ramirez, Dorian Trauchessec, Soufiane Chouaf, Pierre Eustache, Jean-Pierre Pouget, Pierre-Olivier Kotzki, Manuel Bardiès, and Emmanuel Deshayes. Implementation of patient dosimetry in the clinical practice after targeted radiotherapy using [177lu-[DOTA0, tyr3]-octreotate. *EJNMMI Research*, 8(1), nov 2018.

[35] Katherine K. Matthay, John M. Maris, Gudrun Schleiermacher, Akira Nakagawara, Crystal L. Mackall, Lisa Diller, and William A. Weiss. Neuroblastoma. *Nature Reviews Disease Primers*, 2(1), nov 2016.

[36] Libo Zhang, Douglass C. Vines, Deborah A. Scollard, Trevor McKee, Teesha Komal, Milan Ganguly, Trevor Do, Bing Wu, Natasha Alexander, Reza Vali, Amer Shammas, Travis Besanger, and Sylvain Baruchel. Correlation of somatostatin receptor-2 expression with gallium-68-DOTA-TATE uptake in neu-

roblastoma xenograft models. *Contrast Media & Molecular Imaging*, 2017:1–10, 2017.

[37] Natasha Alexander, Paula Marrano, Paul Thorner, Arlene Naranjo, Collin Van Ryn, Daniel Martinez, Vandana Batra, Libo Zhang, Meredith S. Irwin, and Sylvain Baruchel. Prevalence and clinical correlations of somatostatin receptor-2 (SSTR2) expression in neuroblastoma. *Journal of Pediatric Hematology/Oncology*, 41(3):222–227, apr 2019.

[38] J. E. Gains, J. B. Bomanji, N. L. Fersht, T. Sullivan, D. D'Souza, K. P. Sullivan, M. Aldridge, W. Waddington, and M. N. Gaze. 177lu-DOTATATE molecular radiotherapy for childhood neuroblastoma. *Journal of Nuclear Medicine*, 52(7):1041–1047, jun 2011.

[39] B. Emami, J. Lyman, A. Brown, L. Cola, M. Goitein, J.E. Munzenrider, B. Shank, L.J. Solin, and M. Wesson. Tolerance of normal tissue to therapeutic irradiation. *International Journal of Radiation Oncology Biology Physics*, 21(1):109–122, may 1991.

[40] Eleni Kalogianni, Glenn D. Flux, and Alessandra Malaroda. The use of BED and EUD concepts in heterogeneous radioactivity distributions on a multicellular scale for targeted radionuclide therapy. *Cancer Biotherapy and Radiopharmaceuticals*, 22(1):143–150, feb 2007.

[41] George Sgouros, Shannon Squeri, Ase M. Ballangrud, Katherine S. Kolbert, Jerrold B. Teitcher, Katherine S. Panageas, Ronald D. Finn, Chaitanya R. Divgi, Steven M. Larson, and Andrew D. Zelenetz. Patient-specific, 3-dimensional dosimetry in non-hodgkin's lymphoma patients treated with 131i-anti-b1 antibody: assessment of tumor dose-response. *Journal of nuclear medicine : official publication, Society of Nuclear Medicine*, 44:260–268, February 2003.

[42] Rudolf A. Werner, Constantin Lapa, Harun Ilhan, Takahiro Higuchi, Andreas K. Buck, Sebastian Lehner, Peter Bartenstein, Frank Bengel, Imke

Schatka, Dirk O. Muegge, László Papp, Norbert Zsótér, Tobias Große-Ophoff, Markus Essler, and Ralph A. Bundschuh. Survival prediction in patients undergoing radionuclide therapy based on intratumoral somatostatin-receptor heterogeneity. *Oncotarget*, 8:7039–7049, January 2017.

[43] Rudolf A. Werner, Harun Ilhan, Sebastian Lehner, László Papp, Norbert Zsótér, Imke Schatka, Dirk O. Muegge, Mehrbod S. Javadi, Takahiro Higuchi, Andreas K. Buck, Peter Bartenstein, Frank Bengel, Markus Essler, Constantin Lapa, and Ralph A. Bundschuh. Pre-therapy somatostatin receptor-based heterogeneity predicts overall survival in pancreatic neuroendocrine tumor patients undergoing peptide receptor radionuclide therapy. *Molecular imaging and biology*, 21:582–590, June 2019.

[44] Christoph Wetz, I. Apostolova, I. G. Steffen, F. Hofheinz, C. Furth, D. Kupitz, J. Ruf, M. Venerito, S. Klose, and Holger Amthauer. Predictive value of asphericity in pretherapeutic [111in]DTPA-octreotide SPECT/CT for response to peptide receptor radionuclide therapy with [177lu]DOTATATE. *Molecular Imaging and Biology*, 19(3):437–445, oct 2016.

[45] Mathieu Hatt, Florent Tixier, Catherine Cheze Le Rest, Olivier Pradier, and Dimitris Visvikis. Robustness of intratumour 18f-FDG PET uptake heterogeneity quantification for therapy response prediction in oesophageal carcinoma. *European Journal of Nuclear Medicine and Molecular Imaging*, 40(11):1662–1671, jul 2013.

[46] S. Deepa, K. Vijay Sai, R. Gowrishankar, Dwarakarani Rao, and K. Venkataramaniah. Precision electron–gamma spectroscopic measurements in the decay of 177lu. *Applied Radiation and Isotopes*, 69(6):869–874, jun 2011.

[47] M. Ljungberg, A. Celler, M. W. Konijnenberg, K. F. Eckerman, Y. K. Dewaraja, and K. Sjogreen-Gleisner. MIRD pamphlet no. 26: Joint EANM/MIRD guidelines for quantitative 177lu SPECT applied for dosimetry of radiopharmaceutical therapy. *Journal of Nuclear Medicine*, 57(1):151–162, oct 2015.

[48] Lishui Cheng, Robert F Hobbs, Paul W Segars, George Sgouros, and Eric C Frey. Improved dose–volume histogram estimates for radiopharmaceutical therapy by optimizing quantitative SPECT reconstruction parameters. *Physics in Medicine and Biology*, 58(11):3631–3647, may 2013.

[49] W. E. Bolch, K. F. Eckerman, G. Sgouros, and S. R. Thomas. MIRD pamphlet no. 21: A generalized schema for radiopharmaceutical dosimetry–standardization of nomenclature. *Journal of Nuclear Medicine*, 50(3):477–484, feb 2009.

[50] W. E. Bolch, L. G. Bouchet, J. S. Robertson, B. W. Wessels, J. A. Siegel, R. W. Howell, A. K. Erdi, B. Aydogan, S. Costes, E. E. Watson, A. B. Brill, N. D. Charkes, D. R. Fisher, M. T. Hays, and S. R. Thomas. Mird pamphlet no. 17: the dosimetry of nonuniform activity distributions–radionuclide s values at the voxel level. medical internal radiation dose committee. *Journal of nuclear medicine : official publication, Society of Nuclear Medicine*, 40:11S–36S, January 1999.

[51] Mark Konijnenberg, Marleen Melis, Roelf Valkema, Eric Krenning, and Marion de Jong. Radiation dose distribution in human kidneys by octreotides in peptide receptor radionuclide therapy. *Journal of nuclear medicine : official publication, Society of Nuclear Medicine*, 48:134–142, January 2007.

[52] Bin He and Eric C Frey. The impact of 3d volume of interest definition on accuracy and precision of activity estimation in quantitative SPECT and planar processing methods. *Physics in Medicine and Biology*, 55(12):3535–3544, may 2010.

[53] K Sjögreen-Gleisner, D Rueckert, and M Ljungberg. Registration of serial SPECT/CT images for three-dimensional dosimetry in radionuclide therapy. *Physics in Medicine and Biology*, 54(20):6181–6200, oct 2009.

[54] Michael Ljungberg and Katarina Sjögreen-Gleisner. The accuracy of absorbed dose estimates in tumours determined by quantitative SPECT: A monte carlo study. *Acta Oncologica*, 50(6):981–989, jul 2011.

[55] N Lanconelli, M Pacilio, S Lo Meo, F Botta, A Di Dia, L A Torres Aroche, M A Coca Pérez, and M Cremonesi. A free database of radionuclide voxel s values for the dosimetry of nonuniform activity distributions. *Physics in Medicine and Biology*, 57(2):517–533, jan 2012.

[56] Joshua Grimes and Anna Celler. Comparison of internal dose estimates obtained using organ-level, voxel s value, and monte carlo techniques. *Medical Physics*, 41(9):092501, aug 2014.

[57] Massimiliano Pacilio, Ernesto Amato, Nico Lanconelli, Chiara Basile, Leonel Alberto Torres, Francesca Botta, Mahila Ferrari, Nestor Cornejo Diaz, Marco Coca Perez, María Fernández, Michael Lassmann, Alex Vergara Gil, and Marta Cremonesi. Differences in 3d dose distributions due to calculation method of voxel s-values and the influence of image blurring in SPECT. *Physics in Medicine and Biology*, 60(5):1945–1964, feb 2015.

[58] Lisa Bodei, Marta Cremonesi, Mahila Ferrari, Monica Pacifici, Chiara M. Grana, Mirco Bartolomei, Silvia M. Baio, Maddalena Sansovini, and Giovanni Paganelli. Long-term evaluation of renal toxicity after peptide receptor radionuclide therapy with 90y-dotatoc and 177lu-dotatate: the role of associated risk factors. *European journal of nuclear medicine and molecular imaging*, 35:1847–1856, October 2008.

[59] Jeffry A. Siegel, Michael G. Stabin, and Robert M. Sharkey. Renal dosimetry in peptide radionuclide receptor therapy. *Cancer biotherapy & radiopharmaceuticals*, 25:581–588, October 2010.

[60] Raffaella Barone, Françoise Borson-Chazot, Roelf Valkema, Stéphan Walrand, Franck Chauvin, Lida Gogou, Larry K. Kvols, Eric P. Krenning, François Ja-

mar, and Stanislas Pauwels. Patient-specific dosimetry in predicting renal toxicity with (90)y-dotatoc: relevance of kidney volume and dose rate in finding a dose-effect relationship. *Journal of nuclear medicine : official publication, Society of Nuclear Medicine*, 46 Suppl 1:99S–106S, January 2005.

[61] John F. Fowler. The linear-quadratic formula and progress in fractionated radiotherapy. *The British Journal of Radiology*, 62(740):679–694, aug 1989.

[62] Wei Zhao, Pedro Luis Esquinas, Andrea Frezza, Xinchi Hou, Jean-Mathieu Beauregard, and Anna Celler. Accuracy of kidney dosimetry performed using simplified time activity curve modelling methods: a 177lu-DOTATATE patient study. *Physics in Medicine & Biology*, 64(17):175006, aug 2019.

[63] Andreas Delker, Harun Ilhan, Christian Zach, Julia Brosch, Franz Josef Gildehaus, Sebastian Lehner, Peter Bartenstein, and Guido Böning. The influence of early measurements onto the estimated kidney dose in [177lu][DOTA0,tyr3]octreotate peptide receptor radiotherapy of neuroendocrine tumors. *Molecular Imaging and Biology*, 17(5):726–734, mar 2015.

[64] Gustav Brolin, Johan Gustafsson, Michael Ljungberg, and Katarina Sjögreen Gleisner. Pharmacokinetic digital phantoms for accuracy assessment of image-based dosimetry in177lu-DOTATATE peptide receptor radionuclide therapy. *Physics in Medicine and Biology*, 60(15):6131–6149, jul 2015.

[65] Michael Ljungberg and Katarina Sjögreen Gleisner. Personalized dosimetry for radionuclide therapy using molecular imaging tools. *Biomedicines*, 4(4):25, nov 2016.

[66] F. Guerriero, M. E. Ferrari, F. Botta, F. Fioroni, E. Grassi, A. Versari, A. Sarnelli, M. Pacilio, E. Amato, L. Strigari, L. Bodei, G. Paganelli, M. Iori, G. Pedroli, and M. Cremonesi. Kidney dosimetry in177lu and90y peptide receptor radionuclide therapy: Influence of image timing, time-activity integration method, and risk factors. *BioMed Research International*, 2013:1–12, 2013.

[67] Johan Gustafsson, Per Nilsson, and Katarina Sjögreen Gleisner. On the biologically effective dose (BED)—using convolution for calculating the effects of repair: II. numerical considerations. *Physics in Medicine and Biology*, 58(5):1529–1548, feb 2013.

[68] Peter Kletting, Berthold Müller, Bahar Erentok, Jörn Schmaljohann, Florian F. Behrendt, Sven N. Reske, Felix M. Mottaghy, and Gerhard Glatting. Differences in predicted and actually absorbed doses in peptide receptor radionuclide therapy. *Medical Physics*, 39(9):5708–5717, aug 2012.

[69] Gerhard Glatting, Peter Kletting, Sven N. Reske, Kathrin Hohl, and Christina Ring. Choosing the optimal fit function: Comparison of the akaike information criterion and the f-test. *Medical Physics*, 34(11):4285–4292, oct 2007.

[70] David Sarrut, Adrien Halty, Jean-Noel Badel, Ludovic Ferrer, and Manuel Bardiès. Voxel-based multimodel fitting method for modeling time activity curves in SPECT images. *Medical Physics*, 44(12):6280–6288, oct 2017.

[71] M. Lassmann, C. Chiesa, G. Flux, and M. Bardiès. EANM dosimetry committee guidance document: good practice of clinical dosimetry reporting. *European Journal of Nuclear Medicine and Molecular Imaging*, 38(1):192–200, aug 2010.

[72] Mattias Sandström, Ezgi Ilan, Anna Karlberg, Silvia Johansson, Nanette Freedman, and Ulrike Garske-Román. Method dependence, observer variability and kidney volumes in radiation dosimetry of 177lu-DOTATATE therapy in patients with neuroendocrine tumours. *EJNMMI Physics*, 2(1), oct 2015.

[73] Ziv Yaniv, Bradley C. Lowekamp, Hans J. Johnson, and Richard Beare. SimpleITK image-analysis notebooks: a collaborative environment for education and reproducible research. *Journal of Digital Imaging*, 31(3):290–303, nov 2017.

[74] Lee R. Dice. Measures of the amount of ecologic association between species. *Ecology*, 26(3):297–302, jul 1945.

[75] Jennifer E. Gains, Veronica Moroz, Matthew D. Aldridge, Simon Wan, Keith Wheatley, Jennifer Laidler, Connie Peet, Jamshed B. Bomanji, and Mark N. Gaze. A phase IIa trial of molecular radiotherapy with 177-lutetium DOTATATE in children with primary refractory or relapsed high-risk neuroblastoma. *European Journal of Nuclear Medicine and Molecular Imaging*, mar 2020.

[76] J. M. Bland and D. G. Altman. Statistical methods for assessing agreement between two methods of clinical measurement. *Lancet (London, England)*, 1:307–310, February 1986.

[77] Y. K. Dewaraja, E. C. Frey, G. Sgouros, A. B. Brill, P. Roberson, P. B. Zanzonico, and M. Ljungberg. MIRD pamphlet no. 23: Quantitative SPECT for patient-specific 3-dimensional dosimetry in internal radionuclide therapy. *Journal of Nuclear Medicine*, 53(8):1310–1325, jun 2012.

[78] Shozo Okamoto, Anne Thieme, Jakob Allmann, Calogero D'Alessandria, Tobias Maurer, Margitta Retz, Robert Tauber, Matthias M. Heck, Hans-Juergen Wester, Nagara Tamaki, Wolfgang P. Fendler, Ken Herrmann, Christian H. Pfob, Klemens Scheidhauer, Markus Schwaiger, Sibylle Ziegler, and Matthias Eiber. Radiation dosimetry for 177 lu-PSMA i&t in metastatic castration-resistant prostate cancer: Absorbed dose in normal organs and tumor lesions. *Journal of Nuclear Medicine*, 58(3):445–450, sep 2016.

[79] Levent Kabasakal, Mohammad AbuQbeitah, Aslan Aygün, Nami Yeyin, Meltem Ocak, Emre Demirci, and Turkay Toklu. Pre-therapeutic dosimetry of normal organs and tissues of 177lu-PSMA-617 prostate-specific membrane antigen (PSMA) inhibitor in patients with castration-resistant prostate cancer. *European Journal of Nuclear Medicine and Molecular Imaging*, 42(13):1976–1983, jul 2015.

[80] Andreas Delker, Wolfgang Peter Fendler, Clemens Kratochwil, Anika Brunegraf, Astrid Gosewisch, Franz Josef Gildehaus, Stefan Tritschler, Chris-

tian Georg Stief, Klaus Kopka, Uwe Haberkorn, Peter Bartenstein, and Guido Böning. Dosimetry for 177Lu-DKFZ-PSMA-617: a new radiopharmaceutical for the treatment of metastatic prostate cancer. *European Journal of Nuclear Medicine and Molecular Imaging*, 43(1):42–51, jan 2016.

[81] Nichole M. Maughan, Jose Garcia-Ramirez, Matt Arpidone, Amy Swallen, Richard Laforest, S. Murty Goddu, Parag J. Parikh, and Jacqueline E. Zoberi. Validation of post-treatment PET-based dosimetry software for hepatic radioembolization of yttrium-90 microspheres. *Medical Physics*, 46(5):2394–2402, mar 2019.

[82] Irene Virgolini, Valentina Ambrosini, Jamshed B. Bomanji, Richard P. Baum, Stefano Fanti, Michael Gabriel, Nikolaos D. Papathanasiou, Giovanna Pepe, Wim Oyen, Clemens De Cristoforo, and Arturo Chiti. Procedure guidelines for PET/CT tumour imaging with 68ga-DOTA-conjugated peptides: 68ga-DOTA-TOC, 68ga-DOTA-NOC, 68ga-DOTA-TATE. *European Journal of Nuclear Medicine and Molecular Imaging*, 37(10):2004–2010, jul 2010.

[83] V. Lewington, B. Lambert, U. Poetschger, Z. Bar Sever, F. Giammarile, A. J. B. McEwan, Rita Castellani, T. Lynch, B. Shulkin, M. Drobics, A. Staudenherz, and R. Ladenstein. 123i-mIBG scintigraphy in neuroblastoma: development of a SIOPEN semi-quantitative reporting ,method by an international panel. *European Journal of Nuclear Medicine and Molecular Imaging*, 44(2):234–241, sep 2016.

[84] Lisa Bodei, Marta Cremonesi, Chiara M. Grana, Nicola Fazio, Simona Iodice, Silvia M. Baio, Mirco Bartolomei, Dario Lombardo, Mahila E. Ferrari, Maddalena Sansovini, Marco Chinol, and Giovanni Paganelli. Peptide receptor radionuclide therapy with 177lu-DOTATATE: the IEO phase i-II study. *European Journal of Nuclear Medicine and Molecular Imaging*, 38(12):2125–2135, sep 2011.

[85] Eero Hippeläinen, Mikko Tenhunen, Hanna Mäenpää, and Antti Sohlberg. Quantitative accuracy of (177)lu spect reconstruction using different compensation methods: phantom and patient studies. *EJNMMI research*, 6:16, December 2016.

[86] Jorma Heikkonen, Hanna Mäenpää, Eero Hippeläinen, Vappu Reijonen, and Mikko Tenhunen. Effect of calculation method on kidney dosimetry in177lu-octreotate treatment. *Acta Oncologica*, 55(9-10):1069–1076, may 2016.

[87] Jonathan I. Gear, Maurice G. Cox, Johan Gustafsson, Katarina Sjögreen Gleisner, Iain Murray, Gerhard Glatting, Mark Konijnenberg, and Glenn D. Flux. EANM practical guidance on uncertainty analysis for molecular radiotherapy absorbed dose calculations. *European Journal of Nuclear Medicine and Molecular Imaging*, 45(13):2456–2474, sep 2018.

[88] Ho Sze Chan, Erik de Blois, Alfred Morgenstern, Frank Bruchertseifer, Marion de Jong, Wouter Breeman, and Mark Konijnenberg. In vitro comparison of 213bi- and 177lu-radiation for peptide receptor radionuclide therapy. *PLOS ONE*, 12(7):e0181473, jul 2017.

[89] Christophe Nioche, Fanny Orlhac, Sarah Boughdad, Sylvain Reuzé, Jessica Goya-Outi, Charlotte Robert, Claire Pellot-Barakat, Michael Soussan, Frédérique Frouin, and Irène Buvat. LIFEx: A freeware for radiomic feature calculation in multimodality imaging to accelerate advances in the characterization of tumor heterogeneity. *Cancer Research*, 78(16):4786–4789, jun 2018.

[90] L. I. Lin. A concordance correlation coefficient to evaluate reproducibility. *Biometrics*, 45:255–268, March 1989.

[91] Mathias Tesson, Richa Vasan, Andreas Hock, Colin Nixon, Colin Rae, Mark Gaze, and Robert Mairs. An evaluation in vitro of the efficacy of nutlin-3 and topotecan in combination with 177 lu-DOTATATE for the treatment of neuroblastoma. *Oncotarget*, 9(49), jun 2018.

[92] Zain Khurshid, Hojjat Ahmadzadehfar, Florian C. Gaertner, László Papp, Norbert Zsóter, Markus Essler, and Ralph A. Bundschuh. Role of textural heterogeneity parameters in patient selection for 177lu-PSMA therapy via response prediction. *Oncotarget*, 9(70), aug 2018.

[93] Diane Reidy-Lagunes, Neeta Pandit-Taskar, Joseph A. O'Donoghue, Simone Krebs, Kevin D. Staton, Serge K. Lyashchenko, Jason S. Lewis, Nitya Raj, Mithat Gönen, Christian Lohrmann, Lisa Bodei, and Wolfgang A. Weber. Phase i trial of well-differentiated neuroendocrine tumors (NETs) with radiolabeled somatostatin antagonist 177lu-satoreotide tetraxetan. *Clinical Cancer Research*, 25(23):6939–6947, aug 2019.

[94] Damian Wild, Melpomeni Fani, Richard Fischer, Luigi Del Pozzo, Felix Kaul, Simone Krebs, Richard Fischer, Jean E F Rivier, Jean Claude Reubi, Helmut R Maecke, and Wolfgang A Weber. Comparison of somatostatin receptor agonist and antagonist for peptide receptor radionuclide therapy: a pilot study. *Journal of nuclear medicine : official publication, Society of Nuclear Medicine*, 55:1248–1252, August 2014. antagonist or agonist.

[95] Michael S Hofman, John Violet, Rodney J Hicks, Justin Ferdinandus, Sue Ping Thang, Tim Akhurst, Amir Iravani, Grace Kong, Aravind Ravi Kumar, Declan G Murphy, Peter Eu, Price Jackson, Mark Scalzo, Scott G Williams, and Shahneen Sandhu. [177 lu]-PSMA-617 radionuclide treatment in patients with metastatic castration-resistant prostate cancer (LuPSMA trial): a single-centre, single-arm, phase 2 study. *The Lancet Oncology*, 19(6):825–833, June 2018.

[96] C. Kratochwil, F. L. Giesel, F. Bruchertseifer, W. Mier, C. Apostolidis, R. Boll, K. Murphy, U. Haberkorn, and A. Morgenstern. 213bi-DOTATOC receptor-targeted alpha-radionuclide therapy induces remission in neuroendocrine tumours refractory to beta radiation: a first-in-human experience. *European Journal of Nuclear Medicine and Molecular Imaging*, 41(11):2106–2119, jul 2014.

[97] Sara Lundsten, Diana Spiegelberg, Nakul R Raval, and Marika Nestor. The radiosensitizer onalespib increases complete remission in 177lu-dotatate-treated mice bearing neuroendocrine tumor xenografts. *European journal of nuclear medicine and molecular imaging*, 47:980–990, April 2020.

[98] R. L. Wahl, H. Jacene, Y. Kasamon, and M. A. Lodge. From RECIST to PERCIST: Evolving considerations for PET response criteria in solid tumors. *Journal of Nuclear Medicine*, 50(Suppl_1):122S–150S, apr 2009.

[99] Laura A. Dawson, Brian D. Kavanagh, Arnold C. Paulino, Shiva K. Das, Moyed Miften, X. Allen Li, Charlie Pan, Randall K. Ten Haken, and Timothy E. Schultheiss. Radiation-associated kidney injury. *International Journal of Radiation Oncology, Biology and Physics*, 76(3):S108–S115, mar 2010.